

# Effects of friction and gas modelling on vehicle dynamics simulation

---

By

Jan-Sjoerd van den Bergh

Submitted in partial fulfilment of the requirements for the degree:

Masters in Engineering

(Mechanical Engineering)

In the:

Faculty of Engineering, Built Environment

and Information Technology (EBIT)

University of Pretoria

Pretoria

November 2014

## Summary:

<b>Title:</b>	Effects of Friction and Gas Modelling on Vehicle Dynamics Simulation
<b>Author:</b>	Jan-Sjoerd van den Bergh
<b>Study Leader:</b>	Prof. N.J. Theron
<b>Co-Study Leader:</b>	Prof. P.S. Els
<b>Department:</b>	Mechanical and Aeronautical Engineering University of Pretoria
<b>Degree:</b>	Masters in Engineering (Mechanical Engineering)

Validated simulation models have become ever more important in the current technological and economic environment, where simulation is an integral part of the design process. In the field of vehicle dynamics, it is no different, where vehicle manufacturers and researchers are relying more heavily on simulation than ever before. In the competitive field of research and development, the phrase “as accurate as possible, as complex as is necessary” rings true for vehicle models. Due to the “as complex as necessary” approach, many complex phenomena such as suspension kinematics and suspension friction remain un-modelled, as the assumption is made that the effects are negligible. The seemingly negligible effects negatively affect the validity of simulation models, especially when deviating from the specific manoeuvre for which the model was originally created.

In this study, focussed on a vehicle with a hydropneumatic suspension system, the effect of gas modelling methodology, friction, and friction modelling strategy on the validity the suspension unit characteristics, and a full non-linear vehicle dynamics model is presented. The approach to gas modelling included three permutations of the ideal gas formulation, namely isothermal, adiabatic, and a heat transfer dependent thermal time-constant approach. The effects of friction were accounted for using a rudimentary lookup table approach, a LuGre, and a Modified LuGre friction model, while using the case where friction is neglected as reference.

The results showed that the gas modelling approach, and the effects of friction, each have a significant effect on model accuracy and validity when compared to physical test results. The improvement is witnessed on both the single suspension unit characteristic as well as on the full non-linear simulation model. This effectively proves that seemingly negligible effects may have a significant effect on model validity.

## Opsomming:

<b>Titel:</b>	Effekte van Wrywings en Gas modelering op Voertuig Dinamika Simulasie
<b>Outeur:</b>	Jan-Sjoerd van den Bergh
<b>Studieleier:</b>	Prof. N.J. Theron
<b>Mede-Studieleier:</b>	Prof. P.S. Els
<b>Departement:</b>	Mechanical and Aeronautical Engineering University of Pretoria
<b>Graad:</b>	Magister in Ingenieurswese (Meganiese Ingenieurswese)

Gevalideerde simulatie modelle word al hoe meer belangrik in die huidige tegnologiese en ekonomiese omgewing, waar simulatie as 'n integrale deel van die ontwerp proses is. In die voertuig-dinamika veld is dit ook die geval, waar vervaardigers en navorsers meer op simulase staatmaak as ooit tevore. In die navorsings en ontwikkelings veld met sy strawwe kompetisie, word die frase "so akkuraat moontlik, so kompleks as nodig" dikwels ter harte geneem met die ontwikkeling van voertuig modelle. Die "so kompleks as nodig" benadering het die gevolg dat baie verskynsels soos suspensie kinematika en wrywing nie in ag geneem word nie, aangesien daar aanvaar word dat die effekte weglaatbaar klein is. Hierdie oënskynlike weglaatbare effekte, het 'n negatiewe impak op die akkuraatheid en geldigheid van die model waneer daar afgewyk word van maneuvers waarvoor die model oorspronklik ontwikkel is.

In hierdie studie, waar gefokus word op 'n voertuig met 'n hidro-pneumatiese suspensie stelsel, word die effek van gas modelering, wrywing, en wrywings modelering strategie op die geldigheid van die suspensie eenheid karakterestieke, asook die vol nie-linieêre voertuig model voorgelê. Die benadering tot gas modelering sluit drie permutasies van die ideale gas wet in, naamlik isotermies, adiabaties, en die hitte-oordrag afhanklike termiese tyd-konstante formulering. Die effekte van wrywing is op drie maniere in ag geneem, naamklik 'n opsoek matriks, 'n LuGre, en 'n Aangepaste LuGre wrywings model, terwyl die geval waar wrywing weggelaat is gebruik word as verwysing.

Die resultate wys dat die gas modelerings strategie, asook die effek van wrywing elkeen 'n waarneembare effek op die model akkuraatheid en geldigheid het waneer dit vergelyk word met fisiese toets resultate. 'n Verbetering is gesien in die enkel suspensie eenheid karakterestiek sowel as die vol nie-linieêre simulatie model. Dit bewys effektief dat sekere verskynsels, alhoewel dit klein is in vergelyking met ander effekte, 'n groot impak op model geldigheid en akkuraatheid kan hê.

## Acknowledgements

Ek wil graag die volgende persone bedank en erken vir die volgehoue ondersteuning gedurende die verloop van hierdie projek.

- Aan my Vrou: Donna-Lee, baie dankie my engel vir al die ondersteuning, die daar wees waneer ek 'n klankbord nodig gehad het en dat jy saam met my hierdie uitdaging aangepak het. Baie dankie dat jy altyd daar was en vir al jou hulp, raad en bystand deur al ons studie jare saam.
- Aan my Ouers & gesin: Pappa & Mamma, baie dankie vir al die jare se ondersteuning en alles wat julle vir ons gedoen het. Dankie dat julle altyd daar was met 'n helpende hand en ondersteuning in die moeilikke tye. Johann & Riana, baie dankie vir julle ondersteuning deur al die studie jare en al die leiding wat julle vir jul klein boetie gegee het.
- Aan my vriende en familie: Baie dankie vir jul ondersteuning, raad en hulp deur die studie jare wat ons saam gedeel het.
- Aan my studieleier, Prof. Theron: Baie dankie vir al die raad, kommentaar, en leiding gedurende die verloop van die projek.

## Table of Contents

Summary:.....	i
Opsomming:.....	ii
Acknowledgements.....	iii
Table of Contents.....	iv
List of Figures.....	vii
List of Tables.....	x
List of Symbols.....	xi
Abbreviations.....	xiv
1. Introduction.....	1
2. Literature Study.....	2
2.1. Roll Over Statistics.....	2
2.2. Mechanism of Roll Over.....	3
2.2.1. Spring Stiffness – Effects on Vehicle Roll.....	3
2.2.2. Centre of Gravity Position – Effects on Vehicle Roll.....	5
2.2.3. Damping Rate and Transient Effects on Vehicle Roll.....	10
2.3. National Highway Traffic Safety Administration Vehicle Testing Manoeuvres.....	12
2.3.1. Vehicle characterisation-, Handling- and Miss-Use Manoeuvres.....	12
2.3.2. Roll over Propensity Testing Manoeuvres.....	14
2.4. Active and Semi-Active Suspension Systems.....	17
2.4.1. Active Suspension Systems.....	18
2.4.2. Semi-Active Suspension Systems.....	20
2.5. Requirements for Handling and Ride Comfort and Reduced Roll-Over Propensity.....	23
2.5.1. Suspension Requirements for good handling or good ride comfort.....	24
2.5.2. Roll-over prevention strategies and Suspension requirements.....	26
2.6. Friction Effects and Friction Modelling.....	26
2.6.1. Coulomb, Viscous and Stribeck Friction Model.....	27
2.6.2. The Dahl Model.....	28
2.6.3. The LuGre Model.....	29
2.6.4. The Modified LuGre Model.....	30
2.6.5. The Generalised Maxwell Slip model.....	32
2.6.6. General observations from friction models.....	33
2.7. Conclusions from Literature.....	35

3.	Simulation Model and Model Validation .....	36
3.1.	Model Properties .....	36
3.2.	Hydro-Pneumatic Suspension Modelling.....	39
3.2.1.	Hydro-pneumatic suspension modelling, contributing factors .....	39
3.2.1.1.	Thermodynamic effects on hydropneumatic suspension modelling.....	40
3.2.1.2.	Fluid Bulk effects on hydro-pneumatic suspension modelling .....	43
3.2.1.3.	Thermal & bulk effects on hydro-pneumatic suspension modelling.....	44
3.2.1.4.	Gas charging pressure effects .....	45
3.2.2.	Hydraulic Damper Modelling .....	46
3.3.	Friction Modelling .....	47
3.3.1.	Rudimentary, and revised rudimentary compensation for suspension friction.....	47
3.3.2.	Experimental Friction characterisation and LuGre model compensation .....	49
3.3.3.	Modified LuGre Friction Model.....	51
3.3.4.	Comparison of Friction models used for compensation.....	53
3.4.	Model Validation.....	56
3.4.1.	Model Validation spring Force-Displacement Characteristics .....	57
3.4.1.1.	Soft Spring Force-Displacement Validation .....	58
3.4.1.2.	Stiff Spring Force-Displacement Validation .....	62
3.4.2.	Model Validation Severe Double Lane Change.....	66
3.4.3.	Model Validation Constant Radius Test.....	70
3.4.4.	Conclusion of Model Validation .....	73
4.	Simulation Results and Discussion .....	74
4.1.	Gas-Spring modelling Effects on Simulation .....	74
4.1.1.	Simulation results: Gas-Spring Modelling effects on Simulation.....	74
4.1.2.	Discussion: Gas-Spring Modelling Effects on Simulation .....	79
4.2.	Friction modelling Effects on Simulation Model.....	81
4.2.1.	Simulation Results: Friction Modelling effects on Simulation .....	81
4.2.2.	Discussion: Friction Modelling effects on Simulation .....	86
4.3.	Discussion: Friction Effects on Ride and Rollover Dynamics.....	89
5.	Conclusions, Recommendations and Future Work.....	93
5.1.	Conclusions .....	93
5.1.1.	Gas-modelling effects .....	93
5.1.2.	Friction modelling and Frictional effects .....	94
5.2.	Recommendations .....	95

5.3. Future Work.....	97
6. References .....	99
Annexure A: Previous attempts at bulk modulus compensation .....	I
Annexure B: Friction model comparisons for various test inputs .....	III
Annexure B-1: Friction Characteristics for sinusoidal displacement inputs .....	III
Annexure B-2: Friction Characteristics for Triangular displacement inputs.....	VIII
Annexure C: Model Validation Additional figures .....	XII
Annexure C-1: Higher Velocity Double Lane Change Soft Suspension .....	XII
Annexure C-2: Higher Velocity Double Lane Change Stiff Suspension .....	XIV
Annexure D: Friction Effects Additional figures.....	XVII

## List of Figures

Figure 1: Quasi-Static Roll Model Free Body Diagram Gillespie (1992) .....	3
Figure 2: Load transfer effect on tyre Side Force Mitchell (2012) .....	5
Figure 3: Forces acting to produce Roll-Over on a rigidly suspended vehicle Gillespie (1992) .....	5
Figure 4: Forces acting to produce Roll-Over on a suspended Vehicle Gillespie (1992) .....	7
Figure 5: Effect of CG height on Rollover Propensity Whitehead, et al. (2004) .....	9
Figure 6: Effects of longitudinal CG position on vehicle roll-over propensity Whitehead, et al. (2004)	9
Figure 7: Damping effect on Rollover Threshold Gillespie (1992) .....	10
Figure 8: ISO 3888 Double Lane Change Track and Cone Placement International Organisation for Standardisation (1975).....	13
Figure 9: J-Turn Manoeuvre Steering wheel input, Howe, et al. (2001).....	14
Figure 10: Comparison of Fishhook test 1 and 2 Garrot, Howe, and Forkenbrock (1999).....	15
Figure 11: Fishhook test 2 Steering wheel angle as a function of Time, Garrot, Howe, and Forkenbrock (1999).....	16
Figure 12: Suspension Design Space Holdmann and Holle (1999) .....	17
Figure 13: Spring Rate as a function of load for Mechanical, Pneumatic and Hydro-Pneumatic Suspensions, Bauer (2011).....	20
Figure 14: Natural Frequency as a function of spring load for Mechanical, Pneumatic and Hydro- Pneumatic Suspension units, Bauer (2011) .....	21
Figure 15: Circuit Diagram of the 4S <sub>4</sub> Els (2006) .....	22
Figure 16: 4S <sub>4</sub> Spring Displacement Characteristics Els (2006).....	22
Figure 17: 4S <sub>4</sub> Damper Characteristics Els (2006) .....	23
Figure 18: Weighting Function W <sub>b</sub> for vertical vibration measurement on a seated person in the vertical direction British Standards Institution (1987).....	25
Figure 19: Coulomb, viscous and static friction, Van Geffen (2009).....	28
Figure 20: Stribeck friction model, Van Geffen (2009) .....	28
Figure 21: Bristle model of Frictional Interface (Bristles on lower body shown as rigid for simplicity), de Wit, et al. (1995) .....	29
Figure 22: LuGre model simulation results versus measurements showing under and over prediction of two models, Yanada and Sekikawa (2008) .....	31
Figure 23: CG position and Vehicle Dimensions, UYS, et al. (2006b).....	37
Figure 24: Vehicle Wheel and Suspension Track width, Breytenbach (2009) .....	37
Figure 25: Suspension Layout in Simulation Model, Els, et al. (2007) .....	38
Figure 26: Schematic Layout of Front Suspension in the simulation model, Els, et al. (2007) .....	38
Figure 27: Schematic Layout of Rear Suspension in the simulation model, Els, et al. (2007) .....	39
Figure 28: Nelson-Obert Generalized Compressibility Chart, Thermofluids.net (2013).....	41
Figure 29: Force Displacement Characteristic Comparison of Isothermal and Adiabatic gas models, Hard Setting .....	44
Figure 30: Force Displacement Characteristic Comparison of Isothermal and Adiabatic gas models, Soft Setting.....	45
Figure 31: Pre-Load effects on spring characteristics (Soft) .....	46
Figure 32: Friction force velocity characteristic used by Cronjé (2008) .....	48
Figure 33: Revised rudimentary friction model force-velocity characteristic .....	48
Figure 34: Static Friction Characteristics for different pressures, Breytenbach (2009) .....	50



Figure 35: LuGre friction model Force-velocity characteristic.....	50
Figure 36: Modified LuGre Friction model Force-Velocity Characteristic.....	52
Figure 37: Friction Correlation from Breytenbach (2009) .....	54
Figure 38: Comparison of Force Characteristics for three models investigated using 0.025m amplitude, 0.025Hz Sinusoidal displacement input .....	54
Figure 39: Comparison of Force Characteristics for three models investigated using 0.025m amplitude, 0.95Hz Sinusoidal displacement input .....	55
Figure 40: Force-Velocity Characteristic comparison for 0.05Hz Sinusoidal displacement input .....	55
Figure 41: Soft Suspension Characterisation Spring Displacement Input.....	58
Figure 42: Soft Suspension, 0.01 Hz Force-Displacement Correlation, Friction effects .....	59
Figure 43: Soft Suspension, 0.1 Hz Force-Displacement Correlation, Friction effects .....	59
Figure 44: Force-Displacement Correlation 0.01 Hz Soft setting, Measured and Model reactions .....	60
Figure 45: Force-Displacement Correlation 0.5 Hz Soft setting, Measured and Model reactions .....	60
Figure 46: Stiff Suspension Characterisation Displacement Input.....	62
Figure 47: Stiff Suspension, 0.01Hz Force-Displacement Correlation, Friction effects .....	63
Figure 48: Stiff Suspension, 0.1Hz Force-Displacement Correlation, Friction effects .....	63
Figure 49: Force-Displacement Correlation 0.01Hz Stiff setting, Measured and Model reactions .....	64
Figure 50: Force-Displacement Correlation 0.5Hz Stiff setting, Measured and Model reactions .....	64
Figure 51: Soft Suspension Roll angle and Displacement Validation, Thermal Time Constant and Adiabatic models, Double Lane Change 60km/h.....	66
Figure 52: Soft Suspension Force and Roll rate Validation, Thermal Time Constant and Adiabatic models, Double Lane Change 60km/h .....	67
Figure 53: Hard Suspension Displacement Validation, Thermal Time Constant & Adiabatic, Double Lane Change 60km/h .....	69
Figure 54: Hard Suspension Force Validation, Thermal Time Constant and Adiabatic models, Double Lane Change 60km/h .....	69
Figure 55: Constant Radius Test displacement validation using the fixed axis limits.....	71
Figure 56: Constant Radius Test force validation using the same axis limits .....	72
Figure 57: Detailed view of Constant Radius Test force validation .....	72
Figure 58: Bulk Modulus Effect on Soft suspension using Adiabatic Gas model .....	75
Figure 59: Comparison of Adiabatic, Isothermal, and Thermal Time-Constant gas models for Soft suspension .....	76
Figure 60: Bulk Modulus Effect on Stiff suspension using Adiabatic Gas model .....	77
Figure 61: Comparison of Adiabatic, Isothermal, and Thermal Time-Constant gas models for Stiff suspension .....	77
Figure 62: Bulk Modulus effect on Isothermal Constant Radius Test.....	78
Figure 63: Adiabatic and Isothermal gas model effects on Constant Radius Test.....	79
Figure 64: Friction Effects on Soft suspension dynamics for a Double Lane Change .....	82
Figure 65: Detailed view of frictional effects on Left Front Soft suspension displacement for a Double Lane Change.....	83
Figure 66: Friction Effects on Hard suspension dynamics for a Double Lane Change.....	83
Figure 67: Detailed view of frictional effects on Left Front Hard suspension displacement for a Double Lane Change .....	84
Figure 68: Friction Effects on suspension dynamics for a Constant Radius test .....	85

Figure 69: Detailed view of Friction effects on Right Rear Suspension displacement for a Constant Radius Test .....	85
Figure 70: Friction Effects on the DSI for a 60km/h Double Lane Change, Ride-Setting .....	90
Figure 71: Friction Effects on the DSI for an 80km/h Double Lane Change, Ride Setting .....	90
Figure 72: Friction Effects on the DSI for a 60km/h Double Lane Change, Handling Setting .....	91
Figure 73: Friction Effects on the DSI for an 80km/h Double Lane Change, Handling Setting .....	91
Figure 74: Spring Force Displacement Bulk Modulus Compensation Comparison.....	II
Figure 75: 0.05Hz, 0.025m Amplitude Sinusoidal Displacement input Force Characteristic.....	III
Figure 76: 0.1Hz, 0.025m Amplitude Sinusoidal Displacement input Force-Velocity Characteristics...IV	IV
Figure 77: 0.25Hz, 0.025m Amplitude Sinusoidal Displacement input Force Characteristic.....IV	IV
Figure 78: 0.5Hz, 0.025m Amplitude Sinusoidal Displacement input Force-Velocity Characteristics....V	V
Figure 79: 0.5Hz, 0.025m Amplitude Sinusoidal Displacement input Force Characteristic.....V	V
Figure 80: 1Hz, 0.025m Amplitude Sinusoidal Displacement input Force-Velocity Characteristics.....VI	VI
Figure 81: 0.75Hz, 0.025m Amplitude Sinusoidal Displacement input Force Characteristic.....VI	VI
Figure 82: 1.5Hz, 0.025m Amplitude Sinusoidal Displacement input Force-Velocity Characteristics..VII	VII
Figure 83: 0.25m Amplitude, 0.01Hz Triangular displacement input Force response .....	VIII
Figure 84: 0.25m Amplitude, 0.05Hz Triangular displacement input Force response .....	VIII
Figure 85: 0.25m Amplitude, 0.1Hz Triangular displacement input Force response .....	IX
Figure 86: 0.25m Amplitude, 0.5Hz Triangular displacement input Force response .....	IX
Figure 87: 0.25m Amplitude, 1Hz Triangular displacement input Force response .....	X
Figure 88: 0.25m Amplitude, 2Hz Triangular displacement input Force response .....	X
Figure 89: Double Lane Change Displacement validation 70km/h Soft .....	XII
Figure 90: Double Lane Change Force validation 70km/h Soft.....	XIII
Figure 91: Double Lane Change Displacement validation 80km/h Soft .....	XIII
Figure 92: Double Lane Change Force validation 80km/h Soft.....	XIV
Figure 93: Double Lane Change Displacement validation 70km/h Stiff .....	XIV
Figure 94: Double Lane Change Force validation 70km/h Stiff .....	XV
Figure 95: Double Lane Change Displacement validation 80km/h Stiff .....	XV
Figure 96: Double Lane Change Force validation 80km/h Stiff .....	XVI
Figure 97: Friction Effects for 70km/h Double Lane Change Soft Suspension .....	XVII
Figure 98: Friction effects on 70km/h Double Lane Change Soft Suspension, Left Front Detailed view .....	XVIII
Figure 99: Friction Effects suspension displacements for an 80 km/h Soft Suspension Double Lane Change .....	XVIII
Figure 100: Friction Effects on 80km/h Soft Suspension Double Lane Change, Left Front detailed view .....	XIX
Figure 101: Friction Effects suspension displacements for a 70 km/h Stiff Suspension Double Lane Change .....	XIX
Figure 102: Friction Effects on 70km/h Stiff Suspension Double Lane Change, Left Front detailed view .....	XX
Figure 103: Friction Effects suspension displacements for an 80 km/h Stiff Suspension Double Lane Change .....	XX
Figure 104: Friction Effects on 80km/h Stiff Suspension Double Lane Change, Left Front detailed view .....	XXI

## List of Tables

Table 1: Lane Change Track Dimensions (International Organisation for Standardisation 1975).....	13
Table 2: Fishhook test 2 Times and Steering Angles Garrot, Howe, and Forkenbrock (1999) .....	16
Table 3: Classification Working range and Power Requirements for Suspension Systems .....	19
Table 4: Guidelines for comfort according to Weighted RMS British Standards Institution (1987).....	25
Table 5: Mass and Inertial Properties of Base-Line Vehicle Uys, et al. (2006a).....	36
Table 6: Coefficient descriptions and values used for LuGre Friction Model .....	51
Table 7: Coefficient descriptions and values for Modified LuGre Friction Model .....	52
Table 8: Comparative summary of time to model Friction.....	56
Table 9: Corresponding Time Values for Soft Suspension Spring Displacement Input Signals .....	58
Table 10: Force Correlation Comparison with and without Friction for Gas Models Investigated (Soft Spring Setting).....	61
Table 11: Corresponding Time Values for Stiff Suspension Spring Displacement Input Signals .....	62
Table 12: Force Correlation Comparison with and without Friction for Gas Models Investigated (Stiff Spring Setting).....	65
Table 13: Comparison of simulation times with different friction modelling approaches.....	86
Table 14: Friction Effect Peak Percentage Differences, Suspension Displacements .....	87
Table 15: Friction effect Peak Percentage Differences, Roll Rate and Roll Angle .....	87

## List of Symbols

### Roman Symbols:

$A$	Piston Area [ $m$ ]
$a_y$	Lateral Acceleration of CG [ $m/s^2$ ]
$C$	Constant Depending on Overall Steering Ratio
$F$	Force in Pneumatic Spring [ $N$ ]
$F_{Air}$	Spring Force due to Air Compression [ $N$ ]
$F_C$	Coulomb Friction Force [ $N$ ]
$F_f$	Friction Force [ $N$ ]
$F_N$	Normal Force [ $N$ ]
$F_r$	Friction Force (Modified LuGre Friction Model) [ $N$ ]
$F_{rSS}$	Steady State Friction Force [ $N$ ]
$F_s$	Static Friction Force [ $N$ ]
$F_v$	Viscous Friction Force [ $N$ ]
$F_y$	Lateral Force [ $N$ ]
$F_{yi}$	Lateral Force on Inside wheel in the turn [ $N$ ]
$F_{yo}$	Lateral Force on Outside wheel in the turn [ $N$ ]
$F_{zi}$	Vertical Force on Inside wheel in the turn [ $N$ ]
$F_{zo}$	Vertical Force on Outside wheel in the turn [ $N$ ]
$g$	Gravitational acceleration [ $m/s^2$ ]
$g(v)$	Stribeck Effect Function
$h$	Height of Centre of Gravity [ $m$ ]
$h_{max}$	Dimensionless Maximum Lubrication Film Thickness
$h_r$	Roll Centre Height
$h_{SS}$	Dimensionless Steady State Lubricant Film Thickness
$I$	Vehicle Body Moment of Inertia $kg.m^2$

$k_{\beta f}$	Fluid Column Stiffness due to bulk Modulus [ $N/m$ ]
$K_f$	Proportional Constant
$K_{\phi}$	Roll Stiffness [ $N/degree$ ]
$K_S$	Vertical Spring rate of Left and Right springs [ $N/M$ ]
$M$	Mass of Vehicle [ $kg$ ]
$n$	Exponent for Stribeck Curve
$n_p$	Polytropic Gas Constant
$p_{stat}$	Static Pressure [ $MPa$ ]
$R_{\phi}$	Roll Rate [ $degrees/s$ ]
$s$	Distance between Left and Right Springs [ $m$ ]
$t$	Tread/Track width [ $m$ ]
$v$	Relative velocity between Sliding Surfaces [ $m/s$ ]
$V$	Fluid Volume [ $Liters$ ]
$v_b$	Velocity where Steady State Friction is a minimum [ $m/s$ ]
$v_s$	Stribeck Velocity [ $m/s$ ]
$x$	Hydropneumatic Spring Displacement [ $m$ ]
$x_{Air}$	Displacement due to Air Compressibility [ $m$ ]
$x_{Oil}$	Displacement due to Oil Compressibility [ $m$ ]
$x_{stat}$	Static Displacement [ $m$ ]
$\dot{x}$	Sliding Velocity [ $m/s$ ]
$Z$	Gas Compressibility Factor
$z$	Average Bristle Deflection [ $m$ ]
$z_{ss}$	Steady State Bristle Deflection [ $m$ ]

### Greek Symbols:

$\beta_f$	Bulk Modulus of Fluid [ <i>GPa</i> ]
$\mu$	Friction Coefficient between surfaces
$\sigma$	Material Dependent Stiffness Parameter [ <i>N/m</i> ]
$\sigma_0$	Micro Bristle Stiffness [ <i>N/m</i> ]
$\sigma_1$	Micro Bristle Damping Coefficient [ <i>Ns/m</i> ]
$\sigma_2$	Viscous Fluid Friction Coefficient [ <i>Ns/m</i> ]
$\sigma_v$	Viscous Friction Coefficient [ <i>Ns/m</i> ]
$\tau_h$	Time Constant
$\tau_{h0}$	Dwell Time Constant
$\tau_{hn}$	Deceleration Time Constant
$\tau_{hp}$	Acceleration Time Constant
$\phi$	Roll Angle of Vehicle Body [ <i>degrees</i> ]
$\ddot{\phi}$	Roll Acceleration [ <i>degrees/s<sup>2</sup></i> ]

## Abbreviations

ABS	Anti-Lock Braking System
ADAMS	Automatic Dynamic Analysis of Mechanical Systems
CDC	Continuous Damping Control
CG	Centre of Gravity
DSI	Dynamic Stability Index
GMS	Generalised Maxwell Slip Friction Model
GPS	Global Positioning System
ISO	International Standards Organisation
MR	Magneto Rheological
NHTSA	National Highway Traffic Safety Administration
RMS	Root Mean Square
RRMS	Running Root Mean Square
SSF	Static Stability Factor
SSRT	Steady State Rollover Threshold
SUV	Sports Utility Vehicle
VDC	Vehicle Dynamic Controller
2-D	Two-Dimensional
4S <sub>4</sub>	4 State Semi-Active Suspension System

## 1. Introduction

Sports Utility Vehicles (SUVs) are growing ever more popular among vehicle owners. These vehicles are required to have good rough-, and off-road ride comfort and mobility. The required off-road mobility (high ground clearance), leads to the vehicle having a high centre of mass. Many vehicle owners expect these vehicles to have good on-road handling as well due to a misconception in the vehicle name (focussing on the Sports- part of the name Sports Utility Vehicle). The part of the vehicle most directly affecting the vehicles' ride and handling performance is the suspension system.

The suspension system has two main functions for any vehicle. The first, keeping the vehicle tyres in contact with the road, ensuring transmission of control forces. Control forces being longitudinal and side forces acting on the tyres. The second, keeping the vehicle occupant isolated from vibrations caused by irregular road surfaces.

Good ride comfort is achieved by using soft suspension systems, which translate to large suspension displacements. Good handling characteristics are achieved by using stiff suspension systems. Stiff suspension characteristics translate to high load transfers and small suspension displacements. Achieving good ride and good handling in a passive suspension system is a near impossible task. In most cases the setup is a compromise between ride and handling, the bias for SUV suspensions being toward ride comfort. It is however possible to have a single suspension system that achieves both good ride and good handling. This is achieved through the use of active and semi-active controllable suspension systems.

In many top SUVs the suspension is capable of setting ride height depending on driver input or vehicle speed. Certain vehicles also have the capability of changing the damping rate, through use of Magneto-Rheological and other controllable dampers. Ride height is usually a driver controlled system which can be switched between an on-, or off-road setting. The vehicle defaults to the on-road setting when a certain speed is exceeded. During off-road driving the vehicle body is lifted to ensure good ground clearance, whereas on-road driving requires the vehicle body to be lowered thereby improving the roll-over stability and lowering aerodynamic drag.

The development and control of active and semi-active suspension systems relies heavily on accurately modelling suspension units during simulation. However there are some phenomena that influence the characteristics of suspension systems which are in some cases ignored. It is the aim of this study to investigate the effects of friction (or lack thereof) and gas modelling strategy, specifically in the case of hydro-pneumatic suspension units, on vehicle dynamics, for suspension settings biased toward both ride-comfort and handling, focussing on correlation between forces and displacements in the suspension system, as well as on vehicle dynamic parameters such as the roll-rate and roll-angle.



## 2. Literature Study

The aim of this study is to obtain a better insight to the effects of suspension friction on spring and damper characteristics as well as vehicle dynamics. The dynamic properties of interest in this study are forces, accelerations, velocities, as well as displacements in the vehicle system. The quantification of the vehicle dynamics of interest for this study includes handling as well as roll-over dynamics.

In this section the importance of the study will be highlighted by roll over statistics, which shows that any improvement in the understanding or control of vehicle roll over is invaluable. The mechanism of roll over, test manoeuvres and suspension types will also be discussed. Different friction model implementations are also investigated, to form a solid basis from which to investigate frictional effects on vehicle dynamics.

### 2.1. Roll Over Statistics

According to the Department of Transport (2004), single vehicle roll-overs accounted for 39.42% of all fatalities among fatal vehicle accidents in South-Africa in 2003. Head on collisions only accounted for 20.34% of fatalities when excluding pedestrian accidents. According to the National Highway Traffic Safety Administration (2011) SUVs accounted for 17% of all fatalities on North-American roads. Among SUVs involved in fatal accidents in rural areas of America, 41% experienced roll-over. The vehicle type with the second highest roll-over prevalence was Pickup Trucks, with 34% experiencing roll-over, while passenger cars and mini vans only had 23% experiencing roll-over. Frimberger, et al. (2004), notes that 20% of all fatal accidents in Europe involved vehicle roll-over.

Frimberger, et al. (2004), also notes 34% of all roll-overs are tripped roll-overs, which means the vehicle rolled over after colliding with another object (a sidewalk or kerb). The remaining 66% of roll-overs occurred while vehicles were performing dynamic driving manoeuvres. Vehicles with a high centre of gravity (CG), such as SUVs, are more susceptible to roll over on embanked surfaces, further statistics provided by Frimberger, et al. (2004), suggests that 60% of all roll-overs happen on embanked roads.

The statistics underline the need and importance of understanding, and preventing vehicle roll-over. This is proved by the fact that more people are killed in vehicle roll-over accidents than in head on collisions.

## 2.2. Mechanism of Roll Over

The mechanism of vehicle roll is discussed in this section of the literature survey. A quasi-static 2-D rigid body approximate model of vehicle roll will be discussed, where inertial terms in the roll-plane are neglected. The model considered is for pure un-tripped roll in plane with the vehicle, as seen in Figure 1. The effects of different parameters on the model are discussed in the sub-sections that follow.

### 2.2.1. Spring Stiffness – Effects on Vehicle Roll

According to Gillespie (1992), the distance between suspension springs causes the vehicle to have a roll-resisting moment, or roll stiffness, proportional to the difference in roll angle between the vehicle's body and axle. Figure 1, shows the free body diagram used to derive the roll stiffness equation, as per Gillespie (1992), for a steady state cornering manoeuvre.

$$K_{\phi} = 0.5K_s s^2 \dots \{1\}$$

where:

$K_{\phi}$  = Roll Stiffness of the Suspension System

$K_s$  = Vertical Spring Rate of each of the Left and Right Springs

$s$  = Distance between Left and Right Springs

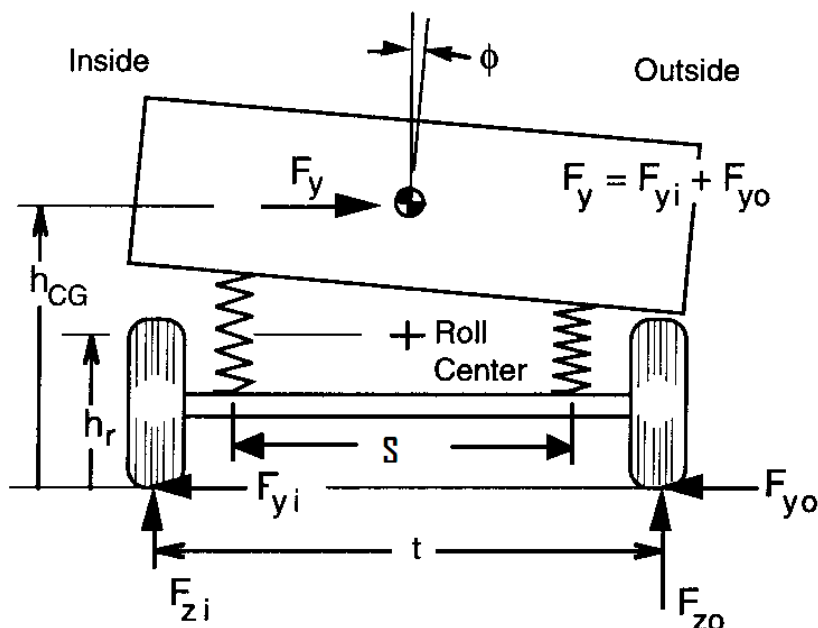


Figure 1: Quasi-Static Roll Model Free Body Diagram Gillespie (1992)

The instantaneous roll centre, also shown above, is an imaginary point at which the lateral forces from the axle are transferred to the vehicle body or vice versa. The roll centre is the instantaneous point about which the vehicle body pivots when a roll-moment is applied. Another description of the roll centre suggests that it is the point at which a lateral force may be applied to the vehicle without causing body roll.

Roll stiffness may be used to quantify load transfer between the inner and outer tyres of a vehicle. Load transfer is established through two mechanisms. Load transfer due to cornering forces on tyres, which is instantaneous. And load transfer due to body roll, caused by the roll dynamics of a vehicle, which usually lags changes in cornering conditions. The difference in vertical load for the inner and outer wheels as found in Gillespie (1992), is given as the following:

$$F_{z_o} - F_{z_i} = 2F_y \frac{h_r}{t} + 2K_\phi \frac{\phi}{t} \dots \{2\}$$

where:

$F_{z_o}$  = Load on Outside wheel in the turn

$F_{z_i}$  = Load on Inside wheel in the turn

$F_y$  = Lateral Force

$h_r$  = Roll Centre Height

$t$  = Tread (track width)

$K_\phi$  = Roll Stiffness of the suspension

$\phi$  = Roll angle of the vehicle body

Even though the load transfer equation derived is for steady state cornering, it does shed light on certain aspects of vehicle roll-over. The first observation is obvious, the higher the load transfer between the wheels, the closer the inside wheel is to lifting and thus the vehicle is to rollover (when ignoring the possibility of vehicle sliding). When minimising load transfer the only parameter dependent on the spring stiffness is roll stiffness and thus roll angle. According to Equation 1, increased roll stiffness results in a lower roll angle, whereas decreased roll stiffness results in an increased roll angle when applying the same roll moment to the vehicle. This creates a trade-off where roll stiffness must be chosen to minimise the second term on the right hand side of Equation 2, minimising the load transfer effect of body roll. This is especially true for vehicles with high Centres of Gravity, where the CG shows large a lateral motion for a supplied roll angle.

If we take vehicle sliding into account, load transfer between the inner and outer wheels becomes vitally important. According to Mitchell (2012), the side force generated by the tyres is a maximum when they experience equal vertical loads as shown in Figure 2. Load transfer from the inner to the outer wheels of a vehicle, causes vehicle tyres to generate smaller than maximum lateral forces than could be achieved without load transfer. Load transfer thus brings tyres closer to the saturation limit where sliding occurs.

**Tire Grip with load transfer: 500 lbs transfer, total grip 1651**

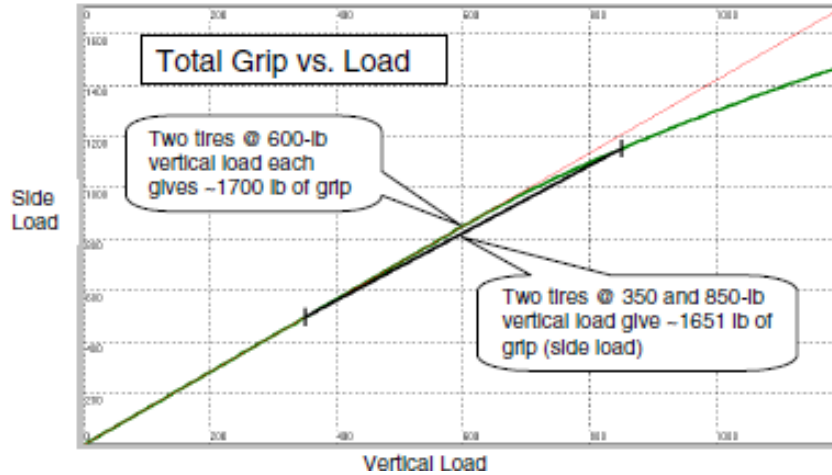


Figure 2: Load transfer effect on tyre Side Force Mitchell (2012)

### 2.2.2. Centre of Gravity Position – Effects on Vehicle Roll

The effect of Centre of Gravity height on vehicle roll-over and lateral stability is easily investigated and explained using a quasi-static vehicle model with rigid suspension (Meaning there is no motion between the vehicle wheels and the vehicle body). Lateral and vertical forces applied to a vehicle during steady state cornering is given in, Figure 3.

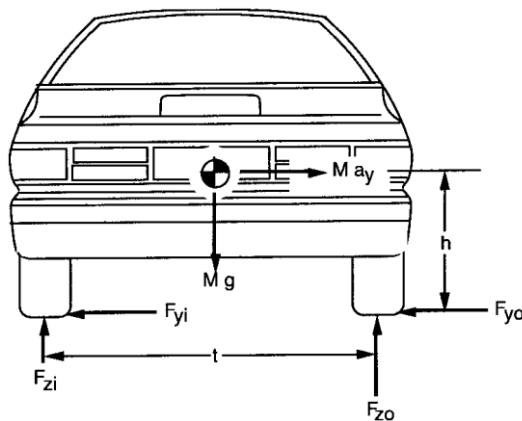


Figure 3: Forces acting to produce Roll-Over on a rigidly suspended vehicle, Gillespie (1992)

Applying Newton’s second law to Figure 3, for the lateral and vertical directions yields the following equations.

Lateral Direction:

$$\sum F_y = F_{yi} + F_{yo} = Ma_y \dots \{3\}$$

Vertical Direction:

$$\sum F_z = F_{zi} + F_{zo} = Mg \dots \{4\}$$

where:

- $F_{yi}$  – Lateral Tyre Force on Inside Wheel  
 $F_{yo}$  – Lateral Tyre Force on Outside Wheel  
 $a_y$  – Lateral Acceleration of CG  
 $F_{zi}$  – Vertical Force on Inside Wheel  
 $F_{zo}$  – Vertical Force on Outside Wheel  
 $M$  – Mass of Vehicle  
 $g$  – Gravitational Acceleration

Taking moments about the contact patch centre of the outside wheel (Gillespie 1992), for a vehicle on a level road on the verge of roll-over ( $F_{zi} = 0$ ), yields the following moment balance equation:

$$\sum M_o = 0$$

$$Mg \left( \frac{t}{2} \right) - Ma_y h = 0$$

which when re-written and simplified yields the quasi-static roll limit as:

$$\left( \frac{a_y}{g} \right)_{roll} = \frac{t}{2h} \dots \{5\}$$

where:

- $t$  – Trackwidth  
 $h$  – Height of Centre of Gravity.

The lateral acceleration where the inside wheel experiences zero vertical force, is the rollover threshold (the quasi-static roll limit is commonly known as the Static Stability Factor, or SSF). It is also desirable to quantify the lateral stability limit for the case where the vehicle slides. Assuming all wheels remain in contact with the road surface; this yields the following relations between vertical and lateral tyre forces.

$$F_{yi} = \mu F_{zi}$$

$$F_{yo} = \mu F_{zo}$$

where:

- $\mu$  – Friction Coefficient between Tyre and Road Surface.

Using the above relations with equations 3 and 4, the following is obtained:

$$Ma_y = \mu Mg$$

which when simplified yields the quasi-static lateral stability (Sliding) limit as:

$$\left( \frac{a_y}{g} \right)_{sliding} = \mu \dots \{6\}$$

From a safety perspective it is desirable to reach the sliding limit before the roll-over limit. This implies that if,  $\left(\frac{a_y}{g}\right)_{sliding} < \left(\frac{a_y}{g}\right)_{roll}$ , i.e.  $\mu < \frac{t}{2h}$ , a vehicle will slide before it rolls-over.

Thus it is clear that lowering the Centre of Gravity height will decrease the roll-over propensity of a vehicle. Ignoring suspension compliance, as done in this analysis, overestimates the roll-over threshold (Gillespie, 1992).

The Steady State Rollover Threshold (SSRT) is considered the maximum value of lateral acceleration a vehicle may resist during steady state driving while not rolling over (Dahlberg, 2002). Dahlberg (2002) notes the SSF as a first order approximation to the SSRT, and as the least conservative estimation of rollover stability.

Considering quasi-static roll-over of a suspended vehicle the lateral forces between the axles and the vehicle body are transmitted through the roll centre. In Figure 4 the roll reactions are shown for a suspended vehicle.

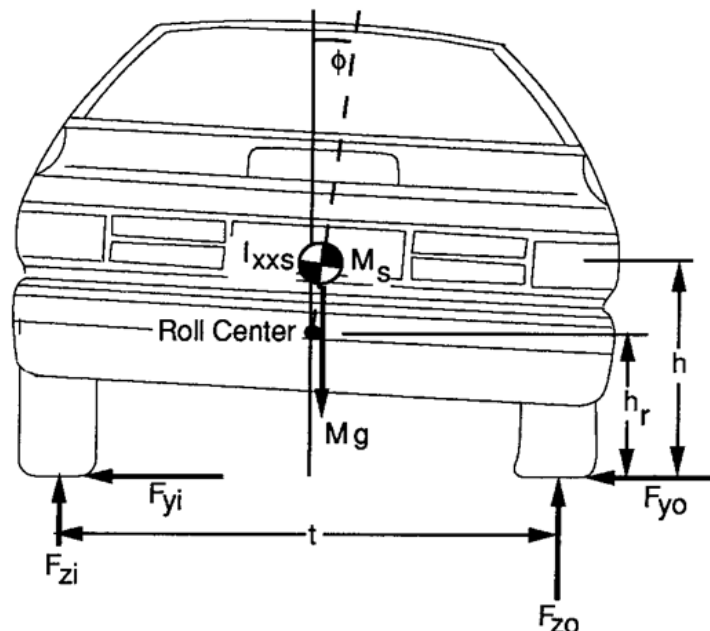


Figure 4: Forces acting to produce Roll-Over on a suspended Vehicle Gillespie (1992)

The moment balance at the verge of roll-over is again taken about the outside wheel contact patch centre, which yields the following as per Gillespie (1992):

$$\sum M_o = 0;$$

$$Mg \left[ \left(\frac{t}{2}\right) - \sin \phi (h - h_r) \right] - Ma_y [h - (h - h_r)(1 - \cos \phi)] = 0$$

where:

$\phi$  – Roll angle

$h_r$  – Roll Centre Height.

Making the small angle assumption, ( $\sin \phi \approx \phi$ , and  $\cos \phi \approx 1$ ) and defining the roll rate as  $R_\phi = \frac{\phi}{a_y} \left[ \frac{\text{Radians}}{g} \right]$  (Roll rate is defined as the rate of change of the roll angle with respect to lateral acceleration, i.e.  $R_\phi = \frac{d\phi}{da_y}$ ), we may re-write the equation above as follows:

$$Mg \left[ \left( \frac{t}{2} \right) - R_\phi \left( \frac{a_y}{g} \right) (h - h_r) \right] - Ma_y h = 0$$

this simplifies to the following:

$$g \left( \frac{t}{2} \right) - a_y R_\phi (h - h_r) - a_y h = 0$$

rewriting it as follows:

$$\left( \frac{a_y}{g} \right)_{Roll} = \left( \frac{t}{2h} \right) \left( \frac{1}{1 + R_\phi \left( 1 - \frac{h_r}{h} \right)} \right) \dots \{7\}$$

Comparing equation 7, to equation 5, shows a factor  $\left( \frac{1}{1 + R_\phi \left( 1 - \frac{h_r}{h} \right)} \right)$  decrease in SSF compared to a rigidly suspended vehicle. The criterion of sliding before rolling thus becomes,  $\mu < \left( \frac{t}{2h} \right) \left( \frac{1}{1 + R_\phi \left( 1 - \frac{h_r}{h} \right)} \right)$ . Gillespie (1992) notes decrease in SSF for a typical passenger vehicle due to suspension compliance is approximately 5 percent.

The relation of roll-centre height and CG height determines lateral shift in CG when the vehicle body rolls. The larger the difference between roll-centre and the CG, the more lateral shift in CG affects the SSF. Vehicles with independent suspension systems mostly suffer more from this phenomenon than vehicles with solid axles. This is due to the high roll centre height and reduced distance from roll centre to CG of solid axle vehicles (Gillespie, 1992). If the roll centre is above the CG, the vehicle experiences inward roll (rolling into the turn), which is not a common occurrence in passenger vehicles.

A similar shift in CG lateral position is caused by lateral tyre deflection, this results in reduced track-width that further reduces the roll-over threshold. Analysing this phenomenon requires a detailed model of the tyres and suspension system of the vehicle which will not be discussed here.

Figure 5 shows the effect of lowering the CG on the roll-over propensity of a vehicle as investigated by Whitehead, et al. (2004), for the case where two wheel lift is experienced during a fishhook test (the fishhook test is discussed in more detail in section 2.3.2.2).

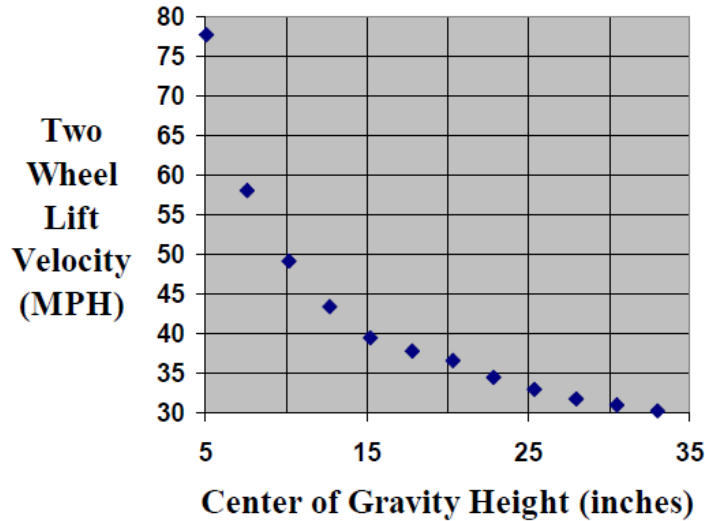


Figure 5: Effect of CG height on Rollover Propensity Whitehead, et al. (2004)

The longitudinal CG position of a vehicle also affects the roll-over propensity, although it is not as obvious as the effect of the CG height. Front to rear weight distribution of a vehicle affects the under-, over-steer characteristics. Steering characteristics of a vehicle affect roll-over propensity. The steering characteristics directly influence lateral acceleration and roll mechanisms. Whitehead, et al. (2004) showed the effects of weight distribution on roll-over propensity through simulation. The results are shown in Figure 6, where the percentage of vehicle weight on the front axle is changed for a fishhook test manoeuvre. Grau (2002), noted the longitudinal CG position to have the greatest effect on lateral vehicle dynamics among all parameters studied in his investigation.

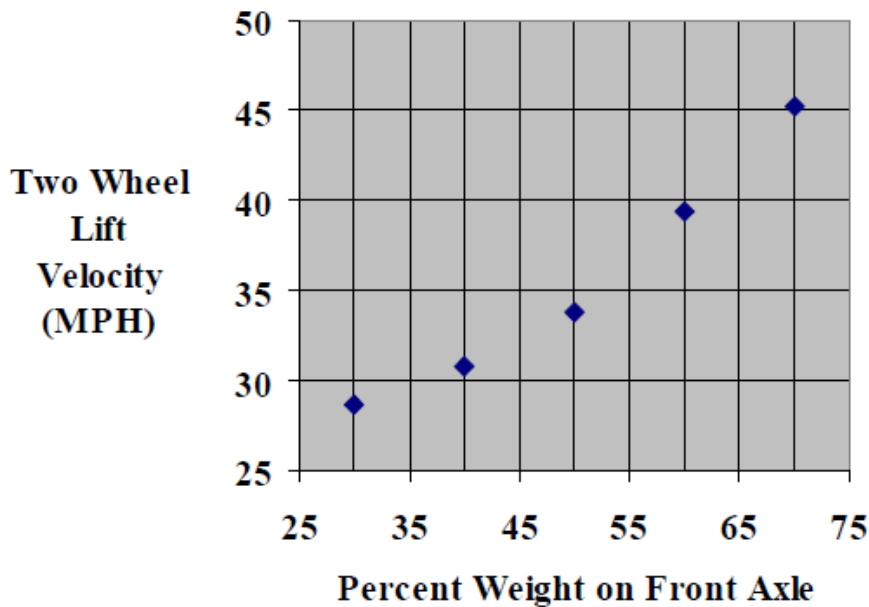


Figure 6: Effects of longitudinal CG position on vehicle roll-over propensity Whitehead, et al. (2004)



### 2.2.3. Damping Rate and Transient Effects on Vehicle Roll

Transient effects cannot be ignored when considering vehicle rollover. Transient effects are due to roll velocities and accelerations which may or may not be beneficial to the roll over stability of a vehicle. The Dynamic Stability Index (DSI) approximates the dynamic roll over threshold of a vehicle, which takes roll energy into account through use of roll acceleration. The DSI is defined by Dukkipati, et al. (2008) as the following:

$$DSI = \frac{a_y}{g} + \frac{I\ddot{\phi}}{mgh} \dots \{8\}$$

where:

$I$  – Moment of Inertia of Vehicle Body.

The DSI gives a closer view of rollover during dynamic testing. If the DSI is larger than the Static Stability Factor, the vehicle will roll-over.

Dampers affect the roll characteristics of a vehicle. Damping increases a vehicles roll over threshold up to one third when going from zero to 50 percent of critical damping. The damping effect on rollover threshold for automobiles, SUVs and trucks are shown in the figure below as per Gillespie (1992).

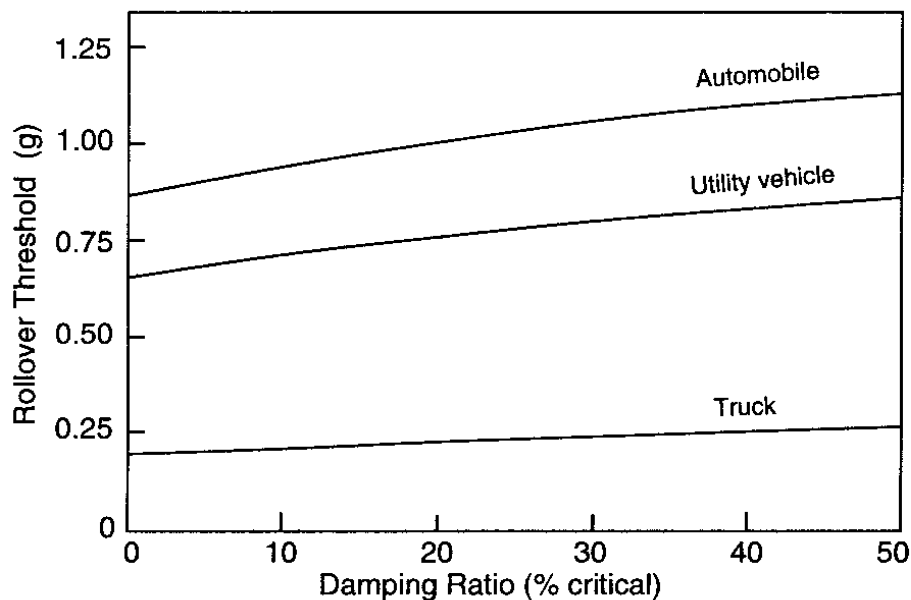


Figure 7: Damping effect on Rollover Threshold Gillespie (1992)

Benefits of roll damping are evident from the figure above. Transient effects during lateral acceleration and cornering manoeuvres may cause a vehicle to rollover before the quasi-static rollover limit is reached. This is due to roll velocity causing the roll angle to overshoot past the equilibrium point for the lateral force applied. The increased roll over threshold with increased damping agrees with the DSI as defined previously. Increased roll damping

lowers peak levels of roll acceleration, thereby decreasing the DSI compared to the SSF, increasing the dynamic roll over threshold. Damping does not affect the steady state or final value, but does dictate the time to reach the steady state as well as the amount of overshoot.

According to Gillespie (1992), an automobile or SUV, subjected to a transient step steer manoeuvre results in a reduction of about 10 percent in rollover threshold of the quasi-static suspended vehicle model. Effects of roll-damping is evident in Figure 7, roll-damping has the greatest effect on overshoot during transient manoeuvres. Frimberger, et al. (2004) notes the effect of increased spring and damper rates on vehicle roll rate, where increased spring and damper rates reduce the vehicle roll rate, while lower spring and damper rates increase the vehicle roll rate.

Roll-resonance affects the rollover threshold of vehicles. Roll-resonant frequencies of passenger vehicles and SUVs are in the order of 1.5Hz, which requires a rapid oscillatory steering input from the driver, and in most cases steering input amplitudes at these frequencies are low. The result from these inputs only creates minor deviations in lateral vehicle position due to attenuation of yaw response at these frequencies, therefore not greatly exciting roll mechanisms. The conclusion is thus that roll resonance is of less significance to rollover in SUVs and passenger vehicles than in large trucks. Lane change and slalom courses, with much slower oscillations do however elicit vehicle responses close to the quasi static behaviour, Gillespie (1992).

## **2.3. National Highway Traffic Safety Administration Vehicle Testing Manoeuvres**

The National Highway Traffic Safety Administration (NHTSA) devised a series of test manoeuvres to quantify the fundamental handling as well as the un-tripped on-road rollover characteristics of road vehicles. The manoeuvres are classified into two classes, vehicle characterisation and un-tripped roll over propensity manoeuvres. The two classes of test manoeuvres are discussed in this section.

### **2.3.1. Vehicle characterisation-, Handling- and Miss-Use Manoeuvres**

Vehicle characterisation manoeuvres are used to characterise the general dynamic properties of a test vehicle. These tests include the following manoeuvres, Pulse Steer, Sinusoidal Sweep, Slowly Increasing Steer, and Slowly Increasing Speed manoeuvres. Vehicle characterisation manoeuvres mostly do not cause a two-wheel lift, or rollover conditions in the vehicle.

Manoeuvres such as the ISO 3888 Double Lane Change, are referred to as handling or miss-use manoeuvres. These manoeuvres do not specifically test roll over propensity but rather the general dynamic handling behaviour of a vehicle. The reason the ISO 3888 Double Lane Change is classified as a handling manoeuvre is that the test is only valid if a clean run is obtained. The manoeuvre consists of a large number of steering inputs, 4 major and, depending on the driver, a number of smaller correction steer inputs. A test run is classified as clean if none of the cones demarcating the route are knocked over. Howe, et al. (2001), noted that in most of the cases tested by the NHTSA, two wheel tip-up, or roll over scenarios were only reached at speeds higher than the highest clean run speeds of the test vehicles. In these cases the vehicle had already lost directional stability (i.e. experienced major over- or under-steer). The ISO 3888 Double Lane Change manoeuvre is very driver dependent, the driver must traverse a specified route which brings driver style, steering input variability, driver anticipation and reaction into the test. The ISO 3888 Double Lane Change is essentially a test of the vehicles road holding ability. The track layout and dimensions for the ISO 3888 Severe Double Lane Change are given in Figure 8 and Table 1 respectively.

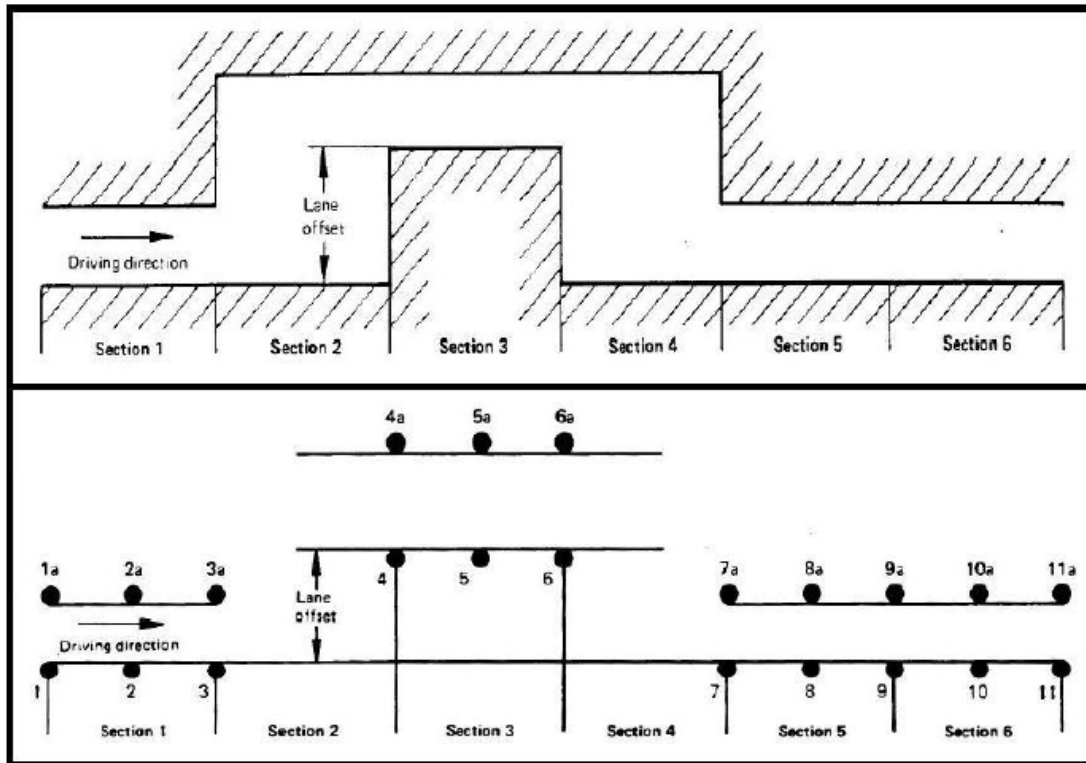


Figure 8: ISO 3888 Double Lane Change Track and Cone Placement International Organisation for Standardisation (1975)

Table 1: Lane Change Track Dimensions (International Organisation for Standardisation 1975)

Section	Width	Length
1	1.1 x Vehicle Width + 0.25m	15m
2	Not Applicable	30m
3	1.2 x Vehicle Width + 0.25m	25m
4	Not Applicable	25m
5	1.3 x Vehicle Width + 0.25m	15m
6	1.3 x Vehicle Width + 0.25m	15m
<b>Lane Offset</b>	3.5m	

The ISO 3888 standard requires the test to comply with the following:

- The lane change track must be marked by cones as shown in the figure above
- The track limit must be tangential to the base circle of the cone as shown in the figure above
- The measuring distance starts at the beginning of section 1 and ends at the end of section 5
- The lane change must be done by a skilled driver
- A passage is faultless when none of the cones positioned as specified have been displaced (International Organisation for Standardisation 1975)

## 2.3.2. Roll over Propensity Testing Manoeuvres

Test manoeuvres for investigating roll over propensity of vehicles, as investigated by the NHTSA are discussed in this section. These manoeuvres are designed to induce large lateral accelerations and load transfers on vehicles, testing their dynamic un-tripped roll over propensity. The tests under consideration are the J-turn and Fishhook Test, with and without pulse braking, Howe, et al. (2001). In contrast to the ISO 3888 Double Lane Change, these tests are open loop, where the steering input is not controlled by a driver (the driver closes the control loop), but by a steering robot, which gives these tests excellent repeatability.

### 2.3.2.1. J-Turn Manoeuvre

The J-turn manoeuvre requires only one major steering input in one direction from the steer robot, up to a pre-determined steering angle. The steer input is shown as a function of time in the following figure. This test models what could happen if a driver initiates a severe turn, Garrot, Howe, and Forkenbrock (1999).



Figure 9: J-Turn Manoeuvre Steering wheel input, Howe, et al. (2001)

This test requires the vehicle to be driven in a straight line up to the desired speed. The steering input is through a programmable steering machine. Starting at 0.0, the programmable steering robot turns the steering wheel in 0.33 seconds from zero to a maximum of 330 degrees at 1000 degrees per second. The steering wheel is held at this maximum steer position for the remaining 4.67 seconds of the test. Once the steering input is supplied the driver releases the throttle, not trying to keep the vehicle speed constant throughout the test.

The NHTSA tests were conducted at speeds ranging from 57.93km/h (36 mph) to 96.56km/h (60 mph), in approximately 3.21km/h (2mph) increments, unless a termination event occurred (Garrot, Howe, and Forkenbrock 1999).

The J-turn with pulse braking is performed in the same way as the J-turn. The difference is a pulse applied to the brake approximately 1 second after the steering wheel reaches the

maximum steering angle. This manoeuvre simulates what happens if a driver brakes sharply after entering a severe turn.

The severity of the J-Turn test is governed by the vehicle initial or entry speed into the manoeuvre, the test should be conducted in a series of left and right turns (Garrot, Howe, and Forkenbrock 1999).

Termination is an event that renders the test un-safe or causes damage to the test vehicle or test surface, it could also be due to excessive over- or under-steer, which prevents the vehicle performing manoeuvre in the desired manner. The termination parameter of interest for this study is a major two wheel lift off. Major two wheel lift-off is defined as two wheels losing contact with the road surface for a clearly discernable amount of time during a test run.

### 2.3.2.2. *Fishhook-Test Manoeuvre*

The NHTSA considered two variations of the fishhook test during their investigation on roll over propensity, where steering angles for fishhook test 1 are determined by the roll-resonant frequency and steering for fishhook test 2 by the steering ratio of the vehicle. The steer rates of the tests are 750 and 500 degrees per second for Fishhook test 1 and Fishhook test 2 respectively. This is clearly seen in Figure 10 which shows a comparison of the steering wheel angle as a function of time for the two tests. Tests end at 8 seconds, the steering inputs after 8 seconds should be ignored, and these are inputs from the test driver regaining control of the vehicle.

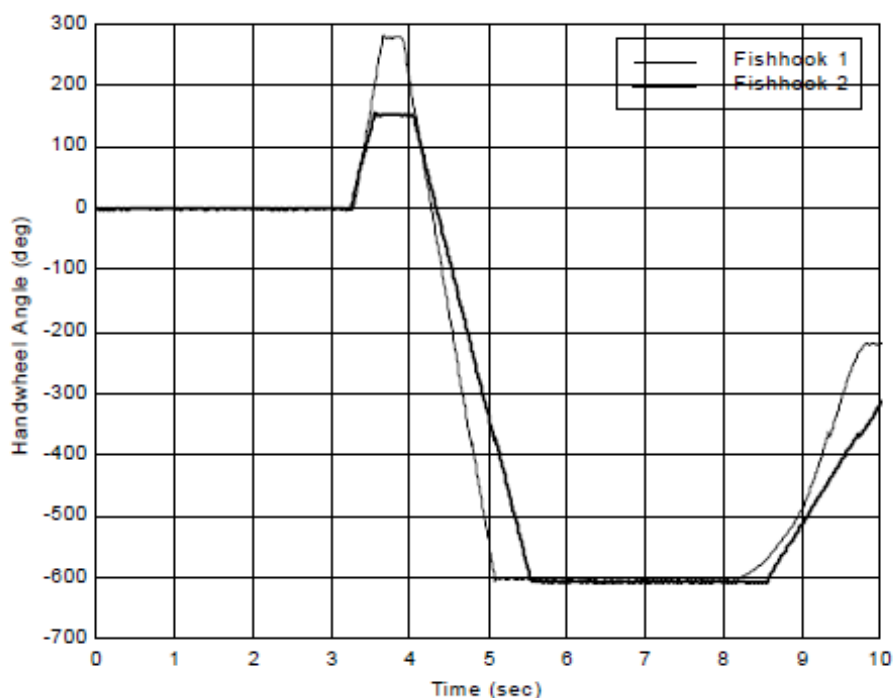


Figure 10: Comparison of Fishhook test 1 and 2 Garrot, Howe, and Forkenbrock (1999)

The aim of the Fishhook test is to induce two wheel tip-up at lower lateral accelerations than the J-turn. In this study we will focus on Fishhook test 2, as the roll-resonant frequency parameter is not as easily attainable as the overall steering ratio of the test vehicle. Fishhook test 2 approximates a drivers' steering response to the recovery of a two-wheel off the road situation, Garrot, Howe, and Forkenbrock (1999).

The steering angles and times to be programmed into the steering robot for Fishhook test 2, is summarised in the following table. The steering rate for Fishhook test 2 is defined as 500 degrees per second for all steering inputs. For the sake of argument the value for C is taken as 250 for the values in Table 2 the corresponding values are shown on Figure 11 for clarity,

Table 2: Fishhook test 2 Times and Steering Angles Garrot, Howe, and Forkenbrock (1999)

Time [s]	Steering Wheel Angle [deg]
0	0
$C/500 = \frac{250}{500} = 0.5$	$-C = -250$
$C/500 + 0.5 = \frac{250}{500} + 0.5 = 1$	$-C = -250$
$2C/500 + 0.5 = \frac{500}{500} + 0.5 = 1.5$	0
$2C/500 + 1.7 = \frac{500}{500} + 1.7 = 2.7$	600
5.0 (End of Test)	600

where:

$$C = 7.5 \times \text{Overall Steering Ratio}$$

The steering input as a function of time for Fishhook test 2 is given in Figure 11.

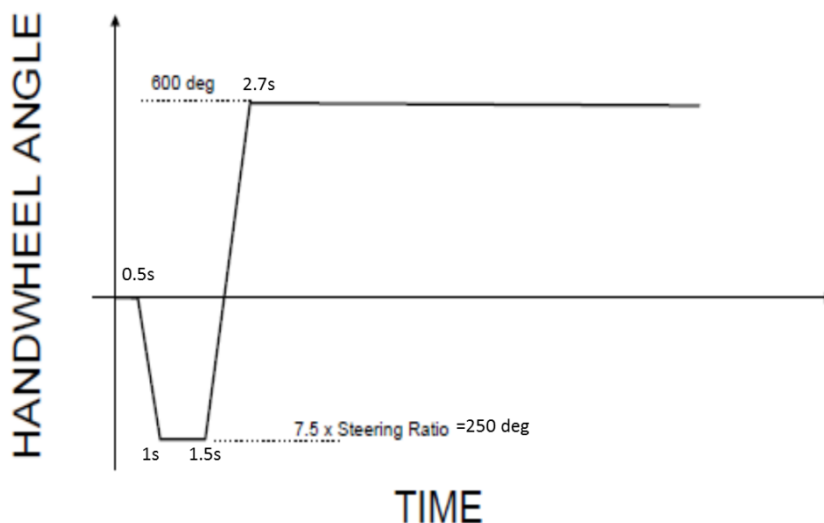


Figure 11: Fishhook test 2 Steering wheel angle as a function of Time, Garrot, Howe, and Forkenbrock (1999)

As with the J-Turn test, the driver releases the throttle when starting the manoeuvre. The entry speed of the manoeuvre again governs the test severity. The Fishhook test manoeuvres as tested by the NHTSA were conducted at speeds from 54.717km/h (34mph) to 80.467km/h (50mph), in approximately 3.21km/h (2mph) increments, unless a termination condition occurred, Garrot, Howe, and Forkenbrock (1999). (Termination conditions are the same as for the J-Turn test)

## 2.4. Active and Semi-Active Suspension Systems

Suspension systems found in most road vehicles are classified as passive systems, meaning suspension characteristics are fixed throughout the useful life of suspension components. Passive suspension systems are in all cases a trade-off between ride and handling characteristics, Els, et al. (2007). Suspension systems, where spring or damper characteristics are changeable using rudimentary tools, also fall under passive suspension systems. In recent times active and semi active suspension systems have become more practical and popular due to the development of microprocessors and actuator technology. The definitions, working and application of active and semi active suspension systems are discussed in this section.

The compromise between Ride and Handling of a vehicle can be seen in Figure 12. The solid lines indicate the spring stiffness characteristics, while the dashed lines indicate the damping rate for specific springs and dampers. Increases along these lines as indicated show the effects on ride comfort and vehicle safety in terms of the dynamic wheel loads. These would indicate that an increase in safety would require a decrease in vehicle ride comfort and vice versa. A passive suspension system only resembles a single point on the graph, typical areas for sports and passenger cars are also shown. The active suspension goal area is indicated by the shaded area, where you can have both good ride and safety characteristics.

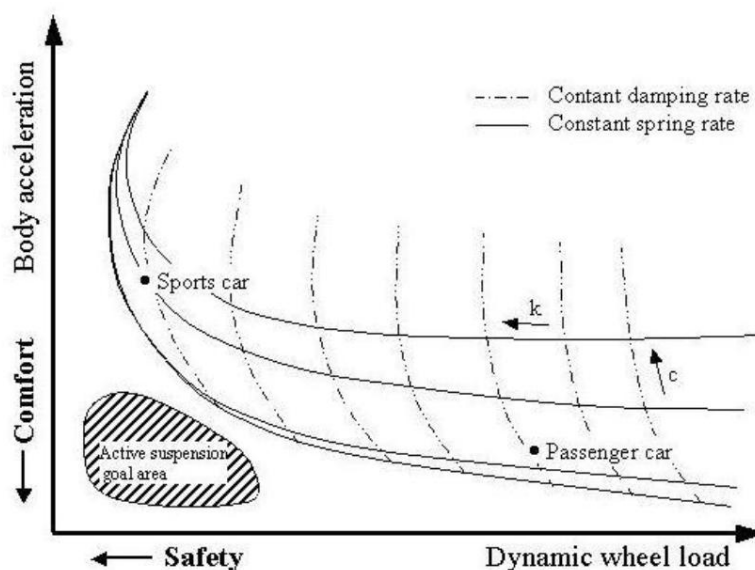


Figure 12: Suspension Design Space Holdmann and Holle (1999)



### 2.4.1. Active Suspension Systems

An active control system is one in which an external power source, powers control actuators that apply forces to a structure in a prescribed manner, Bergman, et al. (1997). This general description of an active control system is also valid for an active vehicle suspension system. Active vehicle suspension systems have the capability of applying forces in a prescribed manner to add, or dissipate energy in the system.

Active suspension systems in many cases use hydraulic, hydro pneumatic and pneumatic actuators (Fischer and Isermann, 2004). These systems have the attractive property of adapting to driving conditions by actuator control and thus influencing various parameters in the suspension system, improving handling, safety as well as the ride perception. Fischer and Isermann (2004) note improvements of more than 30% in ride perception, and 25% in handling capabilities for a vehicle with an active suspension when compared to the same vehicle using a passive suspension system. The power requirements for active suspension systems are quite large when considering the pumps, compressors and actuator requirements. A comparison of power requirements and working ranges for different classifications of suspension systems is shown in Table 3.

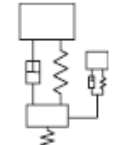
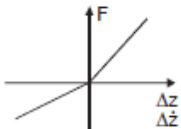
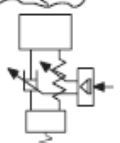
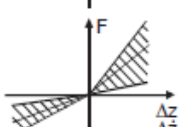
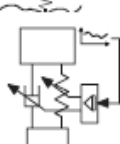
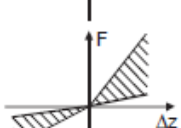
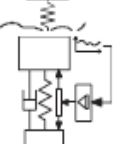
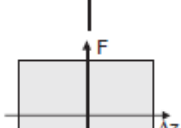
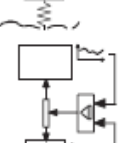
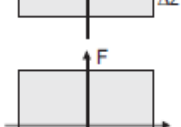
There are many variations in active suspension systems as well as their implementation. One such system is the Mercedes Benz Active Body Control, using a hydraulic actuator in series with a steel spring to control vehicle body attitude.

It is difficult in the conventional sense, to think of controllable dampers. Conventional passive dampers have fixed damping rates and may be tuned to have certain characteristics through pressure dependent valves and intensive design. The characteristics of these dampers do not change significantly during their useful life. Variable-orifice and variable friction dampers are two forms of controllable dampers (Bergman, et al. 1997). Variable-orifice dampers use variable orifice valves, the change in the damping rate is thus dependent on valve reaction time.

Magneto Rheological (MR) Dampers are another type of controllable damper. They are controlled to have a specific damping rate by applying a certain electric or magnetic field to the damper. The reaction of these damper units is in the millisecond range (Bergman, et al. 1997). MR-fluids consist of micron sized magnetically polarizable particles dispersed in a carrier medium such as mineral oil. When a magnetic field is applied to the fluid, particle chains form which increases the viscosity of the fluid. The change in viscosity changes the damping rate without mechanical changes to the damper orifice. MR- and Variable-orifice valve dampers can be controlled continuously, achieving Continuous Damping Control (CDC).

**Table 3: Classification Working range and Power Requirements for Suspension Systems**

 Classification of suspension systems. Natural frequencies:  $f_B$  body and  $f_W$  wheel

System	System representation	Force range	Operation range	Actuator/sensor demand	Max. energy demand	Improvements compared to passive system	
						Comfort	Safety
Passive			—	—	—	—	—
Slowly variable/adaptive			$< f_B$	$4-8/\geq 1$	ca. 50 W	15–20%	10–25%
Semi-active			$f_B - f_W$	$4-8/\geq 8$	ca. 50 W	20–30%	10–25%
Active partially loaded			$0 - f_B$	$4-8/\geq 12$	1–2 kW	> 30%	—
Active fully loaded			$0 - f_W$	$4/\geq 12$	1.5–7 kW	> 30%	25%

## 2.4.2. Semi-Active Suspension Systems

Semi-Active Control systems are a class of active control systems for which external energy requirements are orders of magnitude smaller than fully active control systems. Typically semi-active control devices do not add mechanical energy to the structural system, and are often viewed as controllable passive devices (Bergman, et al. 1997). This is a description of a general semi-active system but is also valid for a vehicle suspension system.

Semi-Active suspension systems may be classed in two discrete groups, Semi-Active Discrete, and Semi-Active Continuous. Semi-Active Discrete systems work on the principle of switching between discrete states for springs and or dampers. One such a system is the 4-State Semi-Active Suspension System (4S<sub>4</sub>), developed by the University of Pretoria, Els (2006), and is described in the section 2.4.2.1. Most Semi-Active Discrete systems work on the same principle as will be described there.

Semi-Active Continuous suspension systems can change suspension characteristics continuously, thus not by switching between different states. This is achieved by Variable Orifice Valves or by MR-Dampers to control the damping rate of the system. Semi-Active springs are mostly based on either Air or Hydro-Pneumatic springs which are non-linear due to their working principles. There are also some cases where air springs are used in combination with coil springs. Most of these systems as reviewed by Els (2006), make use of two or more accumulators with different volumes to achieve different spring rates or continuously variable volume gas accumulators.

The non-linear nature of hydro-pneumatic suspension units is clear in Figure 13, which compares the spring rates of different types of springs, at different loads. There are notable differences between the hydro-pneumatic, pneumatic and mechanical springs. The gas pressure in both hydro-pneumatic and pneumatic springs increases with load, however, the volume of gas in the hydro-pneumatic unit decreases with load, while the pneumatic spring unit has a constant gas volume (Bauer, 2011).

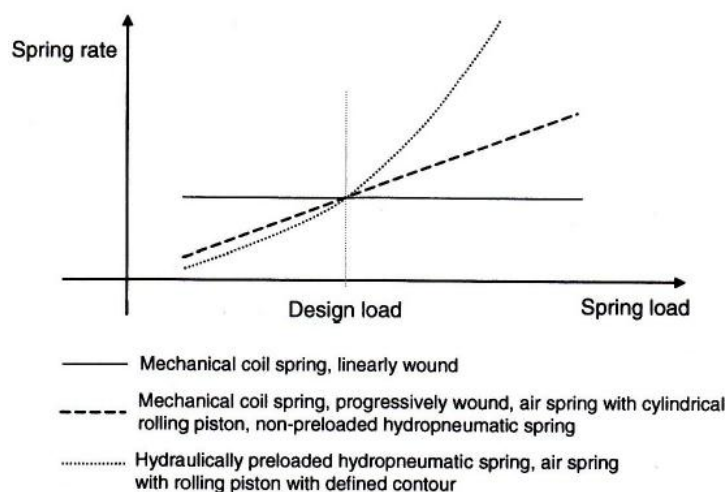


Figure 13: Spring Rate as a function of load for Mechanical, Pneumatic and Hydro-Pneumatic Suspensions, Bauer (2011)

It is clear from Figure 13 that any deviation in design load will affect the spring rate of the suspension. It therefore also affects the natural frequency of the vehicle. The change in natural frequency may adversely affect ride and handling dynamics. The natural frequency for level controlled, pre-loaded pneumatic and hydro-pneumatic suspension systems are less-affected by changes in spring load as seen Figure 14, Bauer (2011).

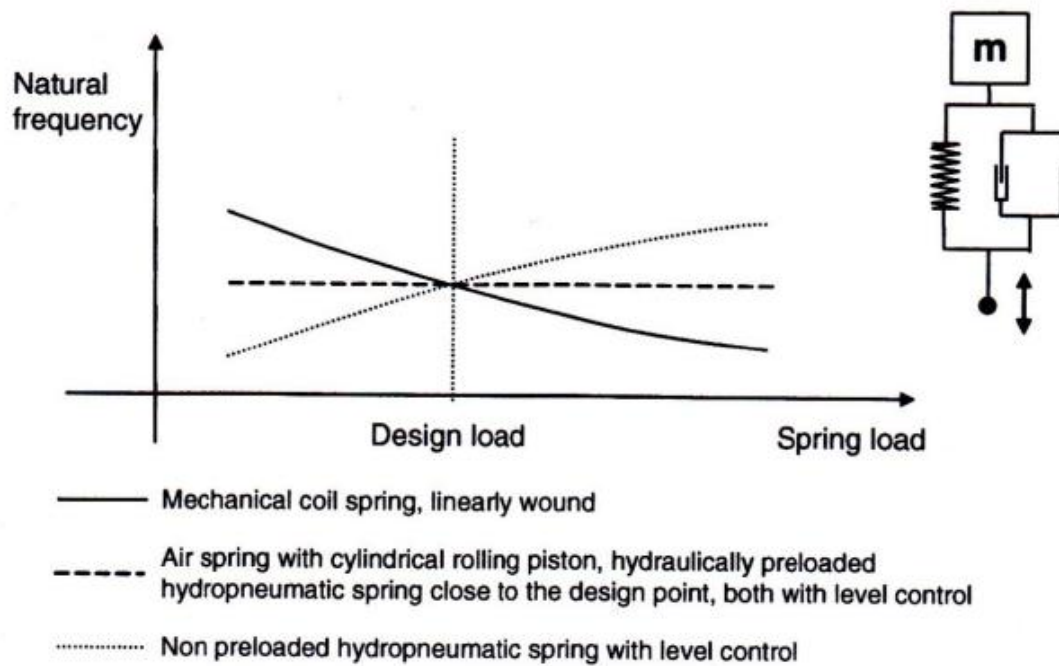


Figure 14: Natural Frequency as a function of spring load for Mechanical, Pneumatic and Hydro-Pneumatic Suspension units, Bauer (2011)

In a survey of commercially available hydro-pneumatic spring systems, Els (1993) identified the working range of hydro-pneumatic springs to be from 2 to 90 MPa. The large operational pressure range may cause discrepancies in the modelling methodology followed, depending on the specific system and application.

#### 2.4.2.1. Four State Semi-Active Suspension System (4S<sub>4</sub>)

A Four State Semi-Active Suspension System (4S<sub>4</sub>), was developed by the University of Pretoria, Els (2006), and is fitted to the test vehicle for this study. The system is based on two switchable hydro-pneumatic spring- and two switchable damper states. The spring states are hard and soft while the damper states are high and low. The oil volume in the suspension struts are controlled using an oil pump, which adds or removes oil from each strut independently to achieve vehicle levelling during the gas charging process. Spring and damper state switching is achieved using solenoid valves. The two spring states are achieved by having gas accumulators of different volumes. The damping states are achieved by valve controlled damper bypass channels. A schematic layout of the system is given in Figure 15.

The gas accumulators, accumulator 1 and 2, have nominal volumes of 0.1 and 0.4 litres respectively, and are filled with Nitrogen. The rest of the system is filled AeroShell 41

hydraulic fluid. The spring setting is controlled by opening or closing valve 3 to achieve soft and stiff spring settings respectively. Damping rates are controlled by opening or closing valves 1 and 2, where high damping is achieved when the valves are closed.

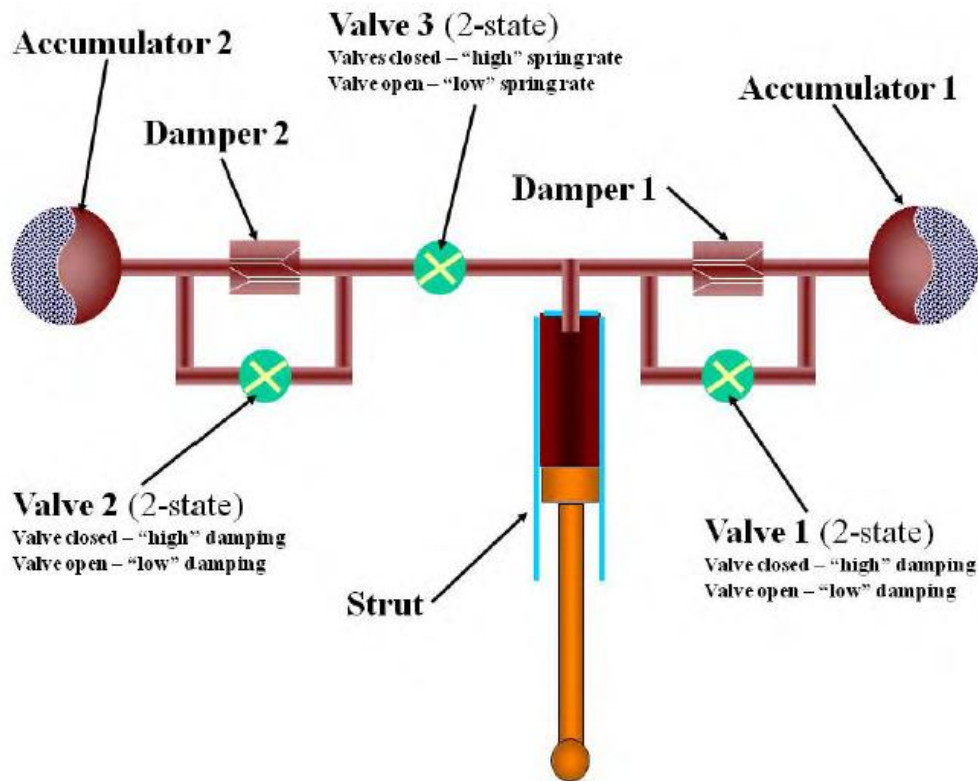


Figure 15: Circuit Diagram of the 4S<sub>4</sub> Els (2006)

Springing is achieved through gas compression, thus the spring rate is nonlinear. The spring force - displacement, and damping force - velocity characteristics for the system are shown in Figure 16 and Figure 17 respectively.

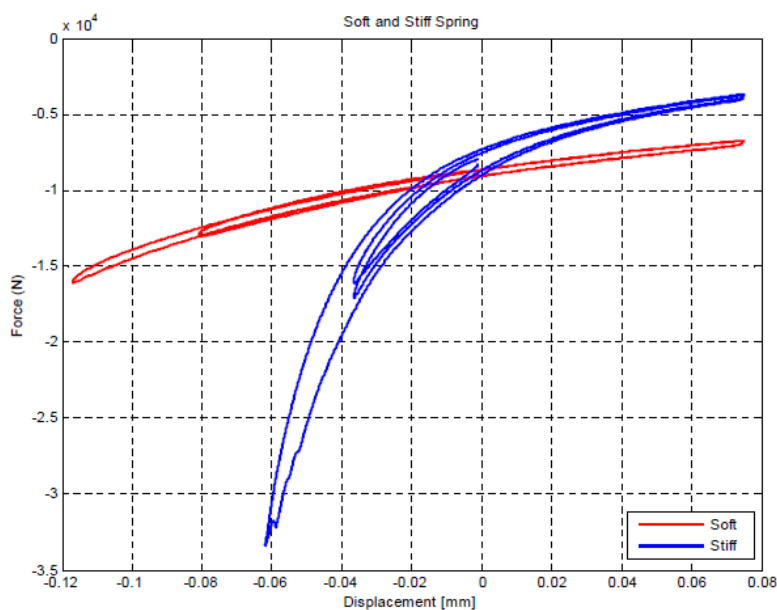
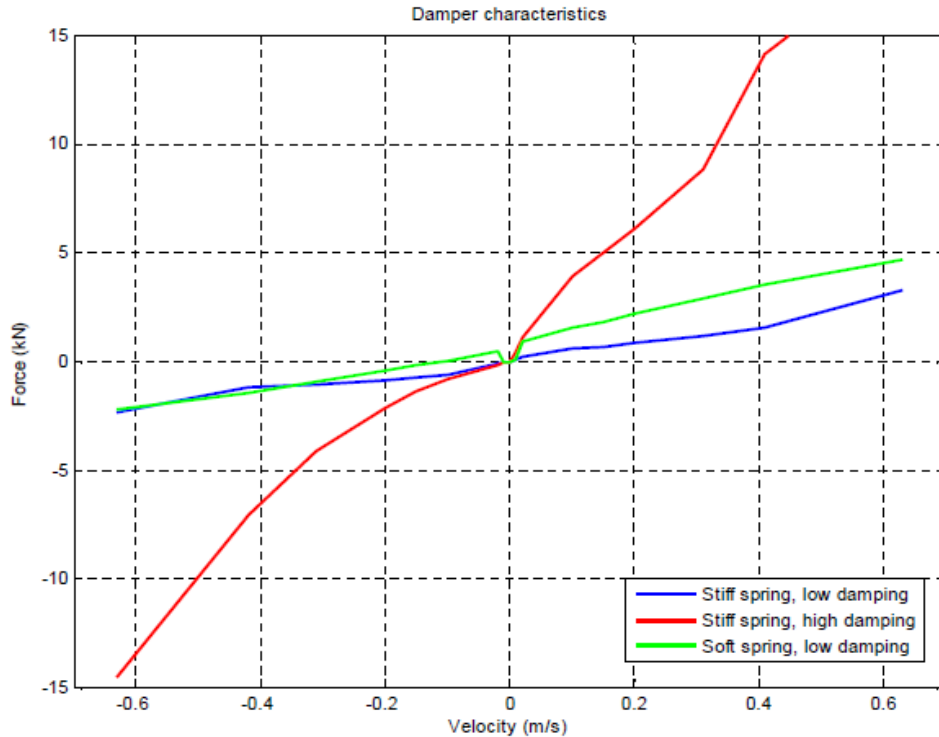


Figure 16: 4S<sub>4</sub> Spring Displacement Characteristics Els (2006)



**Figure 17: 4S<sub>4</sub> Damper Characteristics Els (2006)**

Els (2006) did a number of simulations and tests optimising spring and damper characteristics of the 4S<sub>4</sub> system, and determined the combinations yielding the best possible handling and ride comfort for the specific test vehicle. The results showed a stiff spring (0.1 litre static gas volume for the 4S<sub>4</sub>) and high damping (more than double the baseline damping) is required for good handling. Optimal ride-comfort is obtained using a soft spring (>0.5 litre static gas volume for the 4S<sub>4</sub>) and low damping (less than half of the baseline vehicle).

Breytenbach (2009) noted the ride and handling characteristics both suffer from frictional effects. Friction in the system is caused by hydraulic seals and wear-rings sliding against the suspension cylinder walls, and is inherent to the system and cannot be changed. Friction in the 4S<sub>4</sub> system is substantially higher when compared to that of the standard Land-Rover suspension system.

## **2.5. Requirements for Handling and Ride Comfort and Reduced Roll-Over Propensity**

The conflict between ride and handling characteristics leads to a number of questions, such as what suspension characteristics results in reduced body roll, or reduced roll-over propensity? Another question that may be raised, are the suspension settings required for good ride or handling the same as that required for reduced rollover propensity? This section investigates different suspension settings required to obtain specifically, good handling, good ride-comfort, or reduced rollover propensity.

### 2.5.1. Suspension Requirements for good handling or good ride comfort

Uys, Els, and Thoresson (2006) conducted a study on parameters useful in the quantification and optimisation of vehicle handling. The tests suggested the roll angle as a suitable parameter for quantification as well as optimisation of suspension settings. The study notes a one-to-one relationship between lateral acceleration and roll angle for various drivers on various test tracks and manoeuvres.

Increased roll stiffness decreases body roll angle, therefore increasing the vertical load transfer of the vehicle. Increased load transfer reduces maximum achievable side force from the tyres, improving safety by reducing the roll over tendency of the vehicle when considering the SSF (Cronjé, 2008). Increased roll stiffness can be obtained by using stiffer springs, and/or using anti-roll bars (anti-roll bars reduce the maximum achievable wheel travel).

Studies by Thoresson (2003) and Uys (2007) showed the optimal settings for handling to be high spring stiffness and high damping, while optimal settings for ride comfort were low spring stiffness and low damping. Els (2006), confirmed this through testing obtaining the highest clean run speed through the ISO 3888 Double Lane Change manoeuvre, using high spring stiffness and high damping (tests were conducted on the soft-spring low damping, as well as the base-line vehicle settings).

Holdmann and Holle (1999) investigated possibilities of improving ride and handling of a 3.5 ton delivery vehicle. They found that at frequencies below 4Hz a passive damper with a high damping rate ensures both comfort and safety. Frequencies between 4 and 8 Hz, requires low damping to ensure both comfort and safety. At frequencies above 8 Hz, comfort requires low damping, while high damping improves safety by minimising dynamic wheel loads. They also noted that lateral vehicle dynamics is minimally affected by different damping systems. This is supported by Karnopp and Margolis (1984) noting that changing damping alone is not efficient in stiffening or softening a suspension system.

Sakai and Satoh (1994) theoretically investigated the effects of the roll-centre position on dynamic behaviour of a vehicle. Their findings suggest setting the roll centre higher accelerates the onset of cornering force at high speeds. If one sets the roll centre too high, i.e. at a position above the CG of the vehicle, it may lead to the vehicle leaning into a turn much like a motorcycle. The roll centre of a vehicle is not a fixed point as it is a function of the instantaneous suspension geometry (Frimberger, et al., 2004).

The characteristics required for good handling, are almost the exact opposite of those required for good ride comfort. Ride comfort is measured as the vertical acceleration experienced by the vehicle occupant. Good ride comfort requires the vehicle to have a soft spring and low damping characteristic, isolating the vehicle occupant from harsh vertical accelerations caused by road inputs.



Ride comfort is assessed by calculating the weighted Root Mean Square (RMS) of the vertical acceleration experienced by the vehicle occupant. The weighting filter as proposed by the British Standards Institution (1987) is given in Figure 18. The guideline comfort ratings for the weighted RMS values are given in Table 4.

Table 4: Guidelines for comfort according to Weighted RMS British Standards Institution (1987)

Weighted RMS values	Rating
$< 0.315 \text{ m/s}^2$	Not uncomfortable
$0.315 - 0.63 \text{ m/s}^2$	A little uncomfortable
$0.5 - 1.0 \text{ m/s}^2$	Fairly uncomfortable
$0.8 - 1.6 \text{ m/s}^2$	Uncomfortable
$1.25 - 2.5 \text{ m/s}^2$	Very uncomfortable
$> 2.0 \text{ m/s}^2$	Extremely uncomfortable

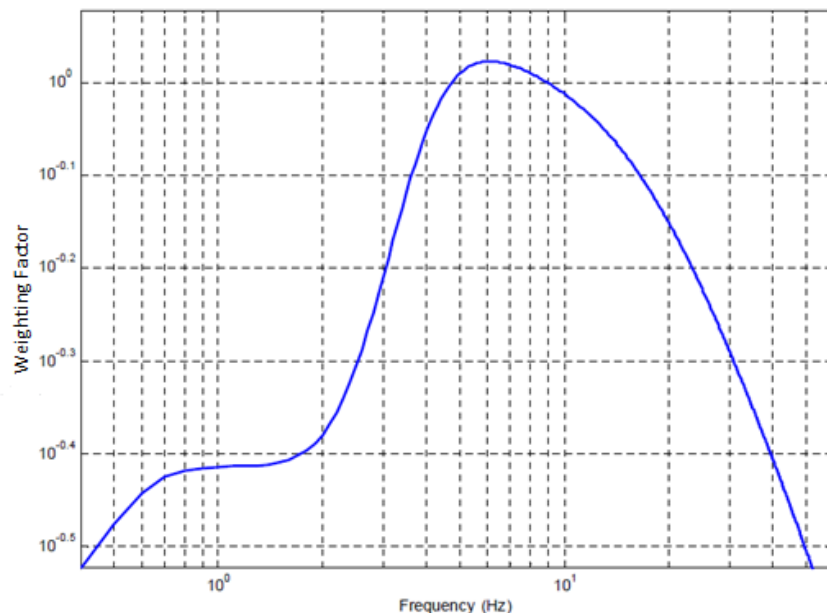


Figure 18: Weighting Function  $W_b$  for vertical vibration measurement on a seated person in the vertical direction British Standards Institution (1987)

Soft spring and damper settings result in low roll stiffness for the vehicle, causing lower levels of vertical load transfer during dynamic manoeuvres. Lower load transfer levels translate to higher maximum achievable tyre side force, causing the vehicle to be more prone to rollover.

Studies by Thoresson (2003), Els (2006), and Uys (2007), proved soft spring and damper settings to be the opposite of what is required for good handling, resulting in large roll angles and higher rollover propensity during dynamic manoeuvres. Uys (2007) noted the suspension requirements for reduced roll-over propensity differs from both ride and handling requirements. The requirement for reduced roll-over propensity found through simulation is that of high damping and low spring stiffness.



### **2.5.2. Roll-over prevention strategies and Suspension requirements**

Roll-over accounts for a large percentage of fatalities in single vehicle accidents. Many investigations have been done, and various strategies developed to reduce vehicle roll-over propensity, and roll-over accidents.

Els (2006), makes use of a 4S<sub>4</sub> suspension system, which switches to handling mode, having high spring stiffness and a high damping, using the Running Root Mean Square (RRMS) of lateral acceleration, as switching criterion. This strategy has been shown to improve the handling capability and reduce roll-over propensity of the test vehicle.

Another strategy is to reduce the vehicle CG height and improving the SSF. This strategy is implemented in the Volkswagen Touareg, which reduces the vehicles' ground clearance from 215mm to 190mm at speeds above 125 km/h (although the driver can set other levels). At speeds above 180 km/h ride height is automatically reduced to 180mm, (Birch, 2002).

Vehicle Dynamic Controllers (VDC), are another approach to roll-over prevention and vehicle stability. VDC mostly use differential braking, making use of the vehicles' Anti-lock Brake System (ABS) to improve stability. Ungoren and Peng (2004) evaluated VDC effects on rollover propensity on a vehicle with an undesirable geometry (such as an SUV with a high CG) through simulation. The author evaluated the roll tendency using worst-case disturbances, and optimised the control inputs for these disturbances. The author concludes a VDC system can improve the rollover stability of a vehicle without changing vehicle geometry.

Active Roll Control is also possible, where vehicle roll angle is reduced by jacking the suspension units on the outside of a turn. This serves to increase vertical load transfer between the inside and outside wheels. The increased load transfer reduces the maximum achievable lateral force improving rollover stability by causing a spin out rather than a rollover event (Van der Westhuizen and Els, 2011).

All of these roll-over prevention strategies were developed and tested to a large extent using vehicle simulation before physical implementation and testing. This highlights the necessity of accurate vehicle dynamics models.

### **2.6. Friction Effects and Friction Modelling**

Friction, nature's Mother in Law to relative motion, a natural manifestation of damping. Friction opposes forces and relative motions components of forces parallel to the friction surface in dynamic systems. Friction is found between sliding solid surfaces, viscous fluid layers, as well as at solid and fluid interfaces as skin friction. Each of the examples given has differing characteristics and driving forces making friction modelling non-trivial. Sliding friction is caused by microscopic surface irregularities causing the surfaces to be in contact

via a number of these asperities, viscous friction is caused by fluid viscosity. Friction is also assumed to be small compared to most suspension forces and is therefore generally ignored or not modelled during simulations as done for example by Lawniczak and Siminski (2009).

Friction in Vehicle suspension systems are to a larger extent between lubricated solid surfaces in sliding contact. The 4S<sub>4</sub> system, fitted to the test vehicle, can effectively be modelled as a hydraulic cylinder; the seals cause a friction level much higher than that of a normal suspension system. The high friction level is noted by various authors working with the specific test vehicle and suspension system, Els (2006), Uys (2007), Cronjé (2008) and Breytenbach (2009). Cronjé (2008) and Breytenbach (2009) achieved improved correlation between measured and simulation results by compensating for friction. Cronjé (2008), compensated using a rudimentary friction model, created by trial and error through simulation correlation studies. Breytenbach (2009) characterised the 4S<sub>4</sub> system friction experimentally, compensating using a LuGre friction model in his mathematical vehicle model. Both Cronjé (2008) and Breytenbach (2009) concluded that the friction modelling in the simulation model required improvement.

Not all friction models investigated are discussed in detail in this section. The friction models that are discussed in detail however form the bases of more complex friction models.

### 2.6.1. Coulomb, Viscous and Stribeck Friction Model

Friction acts as a natural damping force, dissipating energy in dynamic systems. Friction is commonly modelled with static and kinetic states, where friction force depends on normal force and friction coefficient. The kinetic friction coefficient is usually smaller than the static coefficient. Static friction is experienced when no relative velocity between contacting bodies exists. Kinetic friction is experienced when relative velocity between contacting bodies exists. This most basic form of friction modelling is known as the Coulomb friction model, Van Geffen (2009). The equation below is used to calculate the Coulomb friction.

$$F_c = \mu F_n \text{sign}(v)$$

where  $F_n$  is the normal force,  $\mu$  represents the friction coefficient,  $v$  is the relative velocity between the bodies. In lubricated friction, a lubricant film between contacting surfaces adds viscous friction at any non-zero velocity. The viscous friction effect is given by the following equation.

$$F_v = \sigma_v v$$

where  $F_v$  is the viscous friction,  $\sigma_v$  is the viscous friction coefficient, and  $v$  is again velocity. This generally yields a friction characteristic as shown in Figure 19.

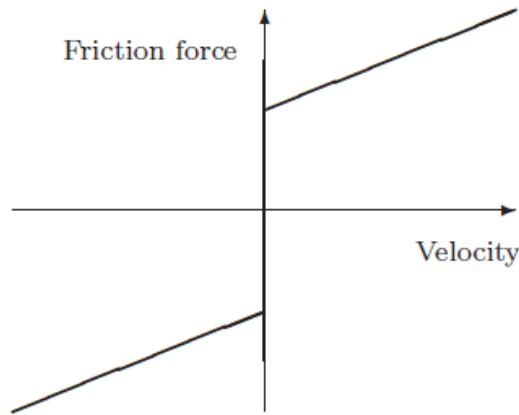


Figure 19: Coulomb, viscous and static friction, Van Geffen (2009)

This model is a crude approximation of reality. The transition between static and kinetic friction is actually more gradual. The gradual transition is caused by a phenomenon known as the Stribeck effect. The Stribeck effect gradually lowers friction over a certain velocity regime from zero to a certain velocity where the viscous fluid effects start dominating increasing friction again. The Stribeck effect is a function of velocity and for simplicity is kept in general form in the equation below.

$$F_f(v) = \mu(v)F_n \text{sign}(v) + \sigma_v v + F_s(v)$$

this yields the friction characteristic seen in Figure 20.

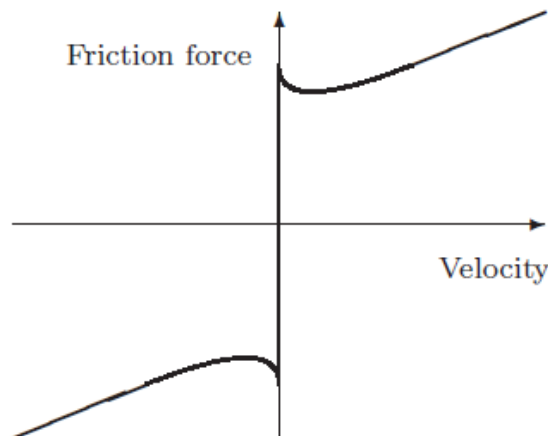


Figure 20: Stribeck friction model, Van Geffen (2009)

The discontinuity found at zero velocity or when crossing the zero velocity, causes numerical modelling problems.

### 2.6.2. The Dahl Model

The Dahl model uses an approach analogous to stress-strain properties of ductile materials to model friction. When subjecting objects to small displacements he observed them returning to their original positions, much like elastic deformation in materials. Subjecting the objects to larger displacements the bonding surface undergoes plastic deformation

causing permanent displacement. The maximum stress of the stress strain characteristic resembles the stiction phenomenon. Dahl assumed friction as not only a function of velocity but of displacement also, Van Geffen (2009). The Dahl model in its time derivative form is given in the equation that follows:

$$\frac{dF_f}{dt} = \frac{dF_f}{dx} \cdot \frac{dx}{dt} = \sigma \dot{x} - \frac{F_f}{F_c} \sigma |\dot{x}|$$

where  $\sigma$  is a material dependent stiffness parameter at equilibrium where the friction force,  $F_f = 0$  [N],  $F_c$  is the Coulomb friction, and  $\dot{x}$  is the sliding velocity. This formulation enables dynamic modelling of pre-sliding displacement and hysteresis caused by friction. Although only representing an approximation to pre-sliding displacements, the Dahl model forms the basis of many more advanced models. The Dahl model is unable to capture effects such as the Stribeck effect and prediction of stick-slip motion. de Wit, et al. (1995), describes the Dahl model as Coulomb Friction with a lag in the friction change when the direction of motion is changed.

### 2.6.3. The LuGre Model

The LuGre model visualises microscopic asperity contact as two rigid bodies in contact through a number of elastic bristles. When a tangential force is applied the bristles deflect like springs and thus give rise to friction force, de Wit, et al. (1995). The bristle model is shown in Figure 21; where for simplicity the bristles on the bottom body are shown as rigid.

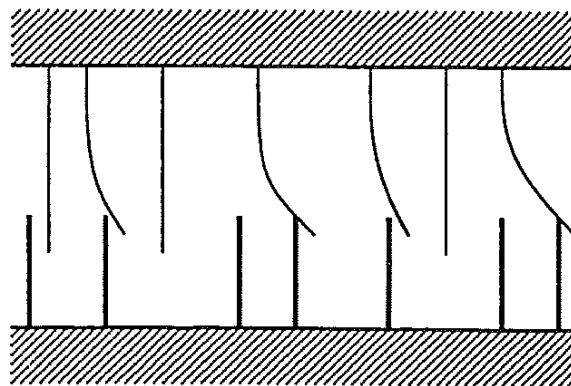


Figure 21: Bristle model of Frictional Interface (Bristles on lower body shown as rigid for simplicity), de Wit, et al. (1995)

If a sufficiently large force is applied some bristles deflect enough to slip. The LuGre model does not make use of random bristle deflection as would physically be the case, but uses average bristle deflection as a simplification, de Wit, et al. (1995).

The function  $g$  characterising the Stribeck effect is given in the following equation as per de Wit, et al. (1995).

$$\sigma_0 g(v) = F_c + (F_s - F_c) e^{-\left(\frac{v}{v_s}\right)^2}$$

where  $F_C$  and  $F_S$  are the Coulomb friction force and Stiction force respectively while  $v_s$  is the Stribeck velocity, and  $\sigma_0$  is the micro bristle stiffness. The Stribeck velocity is the velocity where steady state friction force is almost a minimum.

Bristle deflection is modelled by the following equation where  $z$  is average bristle deflection and  $v$  is relative velocity between surfaces.

$$\frac{dz}{dt} = v - \frac{|v|}{g(v)}z$$

the first term gives deflection proportional to the integral of relative velocity, while the second term causes the deflection to approach a steady state value when velocity is constant, given by the following equation.

$$z_{ss} = \frac{v}{|v|}g(v) = g(v)sgn(v)$$

the function  $g$  is positive, and depends on factors such as material properties, lubrication and temperature, and is not necessarily symmetrical. This implies direction dependent phenomena can be captured. De Wit, et al. (1995) notes the function  $g(v)$  decreases monotonically from  $g(0)$  when velocity increases, corresponding to the Stribeck effect.

Friction force from bristle deflection, and viscous friction is described by the following equation.

$$F = \sigma_0z + \sigma_1 \frac{dz}{dt} + \sigma_2v$$

$\sigma_0$ , is the micro bristle stiffness,  $\sigma_1$  micro bristle damping coefficient and  $\sigma_2$  viscous fluid friction coefficient. These coefficients with the function  $g$ , characterise the model.

#### 2.6.4. The Modified LuGre Model

The modified LuGre model is an extension of the LuGre model improving on several issues highlighted by Yanada and Sekikawa (2008). The LuGre model does not capture un-steady state friction behaviours at a start from rest or under velocity reversals.

Yanada and Sekikawa (2008) note the LuGre model over-predicts forces immediately before velocity reversals, as well as not capturing the reduction in break-away force after one cycle of velocity variation. This is due to the assumption that the lubricant film reacts quickly to velocity variations between contact surfaces in the LuGre model. The shortcomings of the LuGre model are highlighted in Figure 22.

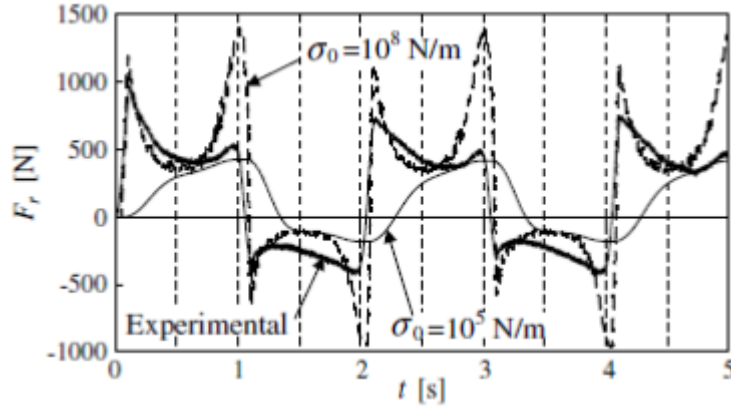


Figure 22: LuGre model simulation results versus measurements showing under and over prediction of two models, Yanada and Sekikawa (2008)

Yanada and Sekikawa (2008) proposed a modification to the LuGre model bringing lubricant film dynamics into consideration while keeping the basic structure of the LuGre model. Lubricant film thickness depends on the relative velocity between contact surfaces. Lubricant film thickness is taken into account by assuming the dimensionless steady state lubricant film thickness can be expressed as follows.

$$h_{ss} = K_f |v|^{2/3} \quad (|v| \leq |v_b|)$$

where  $K_f [(s/m)^{3/2}]$  is a proportional constant and  $v_b$  is the velocity where the steady state friction becomes a minimum. The assumption is made that film thickness does not change for velocities larger than,  $v_b$ , which implies the maximum film thickness is given by the following equation.

$$h_{max} = K_f (v_b)^{2/3}$$

the lubricant film thickness change lags behind the change in velocity, and is dependent on the acceleration or deceleration of contact surfaces. Yanada and Sekikawa (2008) note that the lubricant film thickness decreases during acceleration and increases during deceleration. The magnitude of acceleration/deceleration also affects the difference between the steady and un-steady state film thickness. To take acceleration/deceleration effects into account Yanada and Sekikawa (2008) proposed the following film dynamics model, making use of a varying time constant to account for these effects. This is given by the equation that follows.

$$\frac{dh}{dt} = \frac{1}{\tau_h} (h_{ss} - h)$$

where:

$$\tau_h = \begin{cases} \tau_{hp} & (v \neq 0, h \leq h_{ss}) \\ \tau_{hn} & (v \neq 0, h > h_{ss}) \\ \tau_{h0} & (v = 0) \end{cases}$$

If  $h > h_{max}$  then,  $h = h_{max}$ . The time constant is switched based on the lubricant film thickness, however it may also be switched using acceleration, deceleration and dwell behaviour of the contact area. Using the acceleration and deceleration of the contact area for switching does not greatly affect the results during simulation (Yanada and Sekikawa 2008). Lubricant film thickness is thus not only a function of velocity, but also of the rate of change of the velocity of the contact area.

The modification to the LuGre model incorporating lubricant film dynamics into the Stribeck effect is done using the following equation:

$$\frac{dz}{dt} = v - \frac{\sigma_0 z}{g(v, h)} |v|$$

where:

$$g(v, h) = F_C + [(1 - h)F_S - F_C]e^{-(v/v_s)^n}$$

Comparing the Stribeck effect function here with the one for the LuGre model, it is clear that the Modified LuGre model makes use of the lubricant film thickness, as well as a shape factor,  $n$ , which was given as 2, in the LuGre model. The shape factor as the name suggests, affects the shape or sharpness of the Stribeck effect depending on what is required.

Friction force is given by the following equation:

$$F_r = \sigma_0 z + \sigma_1 \frac{dz}{dt} + \sigma_2 v.$$

The steady state friction characteristic is given by:

$$F_{r_{ss}} = F_C + [(1 - h_{ss})F_S - F_C]e^{-(v/v_s)^n} + \sigma_2 v.$$

The modified LuGre model captures non-symmetric friction effects in the positive and negative velocity ranges, using different coefficients for the positive and negative ranges. The film dynamics model lends the capability of taking time-history into account, capturing the reduction in peak friction after the first velocity cycle. (The model captures the higher peak friction after extended dwell periods during simulation also.)

### 2.6.5. The Generalised Maxwell Slip model

The generalised Maxwell Slip (GMS) model, is based on three explicit friction properties, first the Stribeck curve for constant velocities, second a hysteresis function with non-local memory in pre-sliding and thirdly on the frictional lag in the sliding regime (Al-Bender, Lampaert, and Swevers, 2005). Al-Bender, et al., (2005) describe the GMS model as a parallel connection of  $N$  single state friction models, all subjected to the same inputs and dynamics model, although each of the  $N$  models has a different set of parameter values.

Each of the  $N$  models has a logic state indicating whether an element is sticking or slipping. The dynamics of each elemental model is determined by the following rules.

If an element sticks, the state equation is given by the following.

$$\frac{dz_i}{dt} = v$$

and remains in the stick state until the deflection of the  $i^{\text{th}}$  element equals the velocity weakening Stribeck function for element  $i$ ,  $s_i(v)$ , i.e.  $z_i = s_i(v)$  where  $v$  denotes velocity and  $z_i$  is the  $i^{\text{th}}$  element of the state vector  $z$ .

If the element slips the state equation changes to the following:

$$\frac{dz_i}{dt} = \text{sign}(v)C_i \left(1 - \frac{z_i}{s_i(v)}\right).$$

The element remains slipping until the velocity crosses through zero.  $C_i$ , is an attraction parameter. If  $s_i(v)$  is replaced with a constant parameter the GMS model reduces to the Maxwell-Slip model.

Friction force is the summation of outputs of all elementary state models, with two additional terms accounting for visco-elastic and viscous effects not modelled in elemental states. The friction force is given by the following equation.

$$F_f(t) = \sum_{i=1}^N (k_i z_i(t) + \sigma_i \dot{z}_i(t)) + f(v).$$

The number of unknown parameters depends on the number of Maxwell elements in the system. Each element is characterised by a stiffness coefficient,  $k_i$ , a visco-elastic coefficient,  $\sigma_i$ , an attraction parameter  $C_i$ , and a Stribeck velocity weakening function  $s_i(v)$ .

Al-Bender, et al., (2005) note the number of unknown parameters may be reduced by assuming a common form for the Stribeck function and attraction parameters, across all elements. The parameter identification is then carried out using a suitable optimisation method.

The GMS model is based on the physical phenomenon of asperity contact that causes friction, modelling groups of asperities as an element or elements. Like many other models the GMS model relies on switching criteria to effectively change the state model between sticking and slipping behaviour.

### 2.6.6. General observations from friction models

There are many models available for modelling friction, ranging from simple models such as the basic coulomb friction model to more complex models such as the GMS model following



an elemental approach. Each approach differently affects model fidelity and ease of implementation. Some models rely on easily measurable parameters while others are based on less intuitive parameters, each attempting to find a modelling methodology that is simple to implement yet has high modelling accuracy.

This section is dedicated to discussing different approaches highlighting attributes of each type of model. Friction as a mechanism can be divided into two regimes, pre-sliding and sliding. In pre-sliding friction force is a hysteresis function of position, while in sliding friction force is a function of relative sliding velocity (Lampaert, Swevers, and Al-Bender, 2002).

Bonchis, Corke, and Rye (1999) created a friction model characterising the effects of pressure on friction in double acting hydraulic cylinders. The model depends on 5 coefficients determined using a maximum likelihood approach to find a best fit to measured data. The 5 coefficients are noted by Breytenbach (2009) as having weak physical significance.

Van Geffen (2009) discusses the seven parameter model, which includes a pre-sliding displacement model as well as a Coulomb, viscous Stribeck model with frictional lag. Effectively the 7 parameter model consists of two discrete models, a stiction and sliding phase model. There is also not a clear distinction between the pre-sliding and sliding regime, thus failing to capture transitional behaviour.

Switching models are a class of friction models that switch between discrete modelling states. Van Geffen (2009), notes switching was originally done to avoid numerical problems close to the zero-velocity crossing during simulations. Since the original switching models were introduced various authors have exploited this strategy by switching between modelling states. One state effectively contains a hysteretic pre-sliding characterisation, while the other state describes the sliding friction characteristic. The GMS and 7 parameter models are examples of this.

The modified LuGre model uses two sets of parameters for the positive and negative velocity ranges effectively switching parameter values depending on the velocity range. Using velocity dependent parameters for modelling friction behaviour is also recommended by Márton and Lantos (2007).

Friction models encapsulating pre-sliding effects with local and non-local memory properties, such as the GMS, and seven parameter model, are difficult to characterise, and adds complexity to modelling.

## 2.7. Conclusions from Literature

The conclusions given here are based upon the evidence provided in this chapter.

It is clear from the statistics quoted that a high percentage of vehicle accident fatalities are due to roll over. Any improvement in the roll over propensity or the understanding thereof, can therefore have a substantial effect on the safety of vehicles and their occupants.

A large amount of work has been done to reduce roll over propensity and improve the ride, handling, and dynamic stability of vehicles and specifically SUVs. The mechanism of roll over however, is still not yet wholly understood. There is no vehicle specific parameter that can be compared directly between vehicles to decide which has the better roll over stability.

Literature suggests an increase in spring stiffness and damping, as well as a lower CG improves vehicle handling and reduces roll over propensity at the cost of ride comfort. Spring and damper characteristics required to prevent roll over and the dynamic relationship of the CG and roll over propensity, have only been researched to a limited extent.

Most research on roll over and CG height is based on simplified approximations to the actual problem. The effects of tyres, suspension geometry and suspension friction are neglected in most cases. A validated full vehicle model is potentially a great advantage for vehicle roll over research.

Friction in the 4S<sub>4</sub> semi-active suspension system, although originally ignored, has been noted to cause disparities between simulation and measurement results. The effects of friction have been highlighted previously, although no quantification of frictional effects has been done. A range of complex high fidelity models are available for friction modelling, especially in high precision positioning systems. It is expected however that a complex friction model will be un-necessary for the purposes of this study.

It was decided to follow the guidelines set out here as a plan for this study.

- I. Use a full non-linear vehicle model
- II. Use the ISO 3888 Double Lane Change manoeuvre to investigate vehicle dynamics
- III. Investigate effects of friction and gas modelling methodology on the vehicle model validity against test data
- IV. Identify a friction model and gas modelling methodology among those investigated most improving correlation
- V. Identify and quantify the suspension setting(s) most affected by friction
- VI. Identify and discuss the effects of friction on suspension and vehicle dynamic reactions compared to the case where friction is neglected.

### 3. Simulation Model and Model Validation

The full vehicle simulation model developed by Thoresson (2007), described by Els (2006) and Uys (2007), was used and modified for purposes of simulation. The simulation model was built in MSC.ADAMS (Automatic Dynamics Analysis of Mechanical Systems) based on the physical properties and dimensions of a Land Rover Defender 110, which is used for experimental testing. The physical dimensions of the vehicle were measured or taken from technical drawings of the vehicle and components. Inertial properties for roll, pitch, yaw, as well as the CG point were determined by experimental measurements as described by Uys, Els, Thoresson, Voight and Combrinck (2006a).

Modelling of the hydro-pneumatic suspension system, as well as updates to the model will be discussed in the sub-sections that follow. The validation of the simulation model will also be handled in this section.

#### 3.1. Model Properties

The general model properties are discussed in this section. Special attention is paid to the suspension kinematics and tyre model. The effects of the 4S<sub>4</sub> suspension and outriggers on vehicle parameters such as the Centre of Gravity are also discussed.

Table 5 summarises the mass and inertial properties of the Land Rover Defender 110 as obtained by Uys, et al. (2006a). The masses and moments of inertia quoted are for the base-line vehicle with the standard suspension, without vehicle occupants and without the attachment of outriggers to prevent roll over during testing. Outriggers as well as the 4S<sub>4</sub> affect the CG height and roll moment of inertia of the vehicle.

Table 5: Mass and Inertial Properties of Base-Line Vehicle Uys, et al. (2006a)

Mass Property	Value [Units]
Sprung Mass	1567 [kg]
Sprung Mass Pitch moment of Inertia	2440 [kg.m <sup>2</sup> ]
Sprung Mass Roll moment of Inertia	680 [kg.m <sup>2</sup> ]
Front Un-sprung Mass	229 [kg]
Front Un-sprung Mass Roll moment of Inertia	33.1 [kg.m <sup>2</sup> ]
Rear Un-sprung Mass	229 [kg]
Rear Un-sprung Mass Roll moment of Inertia	33.1 [kg.m <sup>2</sup> ]

The Centre of Gravity (CG) position and vehicle geometry dimensions are given in Figure 23, as determined by Uys, et al., 2006a. There are two CG points of interest shown in the figure, namely the Body CG and the Vehicle CG, which is lower than the body CG. The vehicle suspension and wheel track width is shown in Figure 24, suspension track width being the smaller of the two.

The 4S<sub>4</sub> suspension struts, weighing 40kg each, are considerably heavier than the coil springs used on the standard vehicle. The fitment of two outriggers to prevent roll over during testing adds a further 100kg to the system and increases the vehicles' roll inertia. Vehicle occupants also add mass to the system.

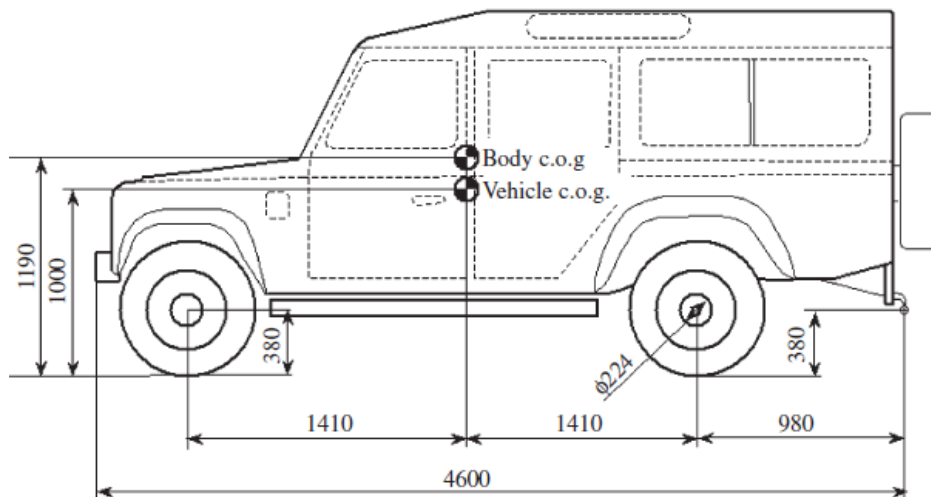


Figure 23: CG position and Vehicle Dimensions, UYS, et al. (2006a)

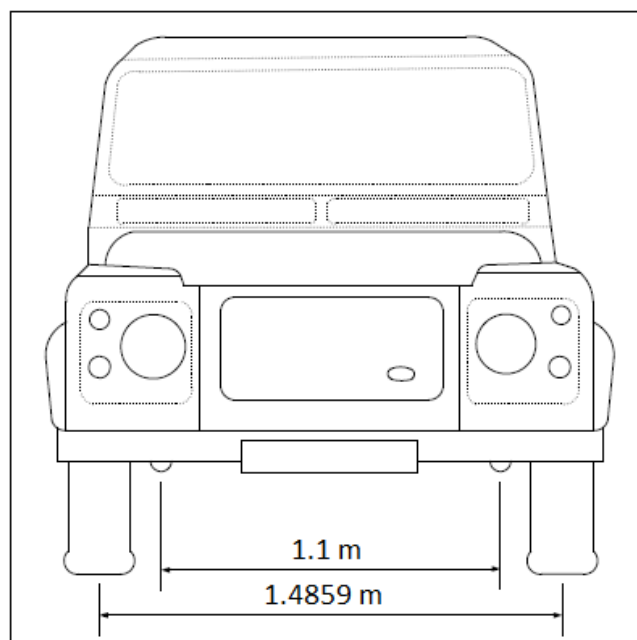


Figure 24: Vehicle Wheel and Suspension Track width, Breytenbach (2009)

The CG height of the vehicle reduces to about 0.95 m while the roll moment of inertia increases to 1298 kgm<sup>2</sup> when taking the effects of outriggers and 4S<sub>4</sub> suspension system into account. The total mass of the vehicle including driver, passenger and instrumentation during testing was 1986.29 kg, the mass of the simulation model was set accordingly along with the re-calculated CG point of the vehicle in test-trim.

The front suspension modelled in MSC.ADAMS consists of a rigid axle, longitudinally located by leading arms connected to the vehicle chassis by rubber bushes, and is laterally located

using a Panhard-Rod. Steering is achieved through a steering angle driver directly connected to the right hand side kingpin with a steering link connecting the left and right wheels. The rear rigid axle is located longitudinally with trailing arms, connected to the vehicle chassis by rubber bushes, and laterally by an A-arm, Els (2006). The leading and trailing arm bushing characteristics are included in the simulation model. The complete suspension layout is shown in Figure 25. Schematics of the front and rear suspension layouts are given in Figure 26 and Figure 27 respectively.

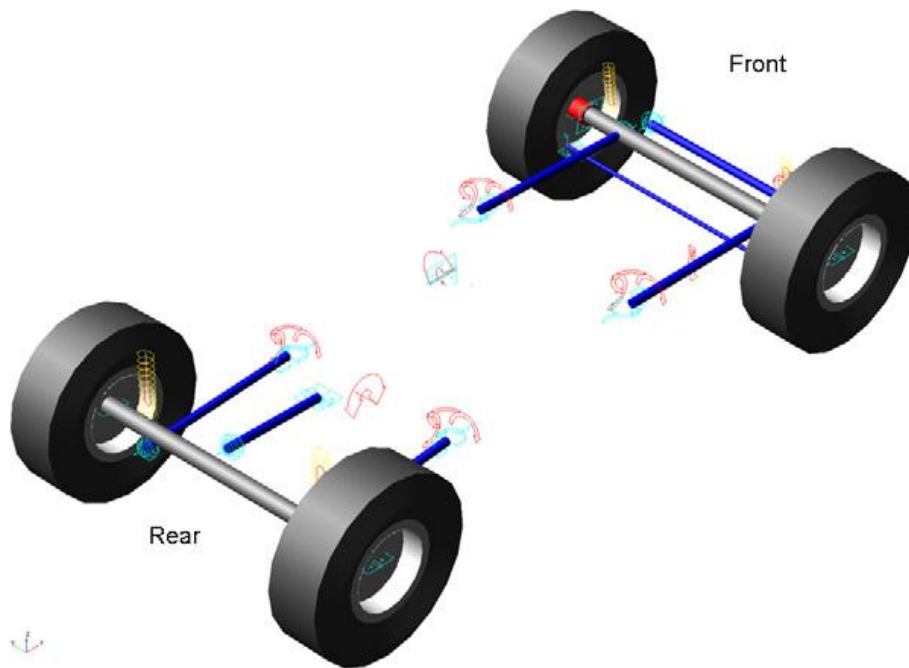


Figure 25: Suspension Layout in Simulation Model, Els, et al. (2007)

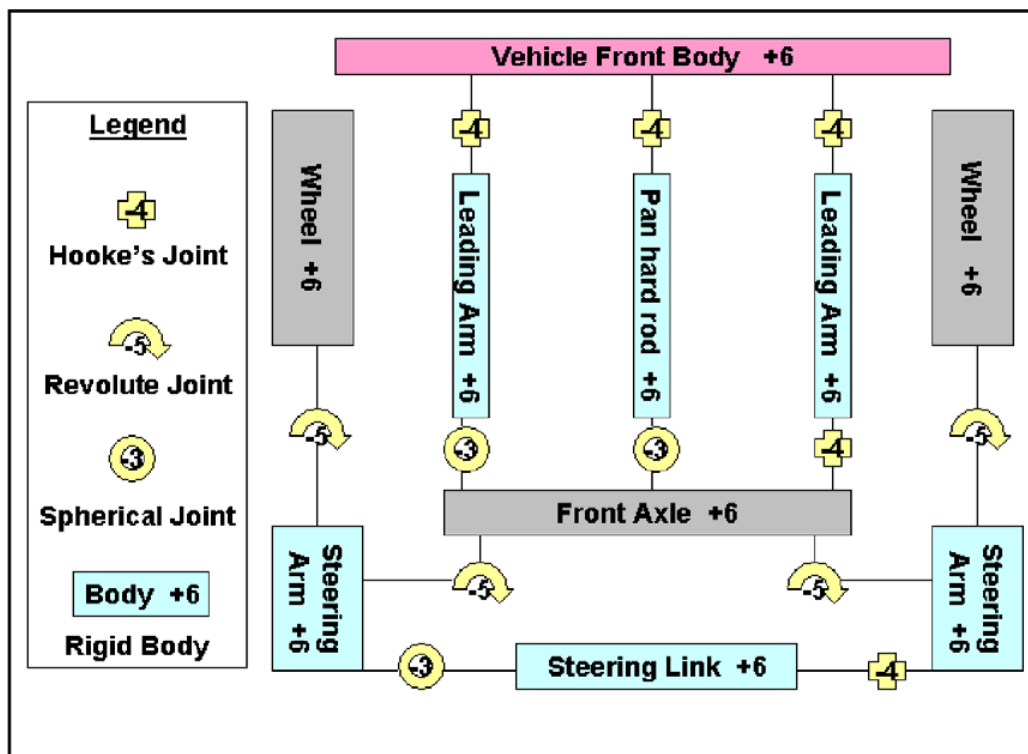


Figure 26: Schematic Layout of Front Suspension in the simulation model, Els, et al. (2007)

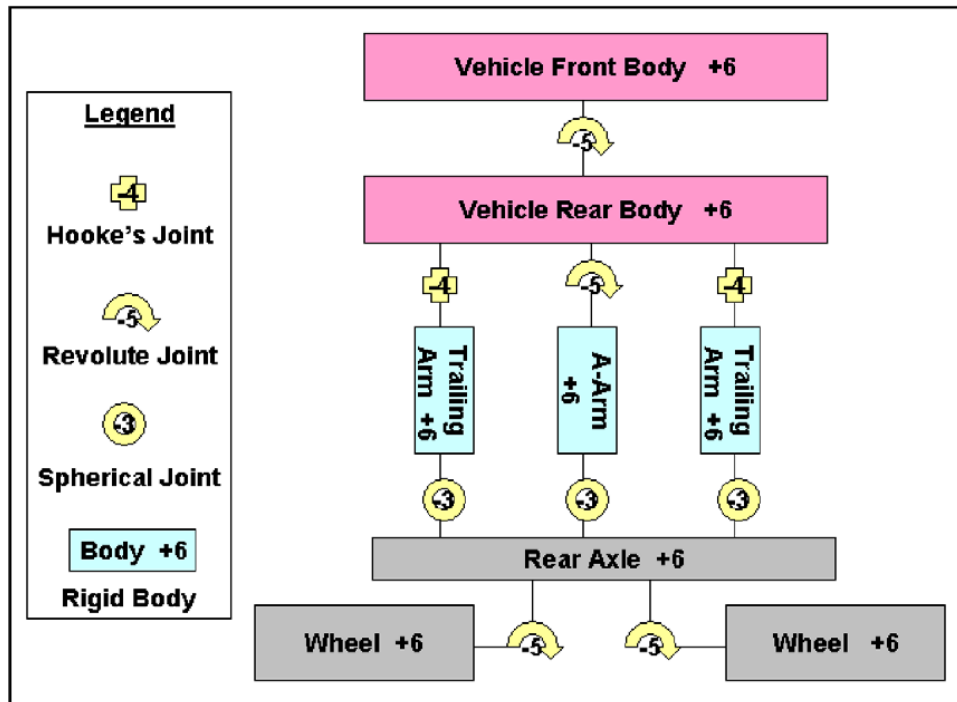


Figure 27: Schematic Layout of Rear Suspension in the simulation model, Els, et al. (2007)

The tyre-road interface in the simulation is modelled using a Pacejka '89 tyre model, (Bakker, Pacejka, and Lidner 1989). The Pacejka tyre model was fitted to experimental side-force vs. slip angle measurements as a function of vertical load, the fitting and fine-tuning was done by Thoresson (2007). Due to a lack of data, and for simplicity during implementation, the longitudinal force and self-aligning moment characteristics of the tyres were excluded. Effects of camber angle were also neglected due to the vehicle having rigid axles for which the camber angle is fixed. The camber effect induced by tyre deflection is also assumed to be small.

### 3.2. Hydro-Pneumatic Suspension Modelling

The working of the hydro-pneumatic 4S<sub>4</sub> suspension system is discussed in section 2.4.2.1. The current section discusses the mathematical modelling of the spring force and damping characteristics of the suspension units. Due to different friction modelling strategies followed by authors previously working with the specific suspension system, suspension friction modelling is discussed in a dedicated subsection.

#### 3.2.1. Hydro-pneumatic suspension modelling, contributing factors

Hydro-pneumatic suspension systems are affected by a multitude of factors. These factors are discussed in the sub sections that follow. The effects of heat transfer and thermodynamics are discussed in section 3.2.1.1, the effect of oil bulk properties on the model characteristics is discussed in section 3.2.1.2, while the effects of accounting for, or disregarding thermodynamic and fluid bulk property effects on the simulation model are shown in section 3.2.1.3.

### 3.2.1.1. Thermodynamic effects on hydropneumatic suspension modelling

The spring force in the 4S<sub>4</sub> system is generated by the compression of nitrogen gas in the system accumulators. Typically this is modelled with an Ideal Gas Model, assuming ideal gas behaviour and polytropic gas compression (Els and Grobbelaar, 1999). They note the gas temperature and pressure can generally vary between -20 °C and +200°C, and 2MPa to 110MPa respectively in commercially used hydro-pneumatic suspension systems, making the ideal gas approach invalid in most cases, especially for pressures above 30MPa.

The 4S<sub>4</sub> system operates at pressures well below 30MPa. The maximum pressure in the system for the highest load case investigated at maximum compression is 20MPa (Els, 2006). The Nelson-Obert generalized compressibility charts for gasses, depending on the reduced pressure and temperature of the gas, is given in Figure 28. The reduced pressure and temperature of the 4S<sub>4</sub> system at its maximum design pressure yields a compressibility factor of around,  $Z = 1.05$ . During testing however the vehicle is rarely loaded to its maximum capacity and normal operation the 4S<sub>4</sub> system has a maximum pressure closer to 6 MPa, which yields a compressibility factor of around,  $Z = 1$ . The compressibility factors for the working range of the 4S<sub>4</sub> system shows that the Ideal Gas model is applicable for modelling the spring force-displacement characteristics.

The spring Force-Displacement modelled using the Ideal gas approach is given by the following equation:

$$F = p_{stat}A \left( \frac{x_{stat}}{x} \right)^{n_p}$$

where:

- $F$  Force in Pneumatic Spring,
- $p_{stat}$  Static Pressure (Constant),
- $A$  Area (Constant),
- $x_{stat}$  Static Displacement (Constant),
- $x$  Hydro-pneumatic spring displacement,
- $n_p$  Polytropic gas Constant.



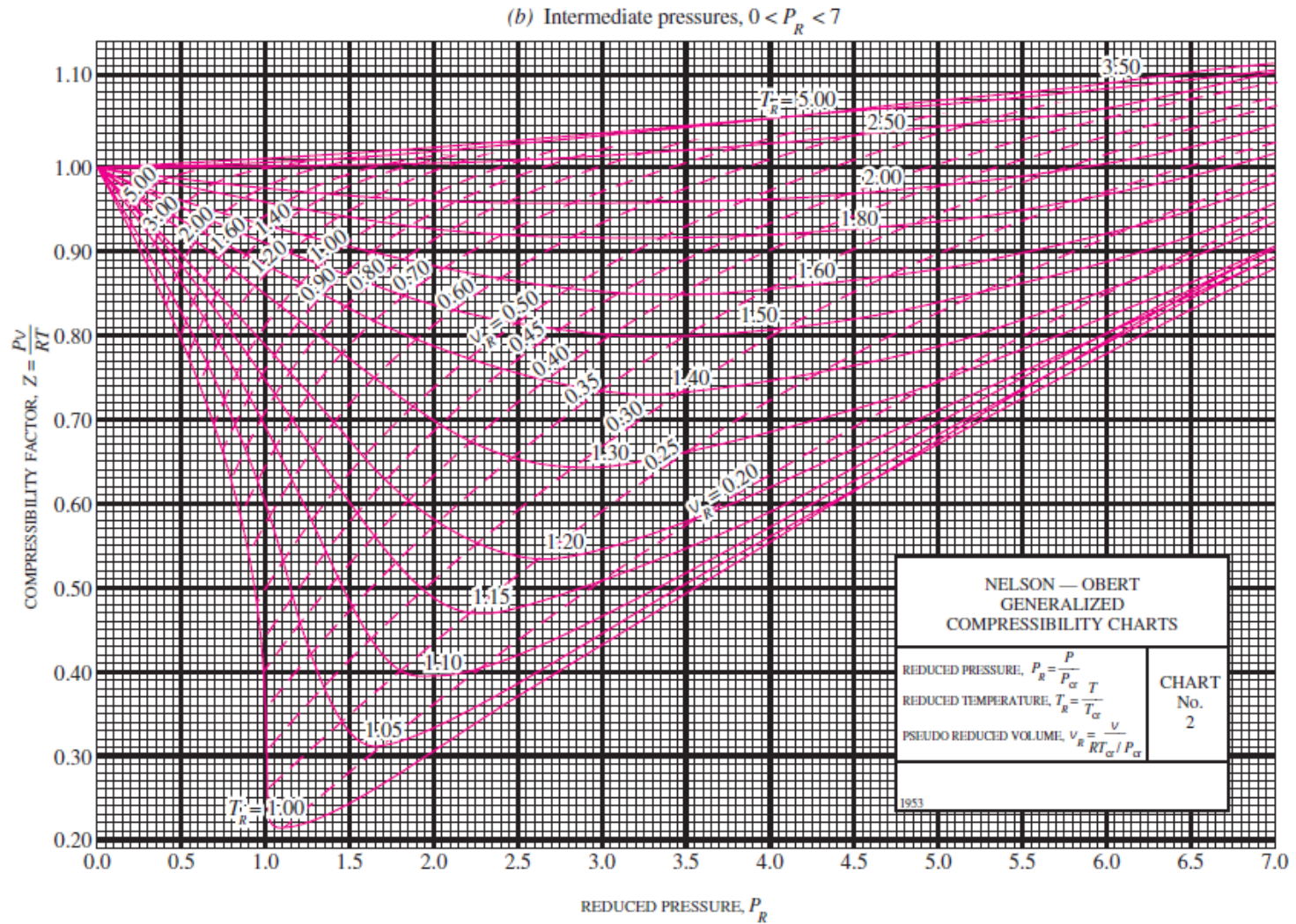


Figure 28: Nelson-Obert Generalized Compressibility Chart, Thermofluids.net (2013)



The problem with modelling the gas using an Ideal gas approach, is that the polytropic gas constant,  $n$ , is assumed to be constant, while this may not physically be the case, (Els, 1993). Els (1993) also noted that the temperature rise in a hydropneumatic suspension system can have significant effects on the characteristics of this suspension type.

Otis and Pourmovahed (1985) accounted for heat transfer by approximating heat transfer with a thermal time-constant model derived from the First law of Thermodynamics. The first law of thermodynamics is given by the following equation.

$$-\dot{U} = -\dot{Q} - \dot{W} \text{ or } -m\dot{u} = -\dot{Q} - \dot{W} \dots \{9\}$$

where:

- $\dot{U}$  Rate of change in Internal energy of the gas
- $\dot{Q}$  Heat transfer rate between the system and environment (In this case from the system to the environment)
- $\dot{W}$  Rate of External work done by the gas on the piston
- $\dot{u}$  Rate of change in specific internal energy of the gas
- $m$  Mass of the gas in the system.

To apply the method proposed by Otis and Pourmovahed (1985), to a hydropneumatic suspension system, Els (1993), assumed the following:

- The system is a closed system.
- Inertial effects are not present during gas compression.
- The process is a homogeneous, quasi-static gas compression process.
- Thermal capacities of the accumulator cylinder wall and piston are negligibly small.

Convective heat transfer from the suspension to the environment may be approximated by the following single time-constant model as derived by Els (1993). The thermal time-constant in the model may be determined either experimentally or analytically.

$$\dot{Q} = \frac{mc_v(T_s - T_g)}{\tau} \dots \{10\}$$

where:

- $c_v$  Specific Heat
- $T_s$  Accumulator cylinder wall/ambient Temperature
- $T_g$  Gas Temperature
- $\tau$  Thermal time Constant.

The rate of piston work, in terms of the piston motion or oil flow is given by the following.

$$\dot{W} = P\dot{V} \dots \{11\}$$

with  $P$  and  $\dot{V}$  the gas pressure and rate of change in volume respectively.

The thermodynamic relation for internal energy per unit mass (neglecting the effect of pressure) is given by the following equation.

$$du = c_v dT_g \dots \{12\}$$

substituting the equations for Convective heat transfer, {10}, Piston work, {11}, and Internal Energy, {12}, into the first law of thermodynamics, {9}, yields the following relation.

$$mc_v \frac{dT_g}{dt} = \frac{mc_v(T_s - T_g)}{\tau} - P\dot{V} \dots \{13\}$$

Simplifying equation {13} leads to the following differential equation for the gas temperature.

$$\dot{T}_g = \frac{(T_s - T_g)}{\tau} - \frac{P\dot{v}}{c_v} \dots \{14\}$$

where  $\dot{v}$  is the rate of change in specific volume of the gas.

The gas temperature differential equation, equation {14} is solved numerically for every simulation step. The calculated temperature is then used to calculate the pressure as using the formulation of the Ideal Gas model shown in equation {15}, where  $R$  is the gas constant for the specific gas.

$$P = \frac{RT_g}{v} \dots \{15\}$$

Accounting for the heat transfer effects should yield a more accurate representation of the gas characteristics. The increased accuracy however adds additional computational complexity and thus increases computational effort.

The model as shown here to be dependent on the gas temperature, will be referred to as the Thermal Time Constant model later in this text. The Thermal Time Constant model accounts for heat transfer effects by approximating the temperature of the gas using the model shown.

Two other models investigated later in this text, are the adiabatic- and the isothermal-ideal gas models. The adiabatic ideal gas model implies the extreme where there is no heat transfer between the gas in the system and the surroundings. The adiabatic model assumes the time allowed for heat transfer is negligibly small and therefore heat transfer is ignored. The isothermal formulation approximates the extreme where there is perfect heat transfer between the gas and the surroundings, and thus the gas remains at a relatively constant temperature.

### 3.2.1.2. Fluid Bulk effects on hydro-pneumatic suspension modelling

The high pressure present in hydropneumatic suspension systems invalidates the assumption that the oil in the system is incompressible. The effect of neglecting fluid

compressibility results in a stiffer overall spring characteristic for the hydro-pneumatic system.

Oil compressibility, caused by the bulk modulus effect, can be modelled as a linear spring. The stiffness of the fluid column only depends on the bulk modulus,  $\beta_f$ , of the fluid. The fluid column stiffness is modelled by the following equation as derived by Breytenbach (2009).

$$k_{\beta_f} = \frac{\partial F}{\partial x} = -\frac{\beta_f A^2}{V}.$$

Breytenbach (2009), noted that by knowing the volume of fluid in the  $4S_4$  system at the time of determination of the bulk modulus (1.6 litres), the diameter of the oil column (50mm) and the bulk modulus of the oil (1.368GPa as experimentally determined by Els (2006)), it is possible to calculate the stiffness of the fluid column to be:

$$k_{\beta_f} = -3.296 \text{ MN/m}$$

Balancing forces between the oil and gas in the accumulator makes it possible to calculate the amount of oil compression. The oil compression effect is added to the suspension displacement to obtain the corrected force displacement characteristics for the suspension system.

### 3.2.1.3. Thermal & bulk effects on hydro-pneumatic suspension modelling

The Bulk Modulus effect is shown in Figure 29 and Figure 30 for the hard and soft suspension settings respectively against experimentally measured isothermal compression data from Els (2006).

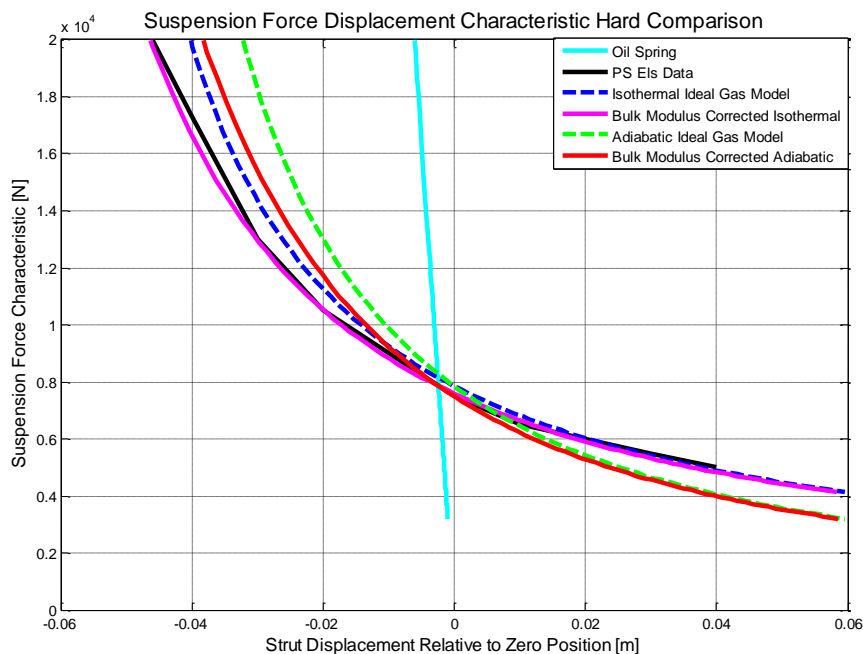


Figure 29: Force Displacement Characteristic Comparison of Isothermal and Adiabatic gas models, Hard Setting

The effect of oil compressibility is clear in Figure 29 and Figure 30. The Ideal gas model in the isothermal, adiabatic, and thermal time-constant formulations, along with bulk modulus effects were used during validation simulations for the hard and soft suspension settings. The three modelling strategies were investigated in terms of accuracy when compared to experimental characterisation measurements of the physical system. The investigation on model accuracy is handled in the model validation section.

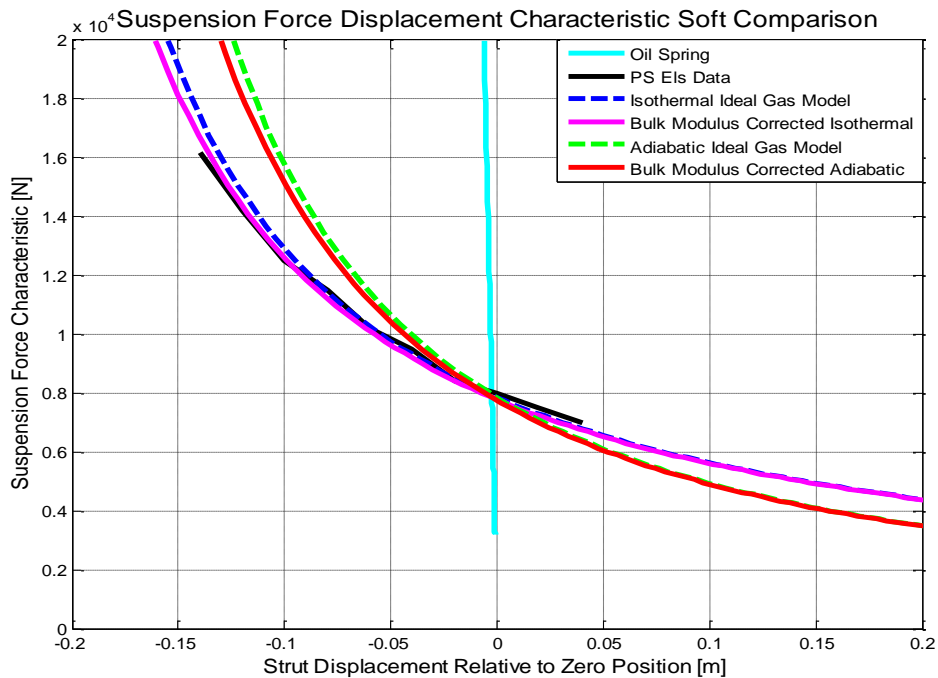
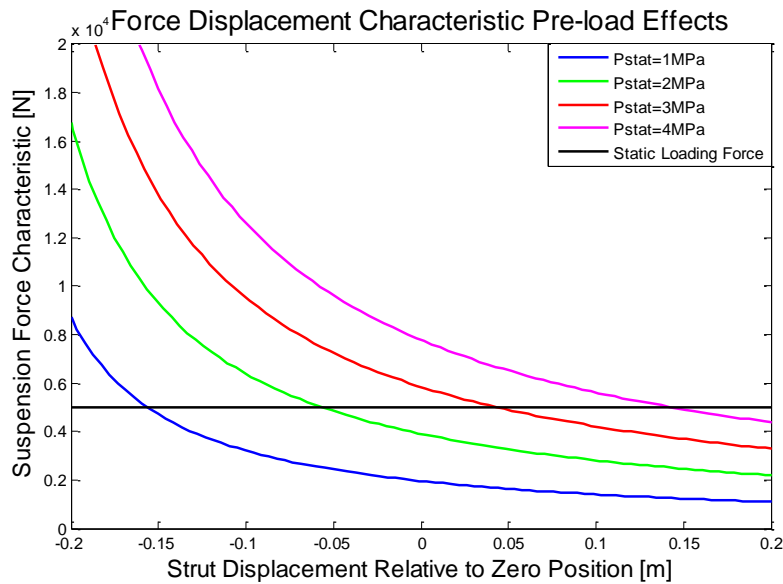


Figure 30: Force Displacement Characteristic Comparison of Isothermal and Adiabatic gas models, Soft Setting

#### 3.2.1.4. Gas charging pressure effects

The gas charging pressure generates a pre-load in the simulation model and is therefore of vital importance. If the pre-load is too high, the suspension strut will extend until equilibrium or the rebound stops are reached, if the pre-load is too low, the suspension strut will compress until equilibrium or the bump-stops are reached. Figure 31, shows the effect of the charging (pre-load) pressure and how it affects the zero/equilibrium strut displacement position. (The static loading force here was taken as 5kN and not 8kN as done previously. This was done to ensure the effect on the 1 MPa charging pressure line is visible in the plotted area)



**Figure 31: Pre-Load effects on spring characteristics (Soft)**

The characteristics directly around the equilibrium position are not the same, as would be expected since the pressure in the strut is a function of displacement. Although the forces at equilibrium are all equal, the spring rate around the equilibrium point is highly dependent on the gas charging pressure in the system.

It is therefore vitally important that the gas-charging pressure specified in the model during simulations be as accurate and close to the actual charging pressure during testing to ensure compatibility between the test and the simulation model.

### 3.2.2. Hydraulic Damper Modelling

Suspension damper characteristics are force-velocity functions. Damping characteristics of the 4S<sub>4</sub> system are well known due to numerous studies done with the specific test vehicle. Although all dampers were intended to have the same characteristic, Breytenbach (2009), notes that due to variations in manufacturing tolerances there is some variation in the characteristics between the struts.

The damper characteristics were modelled by a non-linear function depending on the instantaneous damper velocity and the damping scale factor. The damping scale factor was introduced during previous studies on vehicle ride, handling and roll-over propensity conducted by Thoresson (2003), and Uys (2007), for use as an optimisation variable. The damping scale factor acts as a multiplier of the base-line Land-Rover dampers. The handling characteristic of the 4S<sub>4</sub> system corresponds to a damping scale factor of 2, thus it has double the damping capability compared to the base-line Land-Rover dampers, yielding a high damping characteristic. A damping scale factor of 0.25 is used for the ride mode damping, yielding a low damping characteristic. The damping characteristics obtained with the damping scale factors for ride and handling correspond to the configurations

implemented on the 4S<sub>4</sub> system fitted to the test vehicle. The damper characteristics shown in Figure 17 were used in the simulation model.

Breytenbach (2009) noted the characteristics of both the ride and handling configurations to suffer from a friction induced dead band during characterisation. He notes that the friction is in the most part due to the hydraulic seals and wear rings against the strut cylinder walls. Friction is thus inherent to the system, while the hydraulic viscous damping in the system is controllable and may be used for optimisation purposes. Breytenbach (2009) concluded that it is desirable to model damping and friction separately.

### **3.3.Friction Modelling**

Friction modelling in the simulation of the 4S<sub>4</sub> model is not a new problem; it has been noted by various authors, including Els (2006), Cronjé (2008), and Breytenbach (2009). Razenberg (2009) notes the need for friction modelling on a hydro-pneumatic suspension system used in a rally truck. Sarami (2009) uses a Coulomb model to compensate for friction during the development of a semi-active suspension system for full suspension tractors, showing that friction modelling in hydro-pneumatic suspension systems is necessary.

The need for friction modelling arises from the relatively small error it causes in the suspension force. This small error translates to a small error in the acceleration dynamics of a vehicle. Acceleration being integrated to obtain velocity exacerbates the error, although still being within acceptable limits. The integration of velocity to obtain displacements however aggravates the error to such an extent that it is no longer within reasonable limits. Apart from affecting the displacement calculated during simulation, friction acts as additional damping affecting the transient behaviour of a system. Therefore, it is vital for high fidelity vehicle simulation models to take friction into account. This is especially true for vehicle models containing hydro-pneumatic suspension systems, as these systems suffer from much higher friction levels than normal spring damper suspension units.

#### **3.3.1. Rudimentary, and revised rudimentary compensation for suspension friction**

Cronjé (2008) compensated for friction using a rudimentary friction model, effectively using a lookup table. The friction model was created through comparison between test and simulation data. The static friction limit was obtained by comparing constant radius test data with simulation data subjected to a static friction force. The static friction force was increased until good correlation was found. The dynamic friction force was obtained by comparing Double Lane Change manoeuvre test data with simulation data. The static friction limit was used as a starting point and lowered until a satisfactory correlation was found. The test manoeuvres used were chosen to emulate steady-state and dynamic behaviours. Realising that the Coulomb friction model, containing only the static and

dynamic friction levels, was a crude approximation the Stribeck-effect was included, this yielded the friction model shown in Figure 32.

Upon comparing the friction characteristic in Figure 32, to the experimental static friction characteristic in Figure 34, there is quite a large discrepancy. Firstly the levels of friction in the rudimentary model are too high, and secondly the friction model is symmetric in the positive and negative velocity ranges.

In the present work, the modelling methodology, (building a lookup-table,) was however followed and a more realistic friction model was created based on the experimentally determined friction characteristic, this is shown in Figure 33.

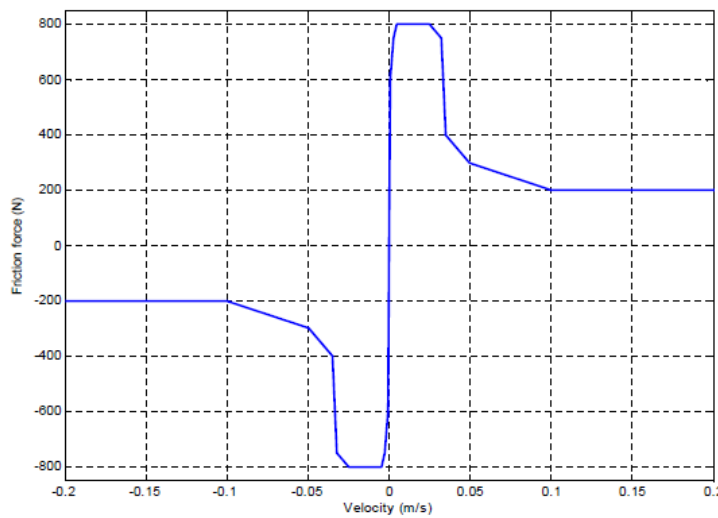


Figure 32: Friction force velocity characteristic used by Cronjé (2008)

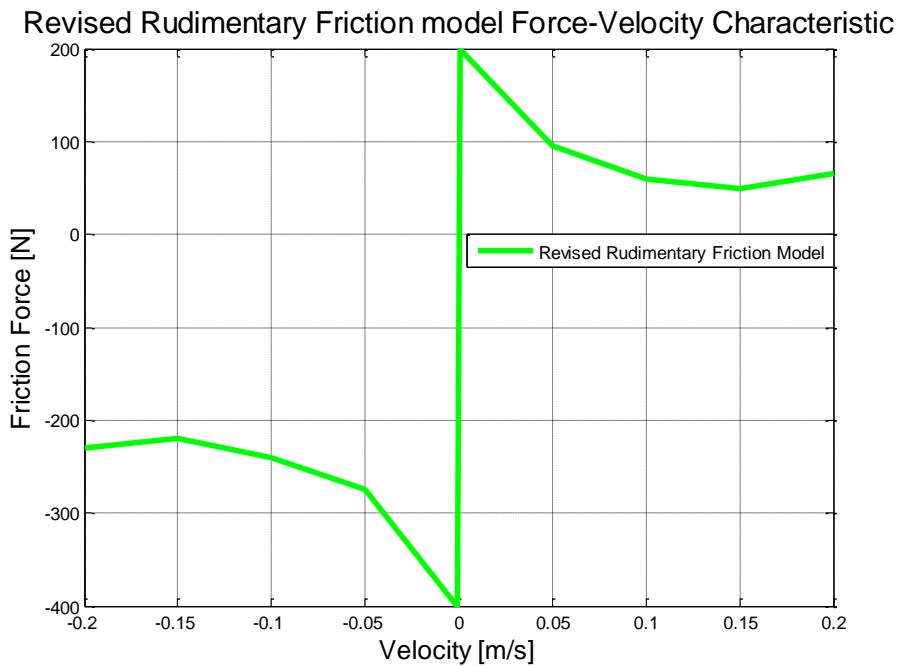


Figure 33: Revised rudimentary friction model force-velocity characteristic

### 3.3.2. Experimental Friction characterisation and LuGre model compensation

Breytenbach (2009) characterised friction in the 4S<sub>4</sub> system experimentally, by removing a suspension unit from the test vehicle, and subjecting it to prescribed displacement testing in a servo-hydraulic dynamic testing machine. The test setup replaced the valve block and accumulators of the 4S<sub>4</sub> system with two inter-connected 5 Litre accumulators and a valve block with large flow passages to negate viscous damping effects. The large accumulators ensured that the gas pressure variation over the total strut stroke was as small as possible. The larger gas volume allowed characterisation of friction at almost constant pressures. The gas and hydraulic fluid were separated in the accumulators by floating pistons. Pressures of the gas and oil in the system were measured with pressure transducers, while the force exerted by the suspension strut was measured using a load cell placed between a servo-hydraulic actuator and the 4S<sub>4</sub> strut.

The tests were conducted at pressures from 500kPa to 3000kPa in 500kPa intervals, with three different prescribed displacement signals. Two triangular displacement signals were used at increasing frequencies and different amplitudes. The triangular signals were used to investigate the friction force at constant velocities. A sinusoidal displacement input was also used to verify the LuGre-friction model generated against measured data. The experimental static friction characteristics are given in Figure 34. The friction model as generated by Breytenbach (2009) was never implemented on the co-simulation vehicle model, but only on the mathematical model used in his study.

(Co-simulation is used in this study where dynamic reactions to forces are modelled using MSC.ADAMS simulation software, while the prescribed forces and control and other phenomena are modelled using MATLAB and Simulink software packages. Co-simulation shares prescribed data as inputs or outputs at each simulation time step between the relevant packages used to construct the model.)



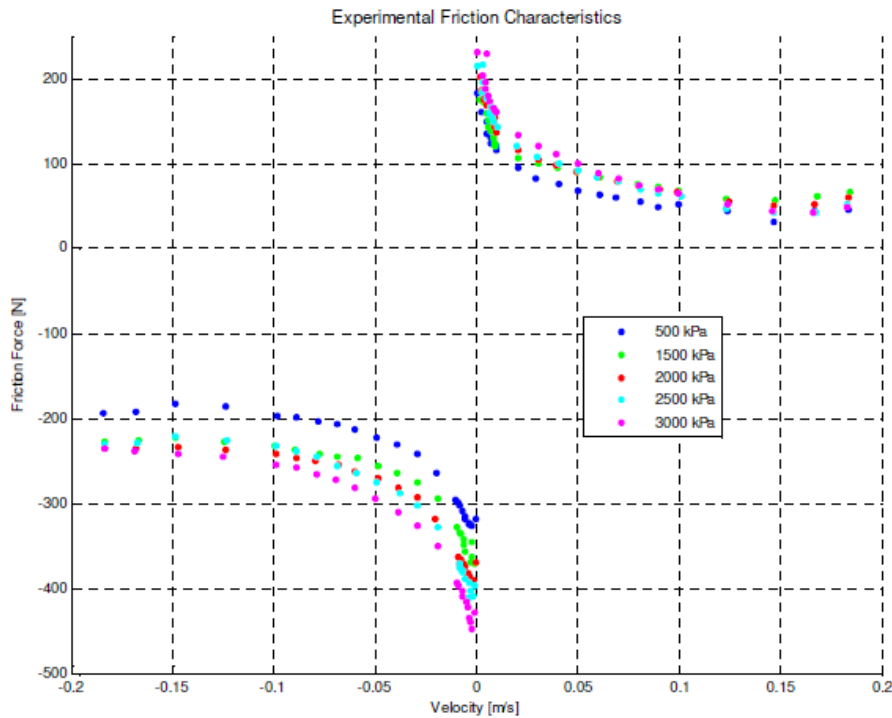


**Figure 34: Static Friction Characteristics for different pressures, Breytenbach (2009)**

A clear dependence between friction and strut pressure exists. Breytenbach (2009) concludes this is likely caused by hydraulic pre-loading of the seals in the system as pressure dependence is biased toward the compression cycle. The friction pressure-dependence in the working range of the system is however small enough to be negligible.

In the present study a LuGre model was fitted to the experimental static friction characteristic, this is shown in Figure 35. The coefficients used for the model are explained in Table 6, along with the values used to generate the model.

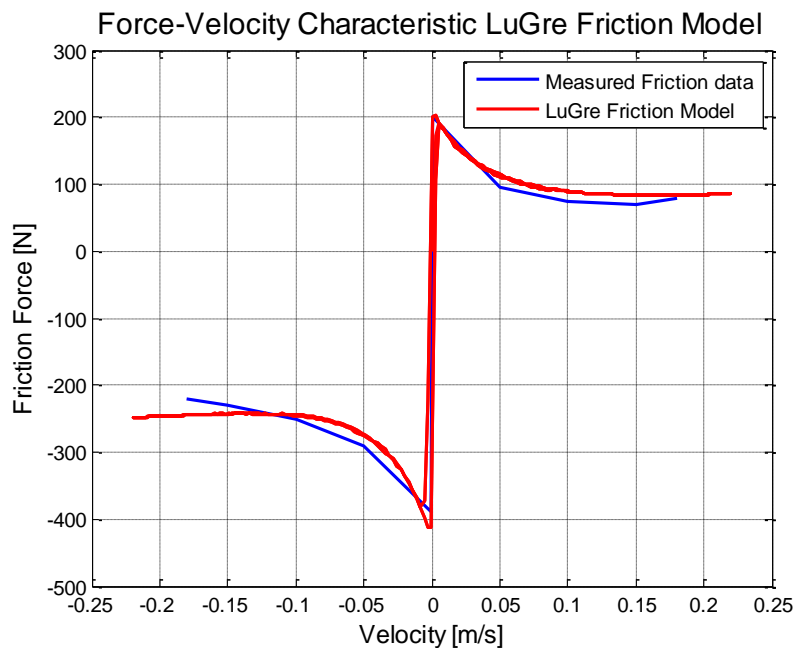


**Figure 35: LuGre friction model Force-velocity characteristic**

It is clear that the LuGre model shown in Figure 35 is a good approximation to the experimental static friction characteristic shown in Figure 34.

Table 6: Coefficient descriptions and values used for LuGre Friction Model

Coefficient	Description	Value		Units
		Positive range	Negative Range	
$F_s$	Maximum Static Friction Force	220	-450	$N$
$F_c$	Coulomb Friction Force	60	-215	$N$
$v_s$	Stribeck Velocity	0.04	-0.031	$m/s$
$n$	Exponent for Stribeck curve	0.849	0.849	-
$\sigma_0$	Bristle Stiffness	$10^8$	$10^8$	$N/m$
$\sigma_1$	Micro-Viscous Friction Coefficient	$10^4$	$10^4$	$Ns/m$
$\sigma_2$	Viscous Friction Coefficient	100	140	$Ns/m$

The model does not take pre-sliding or lubrication effects into account. We therefore expect to see pronounced peaks in the friction force upon velocity reversals.

### 3.3.3. Modified LuGre Friction Model

The popular LuGre model, originally developed by de Wit, et al. (1995), is based on modelling the frictional interface between surfaces as contact between bristles connected to each surface. The average bristle deflection between the two surfaces is used to model the friction. Yanada and Sekikawa (2008) proposed a lubricant film model be added to the LuGre model, giving rise to the Modified LuGre friction model. The Modified LuGre friction model implementation in the simulation model, based on the experimental friction characterisation originally conducted by Breytenbach (2009), is discussed in this section. The mathematical modelling of the Modified LuGre Model is discussed in section 2.6.4.

Due to the fact that friction in the 4S<sub>4</sub> system is non-symmetrical as seen in Figure 34, the model requires two coefficient sets, one for the positive velocity range, and one for the negative velocity range. The coefficients required as input to the model are summarised in Table 7, the resulting force velocity characteristic is shown in Figure 36.

Yanada and Sekikawa (2008) noted the switching criteria being based either on lubricant thickness or acceleration, did not greatly affect simulation accuracy for dynamic friction behaviours on the hydraulic cylinder used in their study. Due to the fact that lubricant film thickness is dependent on the time constant,  $\tau_h$ , it was decided to base switching on the acceleration characteristics. This was done to reduce the computational effort required to achieve switching. The switching criterion in this case thus depends on the velocity history between the two surfaces.

Table 7: Coefficient descriptions and values for Modified LuGre Friction Model

Coefficient	Description	Values		Units
		Positive Range	Negative Range	
$F_s$	Maximum Static Friction Force	220	-450	$N$
$F_c$	Coulomb Friction Force	60	-200	$N$
$v_s$	Stribeck Velocity	0.041	0.091	$m/s$
$n$	Exponent for Stribeck Curve	0.849	0.849	-
$\sigma_0$	Bristle Stiffness	$10^8$	$10^8$	$N/m$
$\sigma_1$	Micro-viscous Friction Coefficient for Bristles	$10^4$	$10^4$	$Ns/m$
$\sigma_2$	Viscous Friction Coefficient	100	140	$Ns/m$
$v_b$	Limit of velocity range where film thickness is varied	0.03	-0.03	$m/s$
$\tau_h$	Time constant for lubricant film Dynamics			$s$
$\tau_{hp}$	Time constant for Acceleration	0.033	0.033	$s$
$\tau_{hn}$	Time constant for Deceleration	2	2	$s$
$\tau_{h0}$	Time constant for Dwell period	10	10	$s$

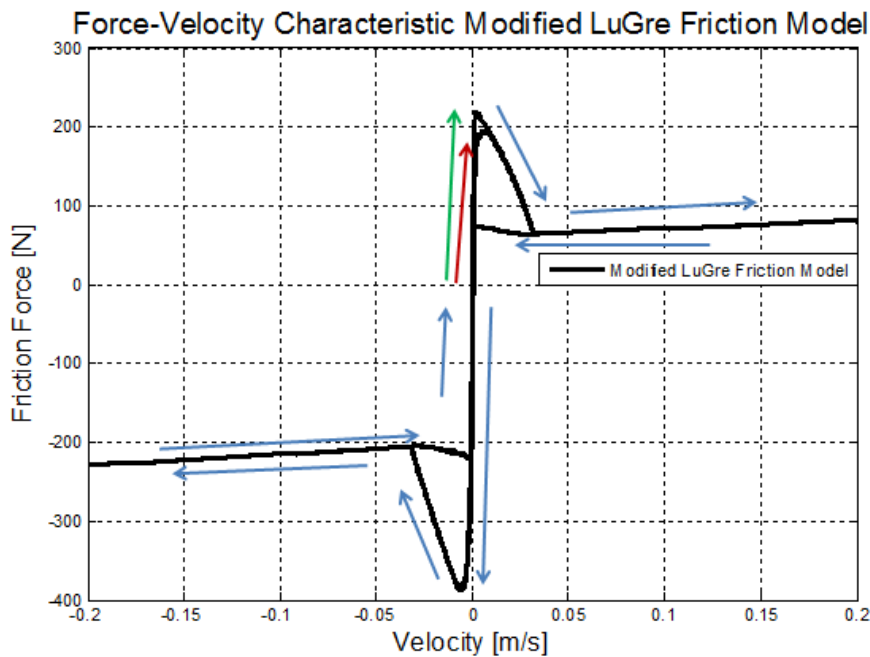


Figure 36: Modified LuGre Friction model Force-Velocity Characteristic

The green line in Figure 36 shows the start and peak friction level of the first cycle after a dwell period. The blue lines indicate the friction force behaviour for sinusoidal velocity inputs. The red line indicates the peak friction level for the second and subsequent cycles of the sinusoidal input.

It is clear that the friction force on the deceleration phase of a sinusoidal input, just before velocity reversal, is lower than the initial peak during the acceleration phase after a velocity reversal. This characteristic is due to the fluid film dynamics model included in the Modified LuGre Friction Model. It is the film dynamics model that gives rise, in part to the hysteretic nature of the model and is the main difference between this and the standard LuGre friction model. The size of the hysteresis loop in the model is controlled by the bristle stiffness. Lower bristle stiffness causes higher pre-sliding displacements, causing the hysteresis loop to be more pronounced.

### 3.3.4. Comparison of Friction models used for compensation

The three models considered each have distinct advantages and disadvantages. It is therefore wise to compare them against one another. In this section the three models will be compared using certain known time-varying inputs. Friction characteristics as well as computational time required for each model is compared.

Considering the characteristic proposed by Cronjé (2008), it is clear that friction is grossly overestimated; however, the implementation of the model is simple and computationally inexpensive. For this reason the revised rudimentary model was suggested, see Figure 33.

The LuGre model, suggested by Breytenbach (2009), is a commonly used model as it is easily implementable, is relatively accurate in the gross-sliding friction regime, and accurately models the Stribeck effect. It is however more computationally expensive than the rudimentary friction model due to the model requiring the numerical solution of a differential equation at each simulation step.

The Modified LuGre model is by far the most computationally expensive model of the three suggested. The computational expense is due to it depending on the numerical solution of two differential equations, one to model film dynamics and the other to model friction characteristics. The Modified LuGre model is however the only one of the three suggestions that takes pre-sliding displacement and lubrication effects into account.

The friction model correlation obtained by Breytenbach (2009), is shown in Figure 37. The displacement signal used was a  $0.025\text{ m}$  amplitude sine wave with increasing frequency.

Figure 38 shows the force characteristic comparison for the three models with a  $0.025\text{ m}$  amplitude sinusoidal input at a frequency of  $0.025\text{ Hz}$ . This frequency corresponds to the lowest frequency used in Figure 37. A comparison of the three friction models using a  $0.025\text{ m}$  amplitude sine wave displacement input with a frequency of  $0.95\text{ Hz}$  is shown in Figure 39.

The differences between force characteristics in the models are clear. The peaks shown by the LuGre and Modified LuGre model after velocity reversals are almost equal and are

independent of excitation frequency, while the peaks before velocity reversals differ due to the film dynamics model.

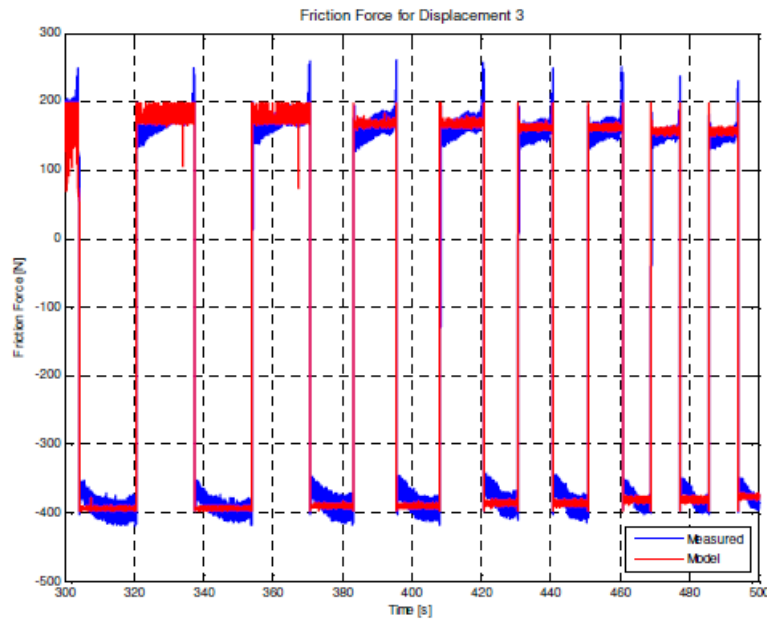


Figure 37: Friction Correlation from Breytenbach (2009)

The transition in the revised rudimentary model on velocity reversals is more gradual than that of the LuGre and Modified LuGre models for the 0.05 Hz displacement signal. The transitions for the 0.95 Hz displacement signal velocity reversals are as rapid as the LuGre and Modified LuGre model.

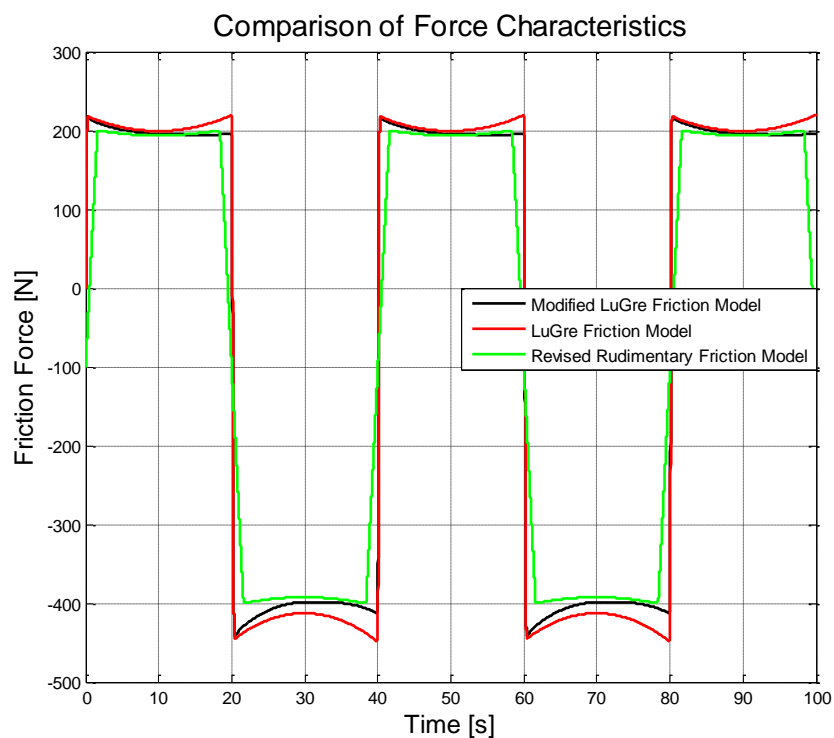
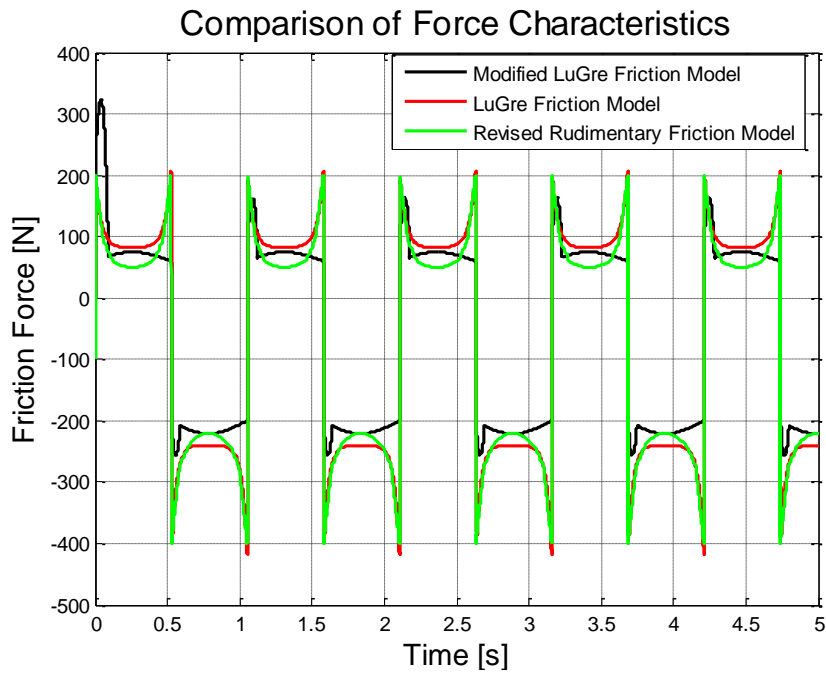


Figure 38: Comparison of Force Characteristics for three models investigated using 0.025m amplitude, 0.025Hz Sinusoidal displacement input



**Figure 39: Comparison of Force Characteristics for three models investigated using 0.025m amplitude, 0.95Hz Sinusoidal displacement input**

The peak friction forces for the revised rudimentary and LuGre friction model clearly stays the same cycle after cycle, whereas the Modified LuGre model shows a larger peak force on the first cycle, the subsequent cycles show a lower peak friction value, which stays constant like the rudimentary and LuGre model peaks. The effect of viscous damping in the Modified LuGre model, due to the lubrication model, is evident in the higher frequency investigation.

Figure 40 shows force-velocity characteristics of the three models for the 0.05 Hz displacement input.

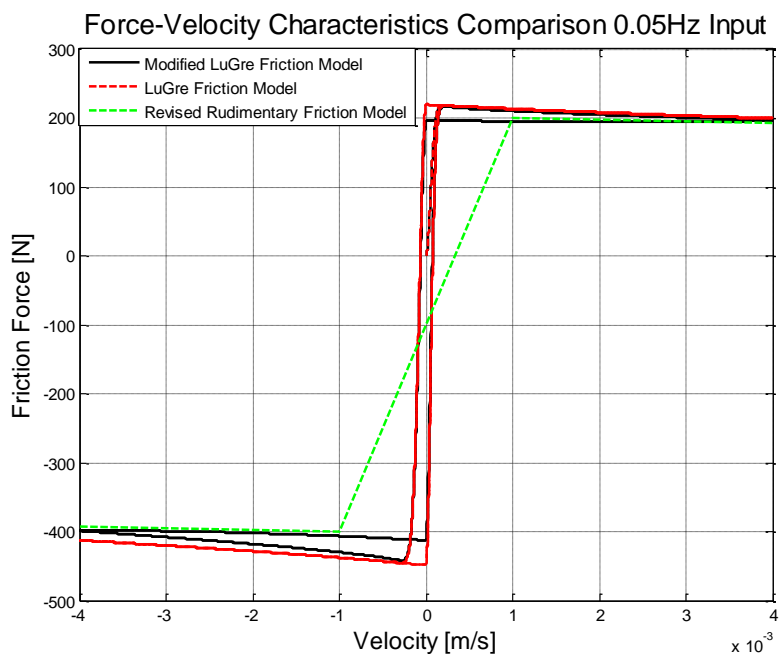


**Figure 40: Force-Velocity Characteristic comparison for 0.05Hz Sinusoidal displacement input**

The computational demand is of paramount importance when aiming to use the model for optimisation purposes, as is the case in many vehicle dynamics studies. To compare the computational expense between the three models, the time taken to model the frictional characteristic with the sinusoidal test input was measured. The table below summarises the times taken by each model to find the friction characteristic for the low frequency test input, i.e. the 100 s simulation data shown in Figure 38.

**Table 8: Comparative summary of time to model Friction**

<b>Model</b>	<b>Time to complete</b>
Revised Rudimentary model	11.300 s
LuGre Friction Model	131.129 s
Modified LuGre Friction Model	270.996 s

It is clear that the revised rudimentary model is by far the least computationally expensive, while the Modified LuGre Model is the most computationally expensive. The reason for the computational expense in the case of both the LuGre and Modified LuGre friction models is the need to solve differential equations numerically. In the case of the Modified LuGre model the initial conditions required for the solution of the differential equations comes from the solution in the previous step, requiring a velocity and lubricant film thickness history stack.

### **3.4. Model Validation**

Physical test data from suspension characterisation tests conducted by Els (2006), was obtained and used to investigate and validate the gas modelling methodology as well as the friction models implemented. Tests on the vehicle were also conducted to capture the dynamic responses of the vehicle which may be used for vehicle characterisation. The severe Double Lane Change, and constant radius tests were chosen as they elicit dynamic and steady vehicle responses respectively. Dynamic and steady responses are vitally important when considering frictional effects, as well as gas modelling methodology on vehicle dynamics.

Validation of the gas model was conducted for the soft and stiff spring settings with the damper packs removed from the 4S<sub>4</sub> system. The data used for the validation of the gas model were obtained by testing one of the 4S<sub>4</sub> suspension units in on a servo-hydraulic test bench. Friction effects are added to the gas-model predicted force by making use of the Modified LuGre Friction model, and compared to measured force data. The model used during validation makes use of measured displacement as input. The calculated force results are compared to measured forces on the strut.

Validation of the full vehicle model will be discussed for both the handling as well as ride comfort settings of the 4S<sub>4</sub> system. The models used for validation purposes use the measured steering, as well as velocity from the GPS system, as inputs for each simulation

manoeuvre. Validation of the suspension forces, suspension displacements, roll angle, and roll rate is achieved by comparing these parameters to the data measured during testing. The models validated use the Isothermal, Adiabatic and Thermal-time constant Ideal Gas approaches to modelling the spring force respectively. The adiabatic approach is expected to show better correlation for dynamic manoeuvres like the Double Lane Change, where suspension displacement frequencies are relatively high. The isothermal approach is expected to show better correlation for steady manoeuvres like the Constant Radius test, where suspension displacement frequencies are relatively low.

The validation is handled in sub-sections for the different models and manoeuvres investigated, as well as the different suspension settings. The first sub-section handles validation of the gas spring-displacement models, while the second sub-section handles the validation for the full vehicle model doing a severe Double Lane Change, the third sub-section handles validation of the full vehicle model for a Constant Radius Test.

### 3.4.1. Model Validation spring Force-Displacement Characteristics

The spring force-displacement characteristics modelled are validated against the measured characterisation data for the system. Characterisation of the spring force-displacement was conducted by Els (2006). Characterisation was conducted for both ride (soft) and handling (stiff), suspension settings, at various frequencies, with the damper-packs removed from the 4S<sub>4</sub> system.

Due to the difficulties that arise from qualitatively comparing different models, it was decided to base validation on the percentage relative-error (%RE) metric as proposed by Kat and Els (2012), given in the equation that follows.

$$\%RE = \left| \frac{Predicted - Measured}{Measured} \right| \times 100\%$$

The %RE is calculated for each data point compared to the corresponding measured data point. The mean relative error is calculated using all %RE values not equal to zero. Ignoring points where measured values are zero serves to remove undefined data points resulting from 0/0 operations: any 0/0 instances are replaced with zeros (i.e. measured value = 0, predicted value = 0, resulting in 0/0). The %RE is also limited, where infinite values resulting from 1/0 operations and errors larger than 100% are set to 100%. The probability of the %RE being smaller than the mean %RE, or a threshold value, is calculated by comparing each %RE to the mean %RE, or threshold. If the %RE is smaller than the reference, it is noted; if it is larger it is ignored. The probability is obtained by dividing by the number of noted instances to the total number of non-zero %RE values.

The probability using the mean %RE is used to test the correlation between data sets. A low mean %RE with a high probability means the data sets correlate well, while a high mean %RE with a low probability means the data sets do not correlate well. The accuracy of data



is tested by using some threshold on the %RE to calculate probability, or a required probability to calculate a threshold %RE. A low threshold %RE with high probability means that the model is accurate, while a high threshold %RE with a low probability means that the model is not accurate.

The %RE metric will be used to compare the different gas model formulations with and without the effects of friction using both the mean %RE probability as well as threshold %RE probability metrics along with the mean %RE.

### 3.4.1.1. Soft Spring Force-Displacement Validation

The soft spring was characterised using triangular displacement inputs with frequencies from 0.01 Hz to 0.5 Hz. The displacement signal for the soft spring is given in Figure 41 that follows while the corresponding time values are given in Table 9.

Table 9: Corresponding Time Values for Soft Suspension Spring Displacement Input Signals

Signal Frequency [Hz]	T [s]	U [s]	V [s]	W [S]	X [s]	Y [s]	Z [s]
0.01 Hz	0	9	50	100	150	191	200
0.05 Hz	0	1.9	10	20	30	38.3	40
0.1 Hz	0	0.97	5	10	15	19.17	20
0.5 Hz	0	0.25	1	2	3	3.9	4

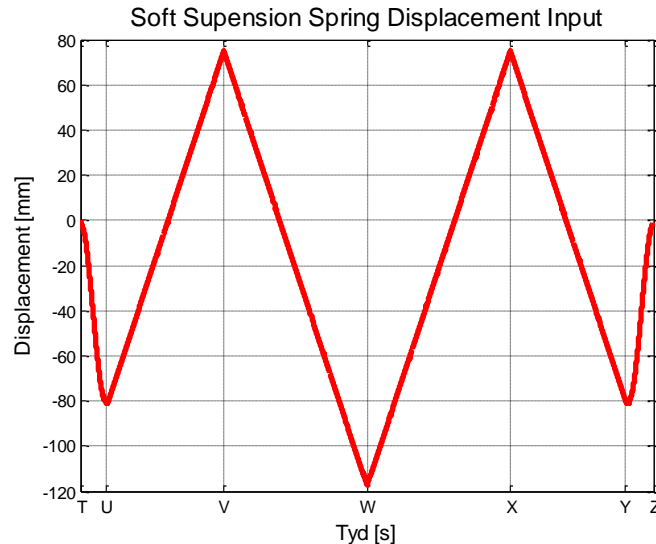


Figure 41: Soft Suspension Characterisation Spring Displacement Input

The force-displacement characteristics for the 0.01, and 0.1 Hz signals are shown in this section in Figure 42 and Figure 43 respectively. The aforementioned figures show the measured and modelled forces of the thermal time constant ideal gas formulation with and without friction effects against measured force data. The Force-displacement correlations shown in Figure 44 and Figure 45 show the predicted forces of the 0.01 and 0.5 Hz displacement signals for the Isothermal, Adiabatic and Thermal-time constant Ideal gas formulations respectively, each accounting for frictional effects.

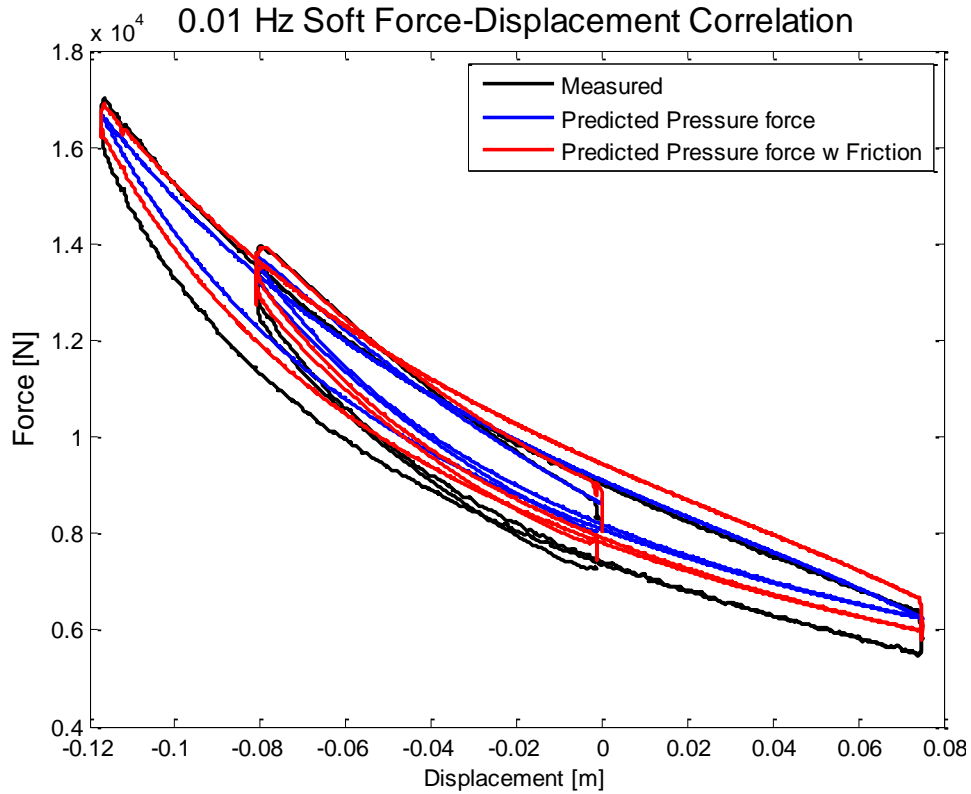


Figure 42: Soft Suspension, 0.01 Hz Force-Displacement Correlation, Friction effects

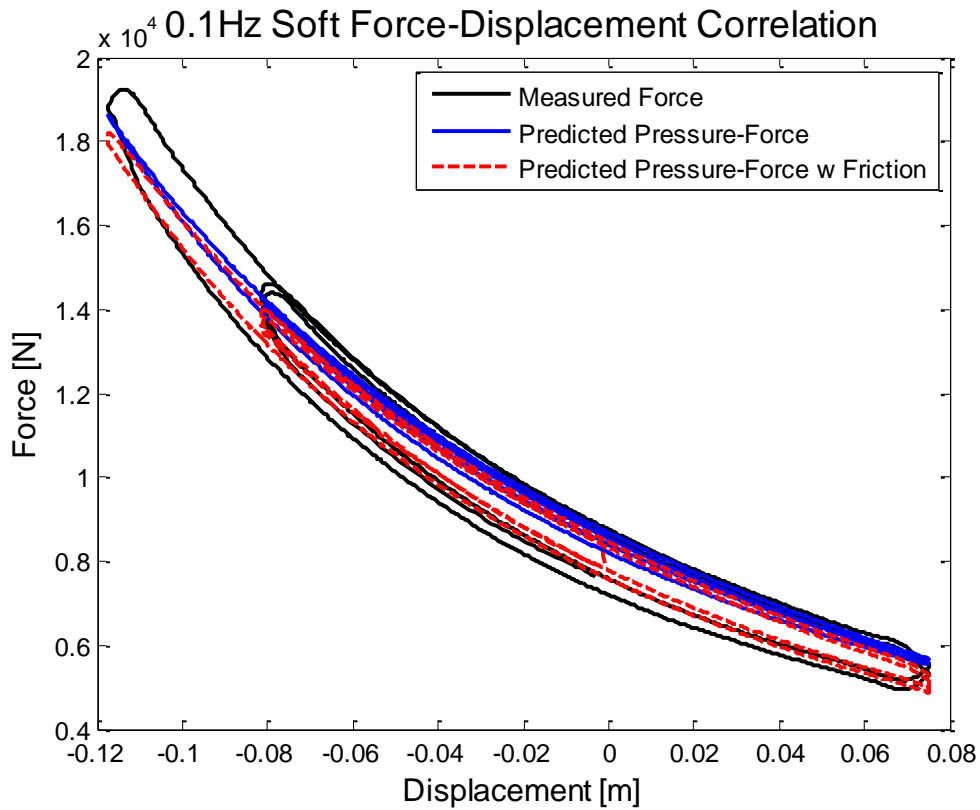


Figure 43: Soft Suspension, 0.1 Hz Force-Displacement Correlation, Friction effects

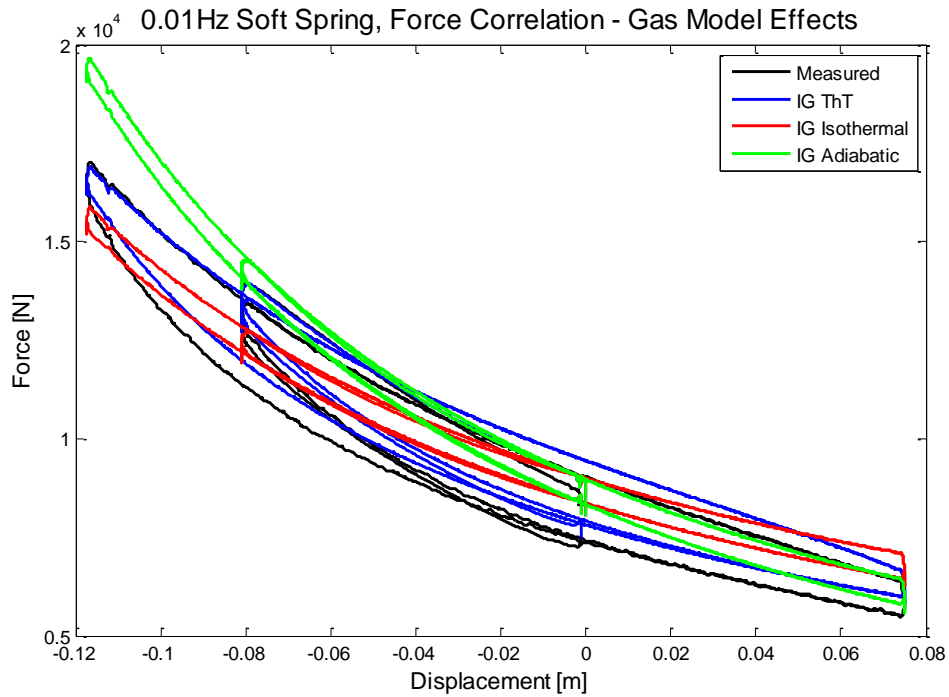


Figure 44: Force-Displacement Correlation 0.01 Hz Soft setting, Measured and Model reactions

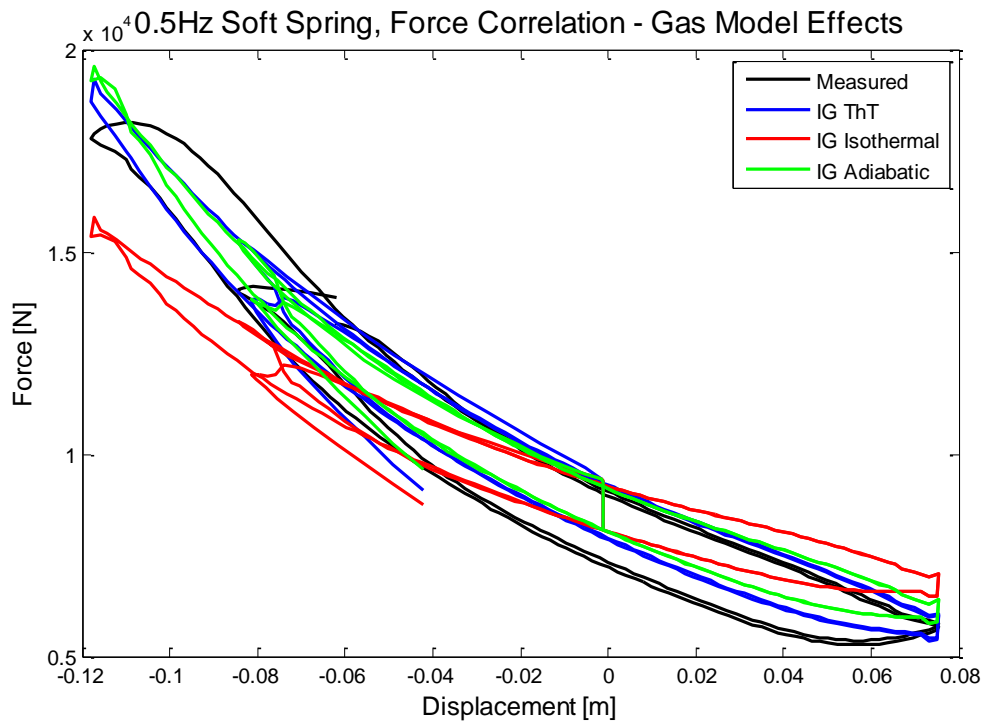


Figure 45: Force-Displacement Correlation 0.5 Hz Soft setting, Measured and Model reactions

The correlation of the modelled force with all the frequencies investigated is shown in Table 10, summarising the percentage relative error (%RE) and probability metrics for the model with and without friction compared to measured force. The threshold %RE and corresponding probability is given for each.

Comparing the correlation results in Table 10, it is clear that the case where friction is taken into account yields superior correlation to the measured results for all three permutations

of the Ideal Gas model. Including friction effects lowers the mean %RE as well as improving the threshold %RE probability. Comparing the three gas model implementations shows the Thermal time constant model, as expected, yields the best correlation considering the entire range of frequencies investigated. At the lower frequencies the isothermal model yields better correlation than the adiabatic model, while this is reversed at higher frequencies.

Table 10: Force Correlation Comparison with and without Friction for Gas Models Investigated (Soft Spring Setting)

Frequency	Gas Model	With/Without Friction	Mean %RE		Threshold %RE	
			M%RE	Probability %	Threshold	Probability %
0.01 Hz	Thermal TC	No Friction	4.70	51.47	5	51.99
		Friction	2.68	49.62	5	86.80
	Isothermal	No Friction	9.17	59.09	5	27.85
		Friction	7.07	52.07	5	22.55
	Adiabatic	No Friction	10.36	57.06	5	24.19
		Friction	7.74	49.87	5	36.41
0.05 Hz	Thermal TC	No Friction	6.63	51.88	5	54.03
		Friction	3.74	57.14	5	78.87
	Isothermal	No Friction	12.43	59.60	5	26.35
		Friction	9.57	53.49	5	27.73
	Adiabatic	No Friction	9.77	52.88	5	49.6
		Friction	6.48	59.09	5	54.09
0.1 Hz	Thermal TC	No Friction	6.08	55.65	10	71.4
		Friction	3.57	52.08	10	100
	Isothermal	No Friction	11.88	58.20	10	49.35
		Friction	9.64	52.98	10	54.98
	Adiabatic	No Friction	8.21	56.30	10	61.95
		Friction	4.94	54.03	10	88.94
0.5 Hz	Thermal TC	No Friction	10.59	56.3	15	71.75
		Friction	8.53	54.03	15	94.24
	Isothermal	No Friction	14.31	60.75	15	59.25
		Friction	12.29	57.39	15	63.66
	Adiabatic	No Friction	11.37	61.25	15	69.50
		Friction	8.66	62.16	15	90.48

The correlation for the thermal time-constant model is very good for most of the tested displacement range at the frequencies tested. At extreme compression and extension, it is seen that the Ideal Gas model deviates from the measured results especially at higher frequencies. The error at these extremes serves to drive the threshold %RE value higher (or decreasing the probability when considering a fixed threshold %RE). The breakdown of the Ideal Gas model at extreme compression is not unexpected. Otis and Pourmovahed (1985), states that it is a well-known fact treating nitrogen as an ideal gas at pressures above 200 bar, (20 MPa is the rated maximum design pressure for the 4S<sub>4</sub> system), can result in

significant errors. The 200mm peak to peak stroke used during the characterisation of the soft 4S<sub>4</sub> setting is around two times the maximum peak to peak displacement expected for the test manoeuvres to be used for this study.

### 3.4.1.2. Stiff Spring Force-Displacement Validation

The stiff spring was characterised using triangular displacement inputs with frequencies from 0.01Hz to 0.5 Hz. The displacement input signal for the 0.01Hz input is of the same form as those of the soft spring however the amplitudes correspond to those seen in Figure 46. Refer to Figure 41 and Table 9 for the input signal time values of the 0.01 Hz input. The signal for 0.05 Hz, 0.1 Hz and 0.5Hz inputs are shown in Figure 46, with the corresponding time values given in Table 11.

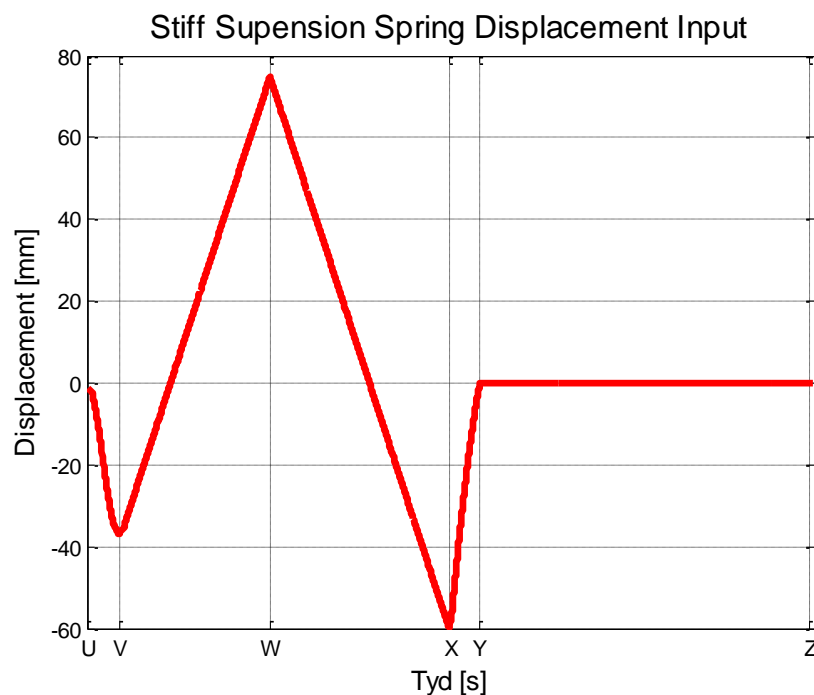


Figure 46: Stiff Suspension Characterisation Displacement Input

Table 11: Corresponding Time Values for Stiff Suspension Spring Displacement Input Signals

Signal Frequency [Hz]	U [s]	V [s]	W [S]	X [s]	Y [s]	Z [s]
0.05 Hz	0	1.8	10.09	19.94	21.63	40
0.1 Hz	0	0.94	5.09	9.97	11.62	20
0.5 Hz	0	0.24	1.08	2.08	3.08	4

The spring force-displacement characteristics for the 0.01, and 0.1Hz signals are shown in this section in Figure 47 and Figure 48 respectively using the Thermal-time constant Ideal gas formulation. The force-displacement correlations shown in Figure 49 and Figure 50 show the predicted forces of the 0.01 and 0.5Hz characterisations Isothermal, Adiabatic and Thermal-time constant Ideal gas formulations respectively, each accounting for frictional effects.

The force correlation of the model with all the frequencies investigated is shown in Table 12, summarising the percentage relative error (%RE) and probability metrics for the model with and without friction to measured data. The threshold %RE and corresponding probability are also shown.

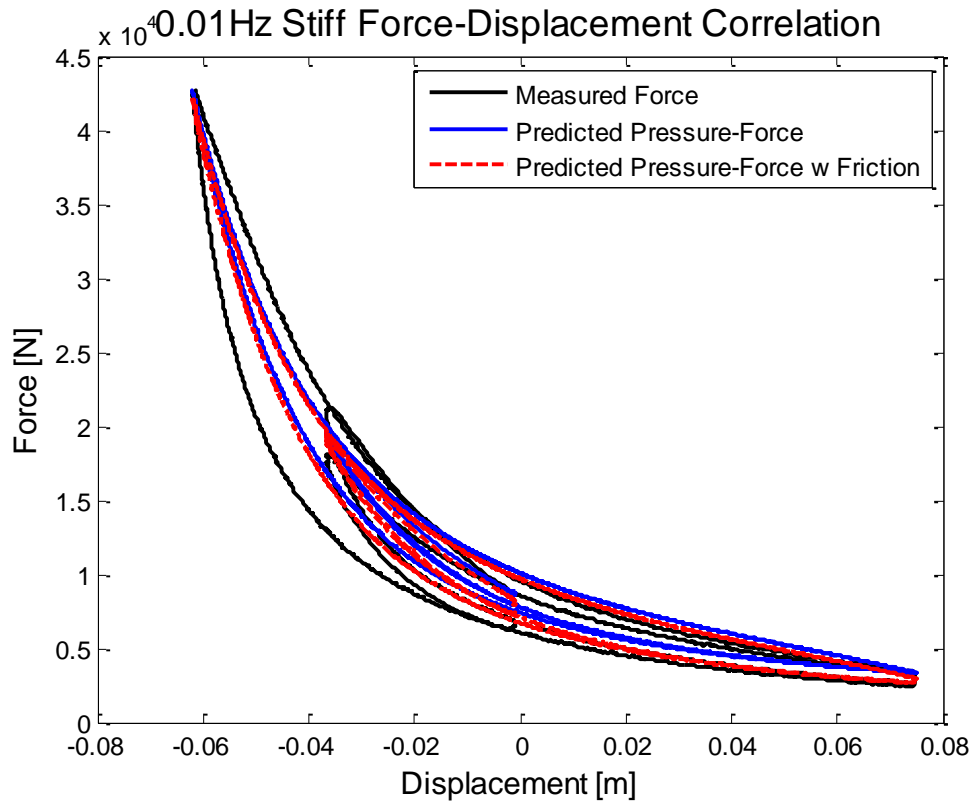


Figure 47: Stiff Suspension, 0.01Hz Force-Displacement Correlation, Friction effects

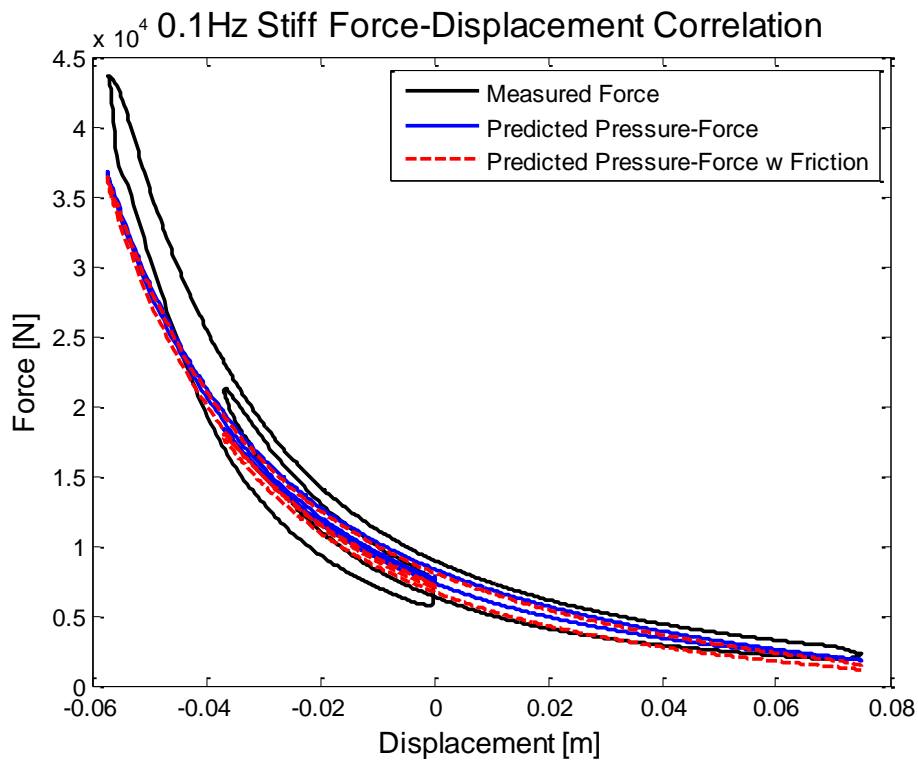


Figure 48: Stiff Suspension, 0.1Hz Force-Displacement Correlation, Friction effects

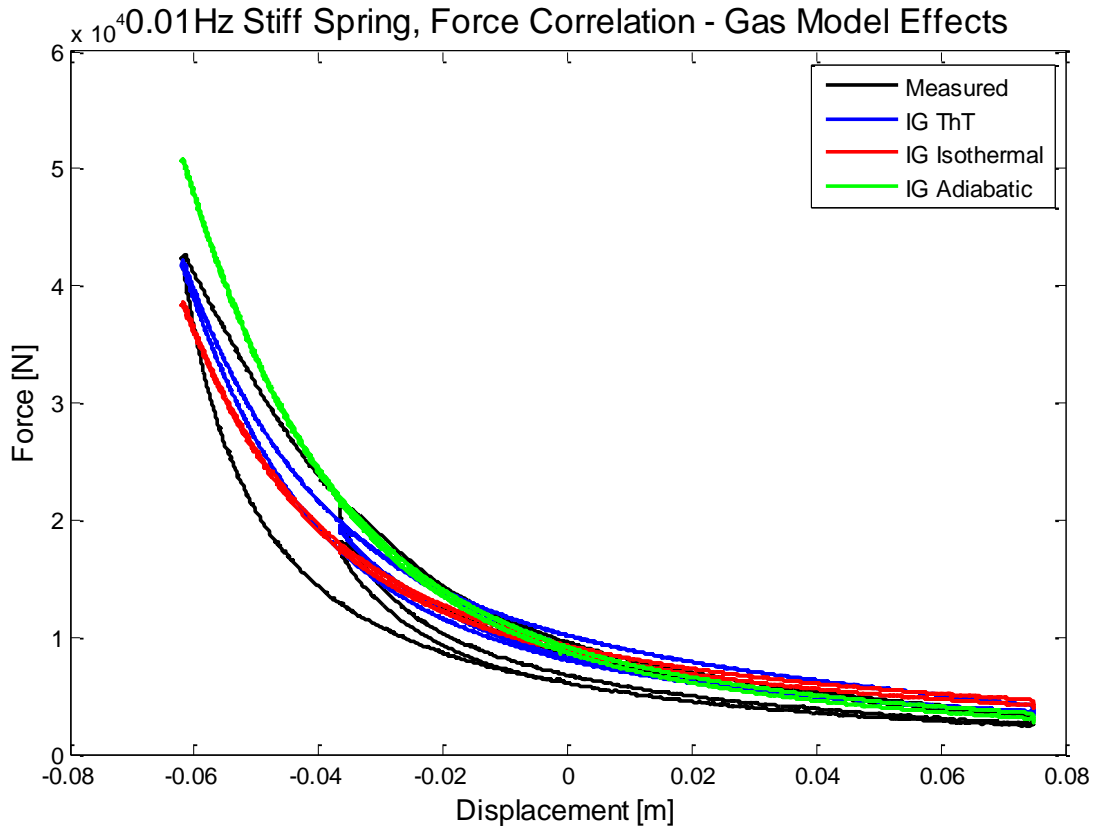


Figure 49: Force-Displacement Correlation 0.01Hz Stiff setting, Measured and Model reactions

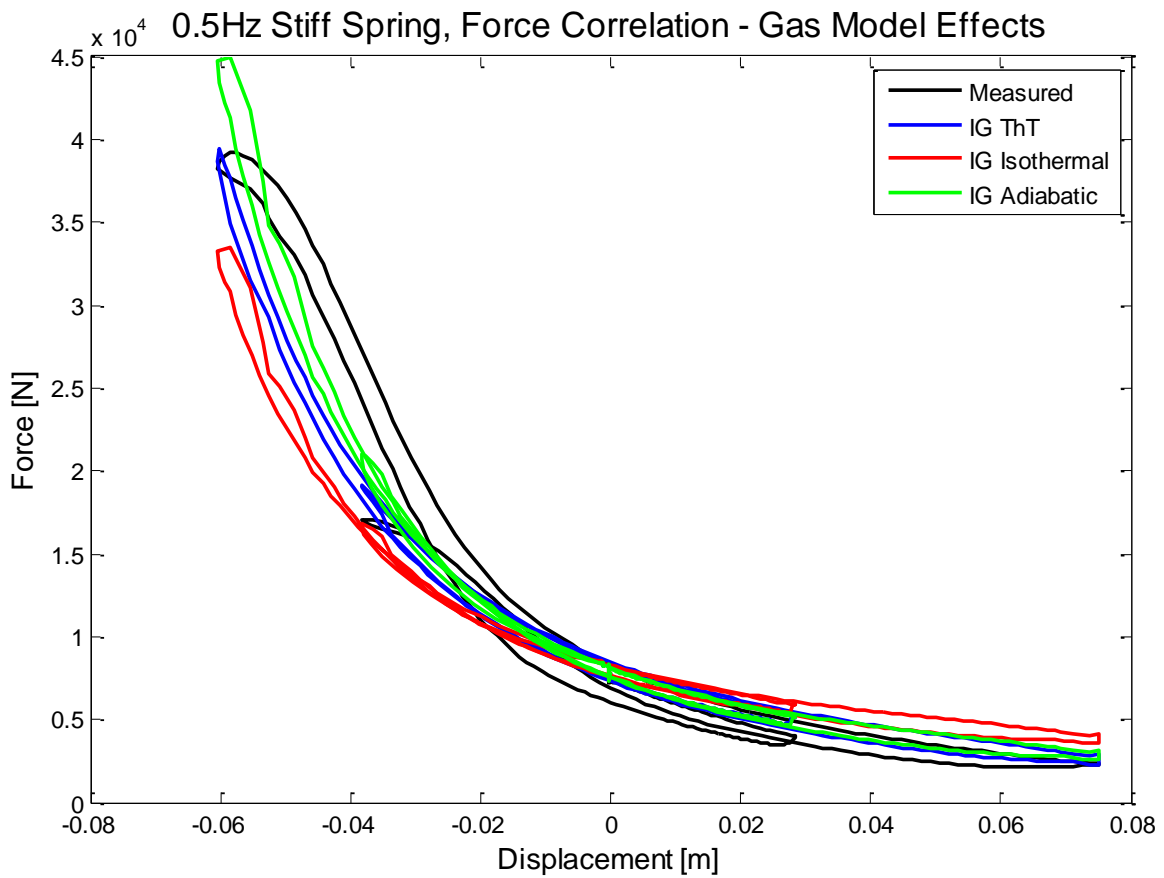


Figure 50: Force-Displacement Correlation 0.5Hz Stiff setting, Measured and Model reactions

The effects of friction on the stiff suspension setting are not as clear as on the soft suspension setting, although ignoring friction does affect the correlation of the data. The correlation of the stiff suspension measured data with the gas model permutations investigated are visibly worse than the correlation obtained with the soft suspension setting. It is however within reasonable error bounds. If considering the peak-to-peak displacement input used during characterisation, compared to the peak-to-peak displacement expected during physical testing, the errors in the operational displacement range are acceptable.

Table 12: Force Correlation Comparison with and without Friction for Gas Models Investigated (Stiff Spring Setting)

Frequency	Gas Model	With/Without Friction	Mean %RE		Threshold %RE	
			M%RE	Probability %	Threshold	Probability %
0.01 Hz	Thermal TC	No Friction	16.71	53.09	10	26.23
		Friction	8.60	56.46	10	68.34
	Isothermal	No Friction	24.66	59.15	10	29.46
		Friction	17.81	50.75	10	35.23
	Adiabatic	No Friction	20.1421	60.14	10	33.56
		Friction	16.38	57.51	10	38.18
0.05 Hz	Thermal TC	No Friction	11.82	64.83	10	55.03
		Friction	9.75	63.79	10	64.77
	Isothermal	No Friction	20.45	62.03	10	37.58
		Friction	14.32	58.46	10	50.34
	Adiabatic	No Friction	15.15	56.85	10	40.70
		Friction	10.38	57.71	10	56.19
0.1 Hz	Thermal TC	No Friction	14.84	56.60	15	57.70
		Friction	10.99	56.88	15	71.89
	Isothermal	No Friction	23.67	64.85	15	42.15
		Friction	16.60	61.23	15	57.98
	Adiabatic	No Friction	16.51	62.20	15	54.00
		Friction	10.23	49.72	15	66.43
0.5 Hz	Thermal TC	No Friction	15.36	56.25	15	55.25
		Friction	12.24	56.64	15	63.41
	Isothermal	No Friction	30.81	58.00	15	33.75
		Friction	24.28	53.88	15	36.59
	Adiabatic	No Friction	18.53	60.25	15	53.00
		Friction	12.30	54.39	15	61.15



### 3.4.2. Model Validation Severe Double Lane Change

The severe Double Lane Change test manoeuvre was conducted at 60, 70, and 80 km/h during physical testing on both the handling and ride-comfort settings of the 4S<sub>4</sub> suspension system. Simulations were conducted using vehicle properties as measured during testing. The steering angle, suspension displacements, suspension strut-pressures, longitudinal lateral and vertical accelerations of the centre of Mass, GPS coordinates of the path, and vehicle velocity were among the variables measured during testing. The measured velocity, steering angle, were used as inputs to the simulation model, while the static suspension strut pressures were used to set the simulation models starting suspension parameters.

#### 3.4.2.1. Double Lane Change, Ride-comfort setting Validation

The model is validated in the time domain using both the Adiabatic and Thermal time-constant ideal gas law formulations, while accounting for friction in the suspension system. This is done as these models showed the best correlation at the higher displacement frequencies. Figure 51, shows the validation of the suspension displacements and roll-angle for the simulation model, including friction effects, against measured data for a 60 km/h Double Lane Change. The validation of the model for higher velocities can be seen in Annexure C-1: Higher Velocity Double Lane Change.

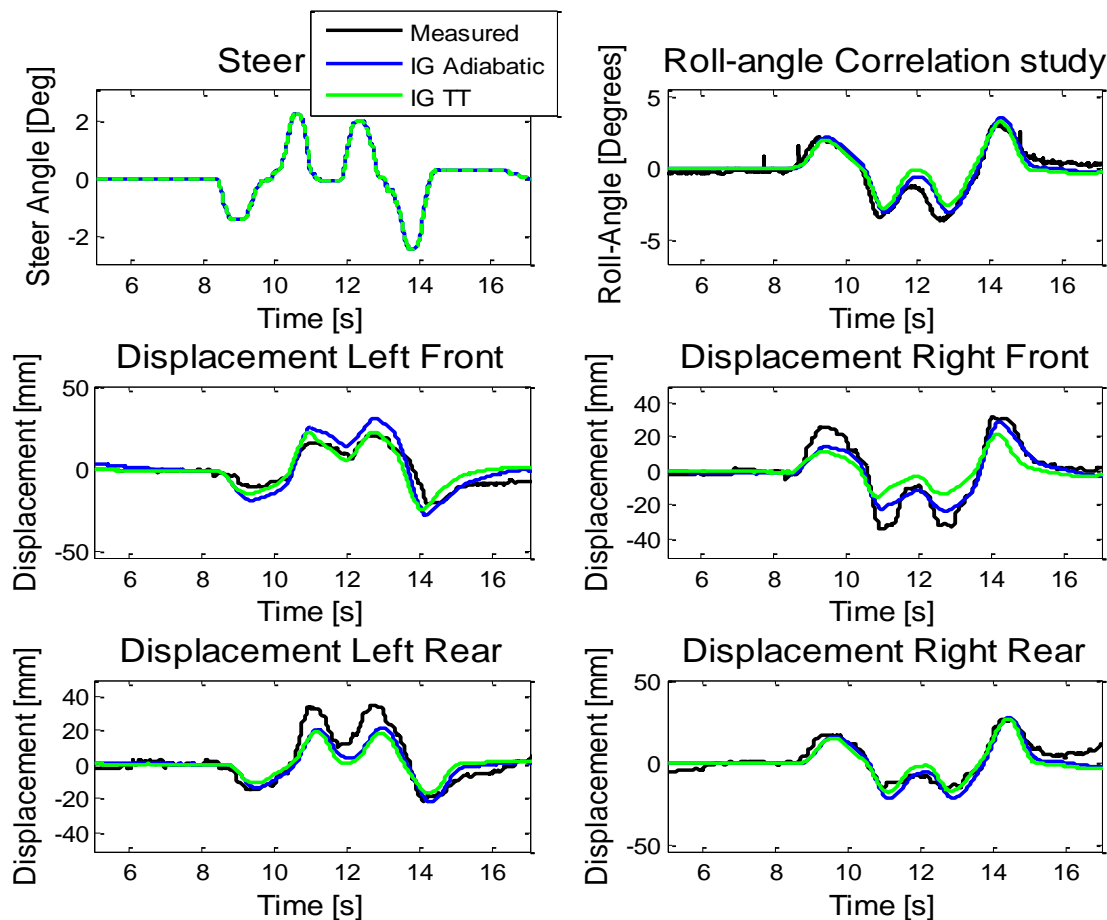


Figure 51: Soft Suspension Roll angle and Displacement Validation, Thermal Time Constant and Adiabatic models, Double Lane Change 60km/h

The roll angle is in very good agreement for both the Adiabatic as well as Thermal Time Constant ideal gas model approaches. The Adiabatic approach gives a very good correlation for the right rear strut in both compression and extension, whereas the left rear shows good correlation in the compression range. The Thermal Time Constant model gives better correlation for the front left, as well as the right rear suspension unit displacements compared to the adiabatic formulation. The differences visible between the two models are due to the heat transfer effects captured by the Thermal Time Constant model, compared to the case of no heat transfer for the adiabatic formulation.

Suspension force characteristic validation is shown in Figure 52 for the measured data, Adiabatic and Thermal Time Constant models. The measured forces for the front and right rear suspension units are re-constituted using the pressures within these struts during testing, while the left rear force was measured using a load-cell. The validation of the model for higher velocities can be seen in Annexure C-1: Higher Velocity Double Lane Change.

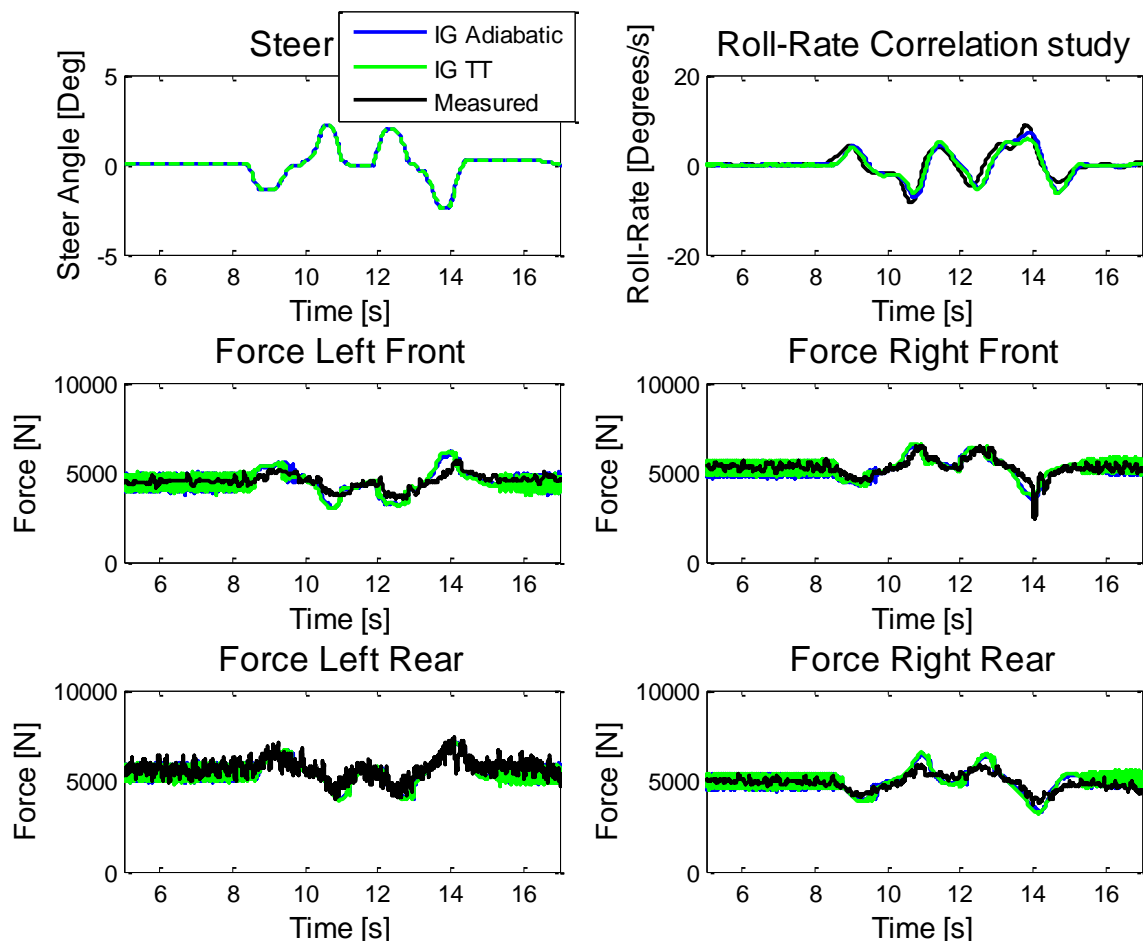


Figure 52: Soft Suspension Force and Roll rate Validation, Thermal Time Constant and Adiabatic models, Double Lane Change 60km/h

The suspension forces and roll rates for both models show good correlation with measured data. The force prediction in the models do suffer from some numerical noise in the steady state, this is due to the non-linearity in the Friction models, which makes it sensitive to changes in velocity around zero. There are minor differences in peak force predictions

between the Adiabatic and Thermal Time Constant models, although these are relatively small. There are visible discrepancies between the measured force and the simulation predictions for the front and right rear suspension units. This is due to the fact that the measured suspension forces are obtained using the measured pressure multiplied by piston area, thus neglecting the effects of friction in the measurements. The left rear suspension unit does not show this discrepancy as the force was measured using a load-cell. The two different measuring strategies are also clear in the measured data, where the load-cell data yields much “noisier” data compared to the pressure transducer data, due to the mechanical filtering effect of friction in the suspension. The force spikes visible in the measured data before and during the double lane change are suspected to be caused by casting lines in the concrete track at Gerotek Test Facilities, used for the vehicle tests. A phase difference is visible in the roll rate and roll angle in the simulation model when using the exact same measured steering input on the vehicle kingpin, this is suspected to be caused by the tyre model used in the simulation.

The suspension forces generally show a better correlation to measured results than displacements. Suspension forces are generally less sensitive to modelling methodology than the suspension displacements. The suspension displacements show clear differences between the Thermal Time Constant and Adiabatic Ideal gas model approaches. Suspension displacements are also very sensitive to changes in the Centre of Gravity (CG) height and lateral offsets. It is due to the uncertainty of the CG position, and the exact gas volumes in each suspension unit, that it is extremely difficult to obtain good correlation on all suspension units simultaneously.

#### ***3.4.2.2. Double Lane Change, Handling setting Validation***

The handling setting model is validated using both the Adiabatic and Thermal Time Constant ideal gas law formulations as they affect the suspension force characteristics. Figure 53, shows the validation of the suspension displacements for the simulation model against measured data for a  $60\text{km/h}$  Double Lane Change. The validation of the model for higher velocities can be seen in Annexure C-2: Higher Velocity Double Lane Change Stiff Suspension.

The Thermal Time Constant ideal gas model formulation again showed better correlation on the front left and right rear suspension unit displacements, as well as on the roll angle, compared to the adiabatic formulation. The left rear and right front suspension displacement correlations are not as good as the other two suspension units, although the correlation is acceptable for the purposes of this study. The clear differences between the reactions of the two gas model formulations are due to the heat transfer effect captured in the Thermal Time constant model, which affects the lateral load transfer of the vehicle also.

Suspension force characteristic validation can be seen in Figure 54 for the measured data, Adiabatic and Thermal Time Constant models. The measured forces in this case are all re-

constituted using the measured suspension pressures, therefore effectively ignoring the effects of friction. The validation of the model for higher velocities can be seen in Annexure C-2: Higher Velocity Double Lane Change Stiff Suspension.

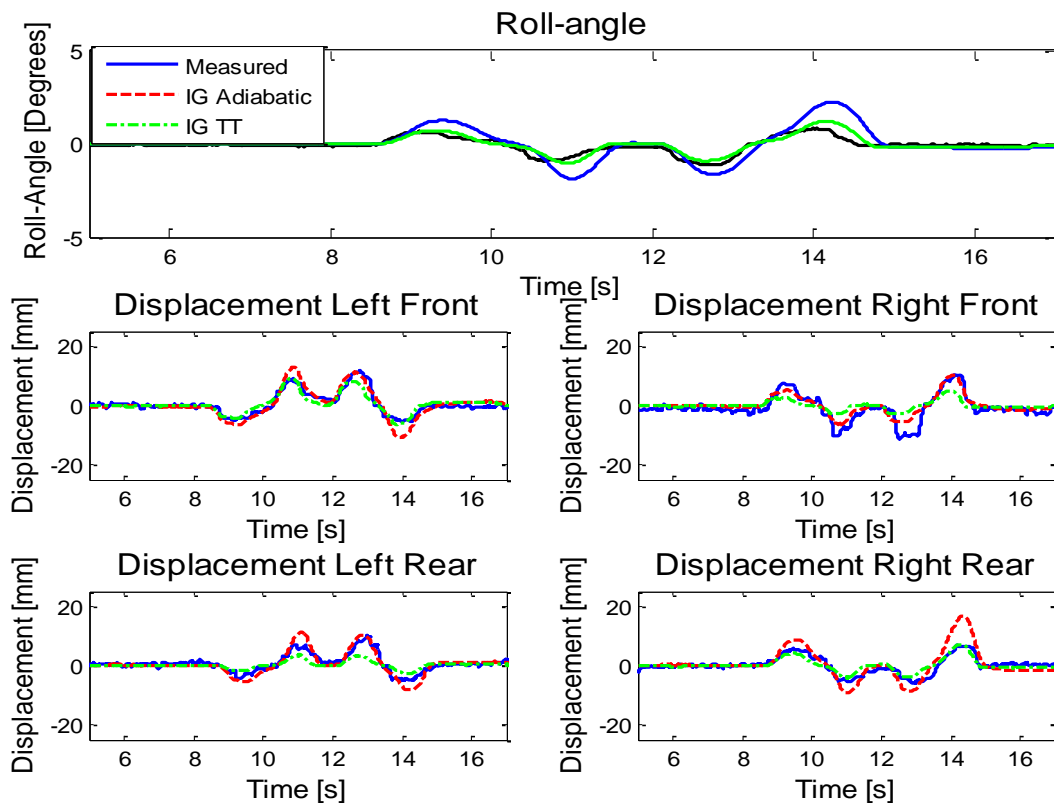


Figure 53: Hard Suspension Displacement Validation, Thermal Time Constant & Adiabatic, Double Lane Change 60km/h

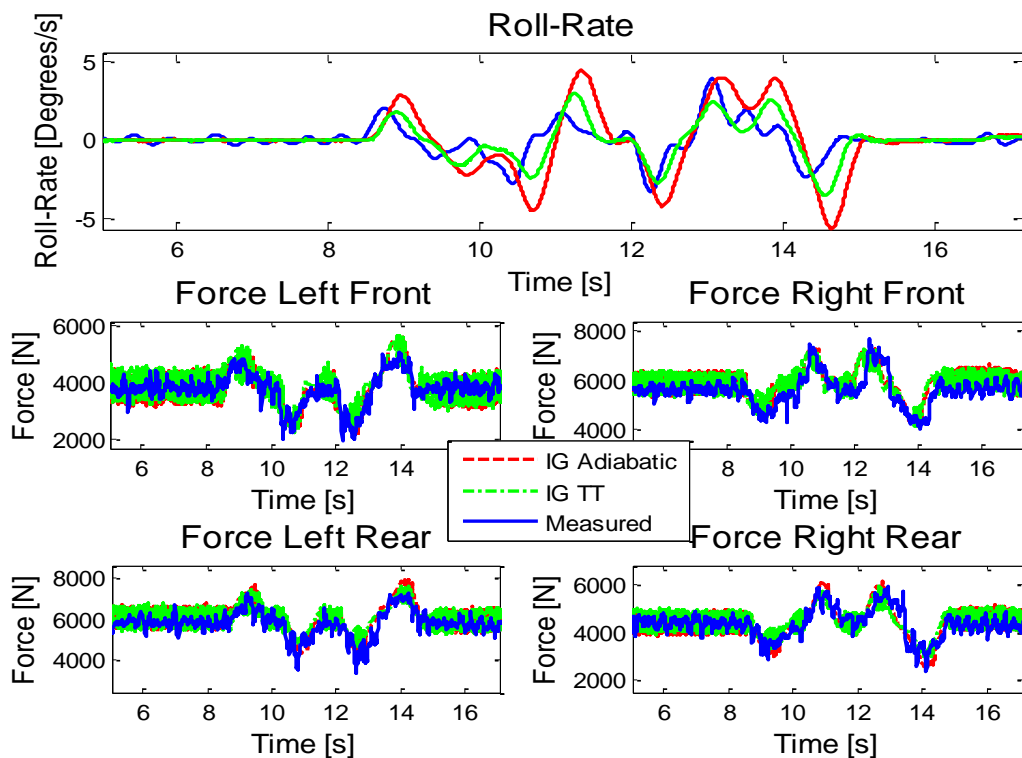


Figure 54: Hard Suspension Force Validation, Thermal Time Constant and Adiabatic models, Double Lane Change 60km/h

Suspension forces for both Thermal Time Constant and Adiabatic formulations show good correlation with one another. Forces in the simulation models do suffer from numerical noise in the steady, or close to steady, state. This is due to the highly non-linear nature of the friction model in the region of zero velocity included in the simulation. There are minor differences in force prediction between the two gas models, although both show excellent correlation with measured data. The roll rate predicted by the Thermal Time Constant model yields better correlation to measured results than that of the adiabatic gas model, this is especially visible on the negative roll rate peak values.

Suspension forces show a better correlation to measured data than suspension displacements. This is most probably due to the statically indeterminate nature of the model, which effectively balances the forces to reach a stable equilibrium point. Suspension forces are generally less sensitive to changes in the vertical Centre of Gravity (CG) position compared to suspension displacements. The CG Height is an important factor in the peak responses of the suspension displacements. The lateral CG offset has the capability of greatly affecting the suspension force, and load transfer characteristics. The discrepancies seen in the simulation model may be due to a number of factors, including the uncertainty of the exact CG position during testing, the exact gas volumes in the 4S<sub>4</sub> accumulators, as well as the shortcomings in the tyre model used.

### **3.4.3. Model Validation Constant Radius Test**

The constant radius test is only validated for the soft ride comfort setting in this section. It has been noted by Breytenbach (2009), that the soft suspension setting is more greatly affected by frictional effects than the stiff suspension setting. The effect of friction is more pronounced on the soft setting due to the low damping rate for the ride setting, the additional frictional damping affects the damping rate substantially.

The validation of the model is done for both the Isothermal and Adiabatic Ideal gas law formulations. The effects of heat transfer on suspension characteristics are clear from the validation of the Double Lane Change Manoeuvre with the two gas model formulations used there. Due to the fact that the constant radius test is subjected to low frequency displacement inputs, meaning closer to isothermal, it was decided to investigate the difference between the adiabatic and isothermal gas models in this section.

Figure 55, shows the correlation of displacements using a fixed axis limits for all four suspension units, facilitating direct comparisons between struts for the Constant Radius Test. The inputs to the simulation were the measured steer angle and velocity. Time is necessary in the simulation to allow settling to be able to compare steady state behaviour, therefore the correlation shown is limited to the last 5 seconds of the simulations.

Acceptable correlation between simulation and measured results are achieved for the suspension displacements and roll angle. The roll angle is effectively constant for the

manoeuvre as would be expected. The differences between the Adiabatic and Isothermal approaches are evident. The adiabatic approach under predicts displacement on all suspension struts. The isothermal approach gives more acceptable correlation on all suspension units. Roll angle correlation is excellent for the isothermal approach, while the adiabatic approach is clearly erroneous for this manoeuvre.

It is evident that the simulation model does under-estimate the displacement somewhat on the right hand suspension units. The roll angle does however give excellent correlation. This is due to the fact that the error in the total displacement between the left and right suspension units is acceptably small.

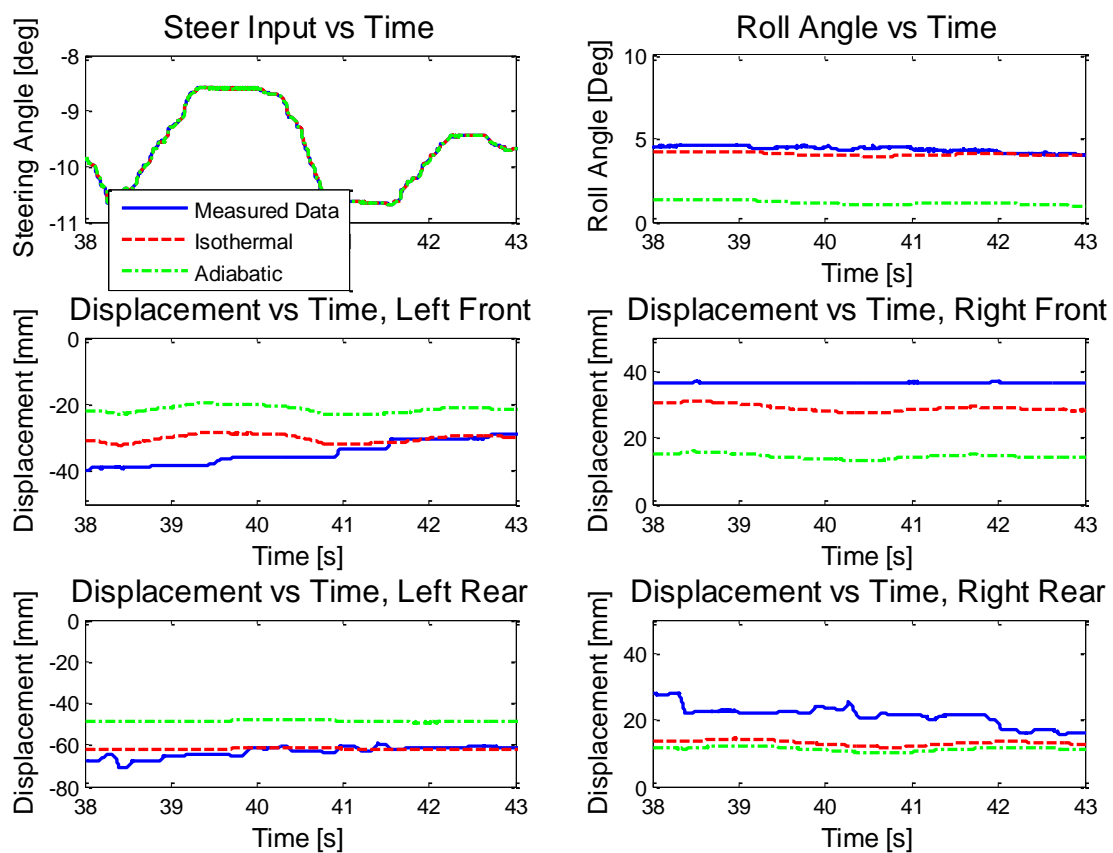
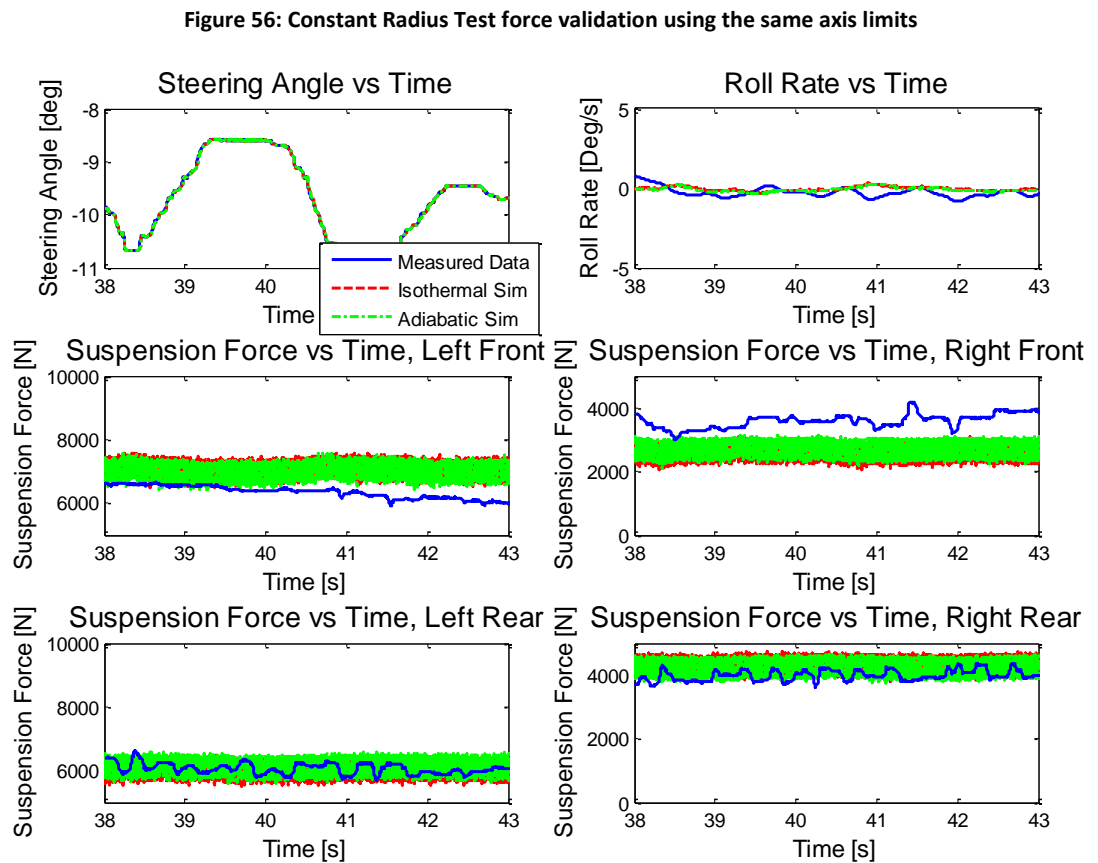
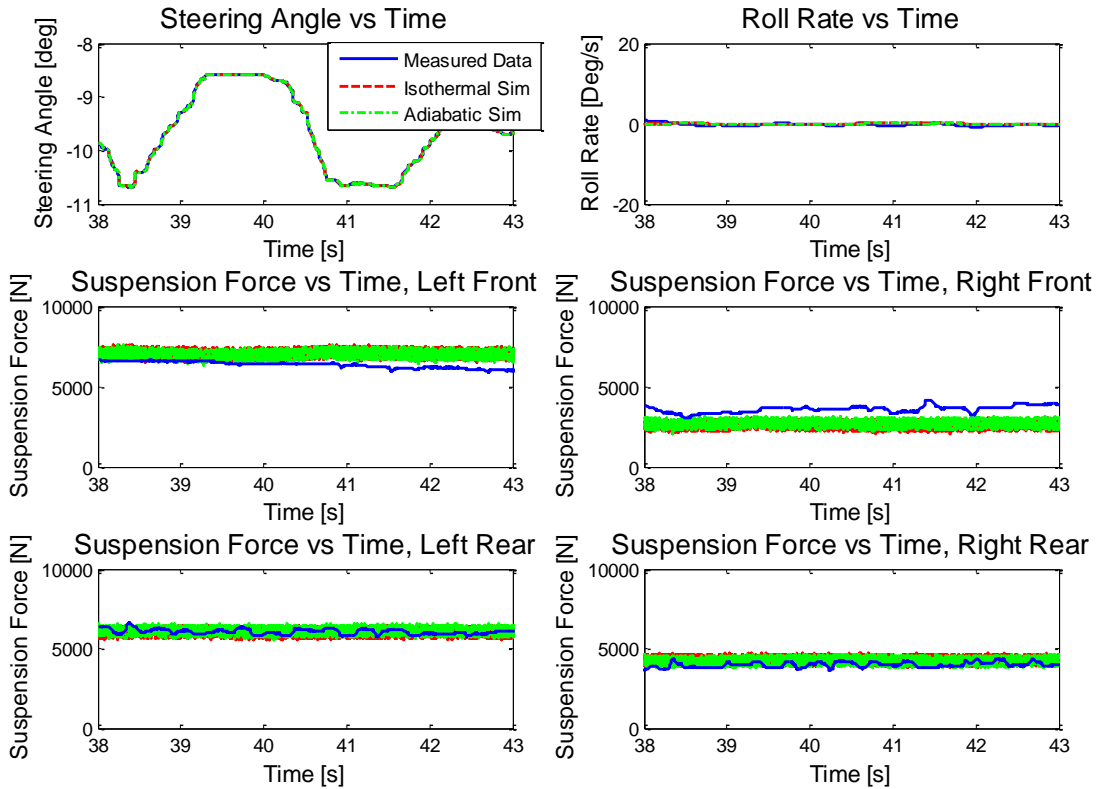


Figure 55: Constant Radius Test displacement validation using the fixed axis limits

Figure 56 shows the correlation of suspension forces and roll rate using a fixed axis limits for all four suspension units facilitating direct comparisons. Figure 57 shows a more detailed view (zoomed in view) of the suspension forces on each suspension unit as well as the roll rate.

Comparing measured and simulated results show good correlation between forces and roll rate. The front suspension forces are over-predicted on the left while being under-predicted on the right implying a lateral CG offset error in the front of the model. Rear suspension force and roll rate correlations are good. The measured and simulated roll rates are seen to be effectively zero as would be expected. The noise on the simulated suspension forces is due to the high non-linearity in the friction model near zero velocity.



### 3.4.4. Conclusion of Model Validation

The model as presented here shows a good correlation for the Double-Lane Change on hard and soft suspension settings, and also shows acceptable correlation for the Constant Radius Tests when compared to measured data. Suspension forces, displacements, as well as roll-angle and roll-rate (roll-velocity), have been presented for the ride and handling setting. The correlations between the measured and simulated results are acceptable for the parameters investigated.

The simulation model over-predicts displacements for certain suspension units, while it under-predicts displacements for other units. These discrepancies may be caused by a number of factors including the uncertainty of the CG position, uncertainty about the exact gas volume in the system accumulators, un-modelled friction in the joints of the simulation model, and possibly by shortcomings in the tyre model used during simulation. It is suspected, due to the over- and under-predicting nature of the discrepancies, that they are caused by a minor error in the CG position and gas volumes of the simulation model compared to the actual test vehicle.

Implementing the Ideal Gas model in Isothermal, Adiabatic or Thermal Time Constant form clearly affects suspension displacement dynamics as expected. Comparing the physical spring with the isothermal and adiabatic ideal-gas formulations, it is clear that the isothermal formulation yields a softer spring, while the adiabatic formulation yields a stiffer spring. The thermal-time constant model is somewhere between the two extremes (Isothermal and Adiabatic) and is frequency dependent, closer to the physical characteristic. The effect of the gas model implementation is much less noticeable when considering suspension forces due to the statically indeterminate nature of the model making the forces balance.

The Thermal Time Constant implementation of the Ideal Gas model showed better displacement correlation for the Double Lane Change for both ride and handling settings compared to the adiabatic formulation, while the Isothermal implementation showed better correlation for the Constant Radius Tests compared to the adiabatic formulation. The Thermal Time Constant Ideal Gas model showed much better correlation and accuracy compared to both Isothermal, and Adiabatic formulations across the entire characterisation frequency range.

The simulation model was validated while taking account of friction in the suspension system. The simulation results presented in the next chapter investigates the effects of different gas and friction models on the dynamic vehicle responses. The computational effort for the full vehicle model with the different gas models and friction compensation strategies will also be investigated.



## 4. Simulation Results and Discussion

The simulation results shown in this section shows the effects of different modelling methodologies pertaining to friction modelling as well as gas-spring modelling. The modelling methodologies are investigated to see the effects of the different approaches.

The first subsection is dedicated to the effects of gas-spring modelling. The differences between accounting for and disregarding fluid compressibility are clear in Figure 29 and Figure 30. The differences between the isothermal, adiabatic, and thermal time-constant ideal gas modelling approaches, are clearly shown in the model validation section. The effects of the gas modelling methodology on simulation predicted results, the aim of this section, will be handled for the following instances of the ideal gas model: Isothermal, Adiabatic, and Thermal Time Constant formulations. The different gas model effects and their effects on vehicle dynamics simulations are discussed in this section. Effects of the bulk modulus on the isothermal and adiabatic modelling approaches are also shown in this section.

The effects of friction on simulation results and the various strategies of compensating for friction will be handled in the second subsection. The simulation model will be investigated for the following cases of friction compensation: no-compensation, rudimentary compensation (Lookup-table), LuGre compensation, and Modified LuGre compensation. The effects of the additional computational expense on the simulation model will also be discussed along with the effects of each friction compensation method.

### 4.1. Gas-Spring modelling Effects on Simulation

The gas model intrinsically affects the spring characteristic of the suspension system. The effects of the different approaches were clear during model validation although they were not discussed. Simulations using the same vehicle model, parameters and variables with the different gas model implementations are used to show the effect of each of the approaches. Although many of the simulations are similar the simulation results shown in this chapter were not previously shown or discussed in chapter 3.

The ideal gas model was used in the adiabatic, isothermal, and Thermal Time Constant formulation. The adiabatic and isothermal models are at the extremes of heat transfer, where isothermal implies perfect heat transfer, and adiabatic implies no heat transfer. In reality the reaction of the system is somewhere between these two extremes, this is modelled using the thermal time constant formulation.

#### 4.1.1. Simulation results: Gas-Spring Modelling effects on Simulation

The gas model not only affects the displacements on the simulated suspension strut responses, but also the simulated dynamic behaviour of the vehicle. The effect of the gas modelling approach is discussed for the Double Lane Change Manoeuvre and also for the

Constant Radius test. Model validation in section 3.4 suggests the Thermal Time Constant approach would be better suited to the Double Lane Change, while the isothermal approach is better suited for the steady Constant Radius Test when compared to the adiabatic approach respectively. The effects of the different approaches are presented for the two manoeuvres in the sub-sections that follow.

#### 4.1.1.1. Double Lane Change

The suspension force and displacement reactions of the vehicle simulation model, using the different gas modelling approaches, are compared in this section. The vehicle model parameters and suspension pressures remain consistent for each approach. The effect of the bulk modulus on the adiabatic ideal gas model formulation for the soft suspension for a double-lane change at 60km/h model is shown in Figure 58.

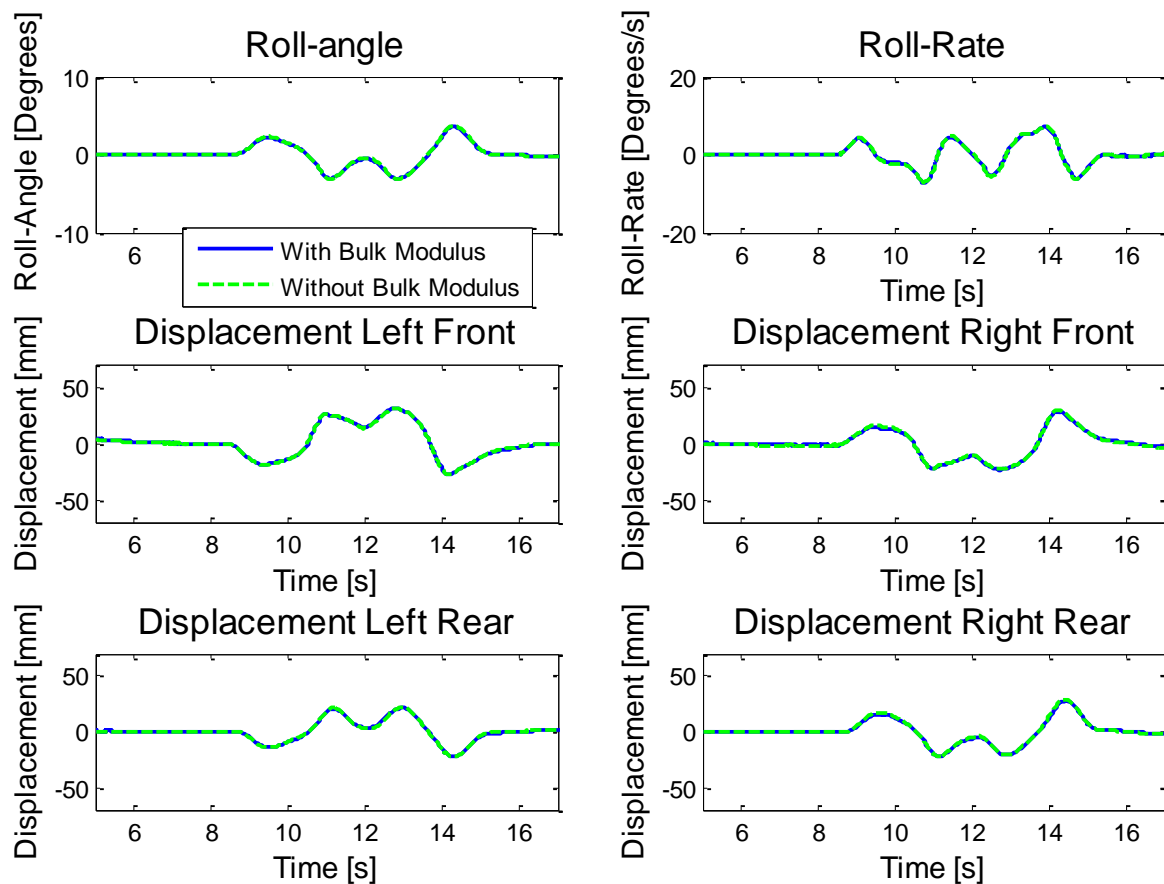


Figure 58: Bulk Modulus Effect on Soft suspension using Adiabatic Gas model

It is notable that the bulk modulus has no clearly discernable effect on the suspension displacements, roll rate, or roll angle dynamics when using the ride comfort setting of the 4S<sub>4</sub> suspension system for a double lane change. The bulk modulus effect is only barely visible on the static suspension displacements (i.e. where the suspension struts have zero displacement during the manoeuvre, thus during the time interval of 6 s to 8 s) and on the peaks in suspension rebound. This is due to the relatively narrow displacement band excited during the dynamic manoeuvre.

The suspension displacements for a 60km/h double lane change on the soft suspension setting, using the Adiabatic, Isothermal, and Thermal Time Constant ideal gas models is shown in Figure 59.

The three gas models show clear differences in suspension displacements, roll angle, and roll rate. The isothermal gas model effectively yields a softer spring characteristic, translating to higher peak suspension displacements and roll angles.

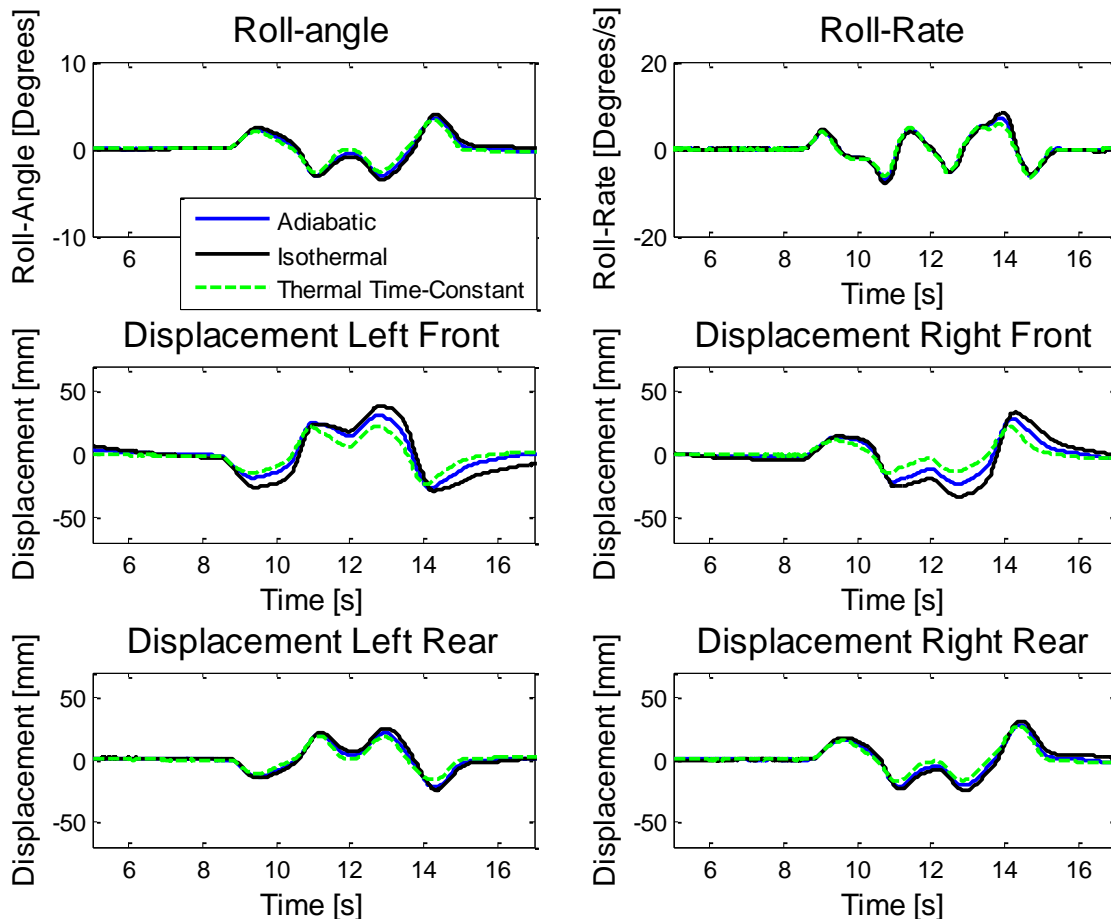


Figure 59: Comparison of Adiabatic, Isothermal, and Thermal Time-Constant gas models for Soft suspension

Interestingly, from simulation results it would seem that the Thermal Time-Constant model yields a stiffer spring characteristic compared to both the adiabatic and isothermal models. This indicates that the dynamics of the full vehicle model is most greatly affected by the suspension gas model used during simulation. It also shows the effect that heat build-up may have on suspension characteristics.

The effect of the bulk modulus on the adiabatic ideal gas model formulation for the stiff suspension model is shown in Figure 60 for a 60km/h Double Lane Change manoeuvre. The bulk modulus has a more pronounced effect on the stiff suspension compared to the soft suspension setting. Although the effect is not evident for the relatively low velocity (compared to the velocities at which tests were conducted) manoeuvre shown, higher velocity manoeuvres are subjected to more considerable Bulk-Modulus effects (consider

Figure 29 for Bulk Modulus Effect on Stiff-suspension displacement characteristic). The bulk modulus effectively softens the stiff suspension, causing higher displacements and larger dynamic peak responses, although these effects are not as pronounced in the figure shown due to the relatively small displacement range excited during dynamic manoeuvres.

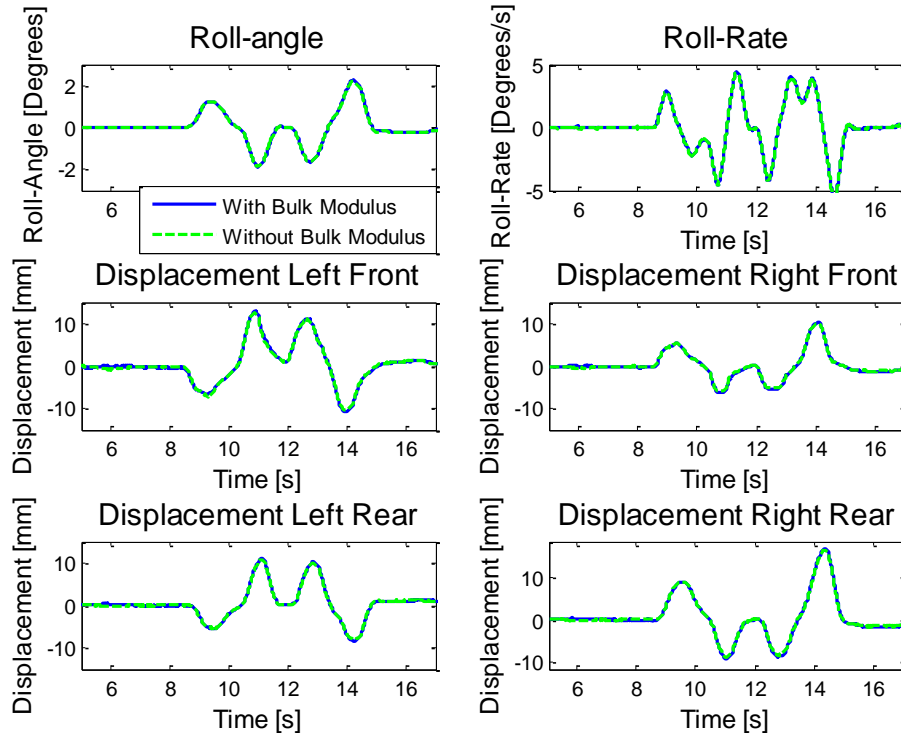


Figure 60: Bulk Modulus Effect on Stiff suspension using Adiabatic Gas model

The gas modelling approach in the simulation model has an appreciable effect on the vehicle dynamics for the handling setting of the 4S<sub>4</sub> system, as can be seen Figure 61.

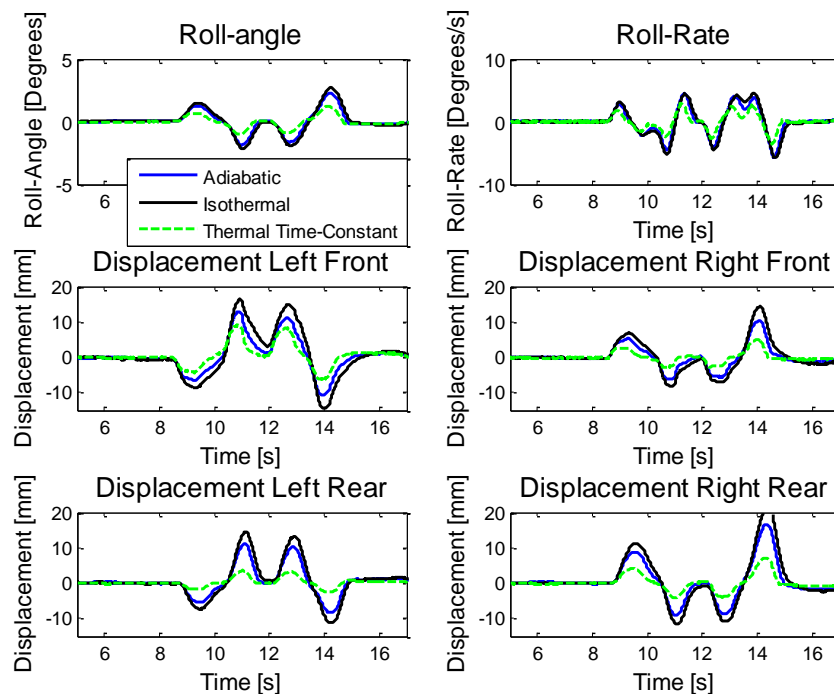


Figure 61: Comparison of Adiabatic, Isothermal, and Thermal Time-Constant gas models for Stiff suspension

The isothermal gas modelling approach again effectively yields a lower spring stiffness compared to the stiffness achieved when using the adiabatic or thermal time constant approach. The isothermal approach yields considerably higher dynamic response peaks in the extension range, while the compression cycle shows this phenomenon to a lesser extent. The thermal time-constant model, as with the soft suspension setting, seemingly yields a higher spring stiffness characteristic during simulation, compared to the isothermal and adiabatic formulations. This is once again an indication that the simulation model is highly sensitive to the gas modelling methodology and heat build-up in the suspension units.

#### 4.1.1.2. Constant Radius Test

Suspension force and displacement reactions for the vehicle simulation model for the isothermal and adiabatic ideal gas-model approaches are given here. The vehicle model parameters and suspension pre-load pressures are kept constant for all approaches.

Figure 62 shows the bulk modulus effect on the isothermal gas spring model for a constant radius test using the soft suspension setting.

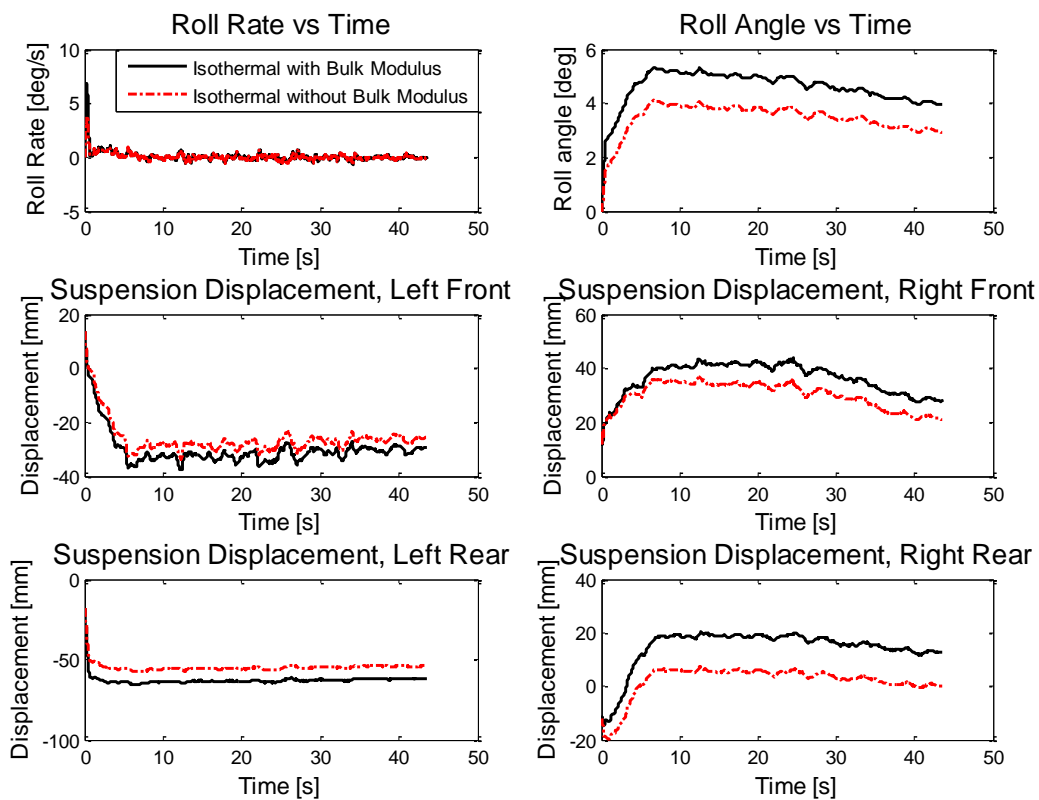


Figure 62: Bulk Modulus effect on Isothermal Constant Radius Test

Figure 63 shows a comparison of the adiabatic and isothermal gas spring models for a constant radius test using the soft suspension setting.

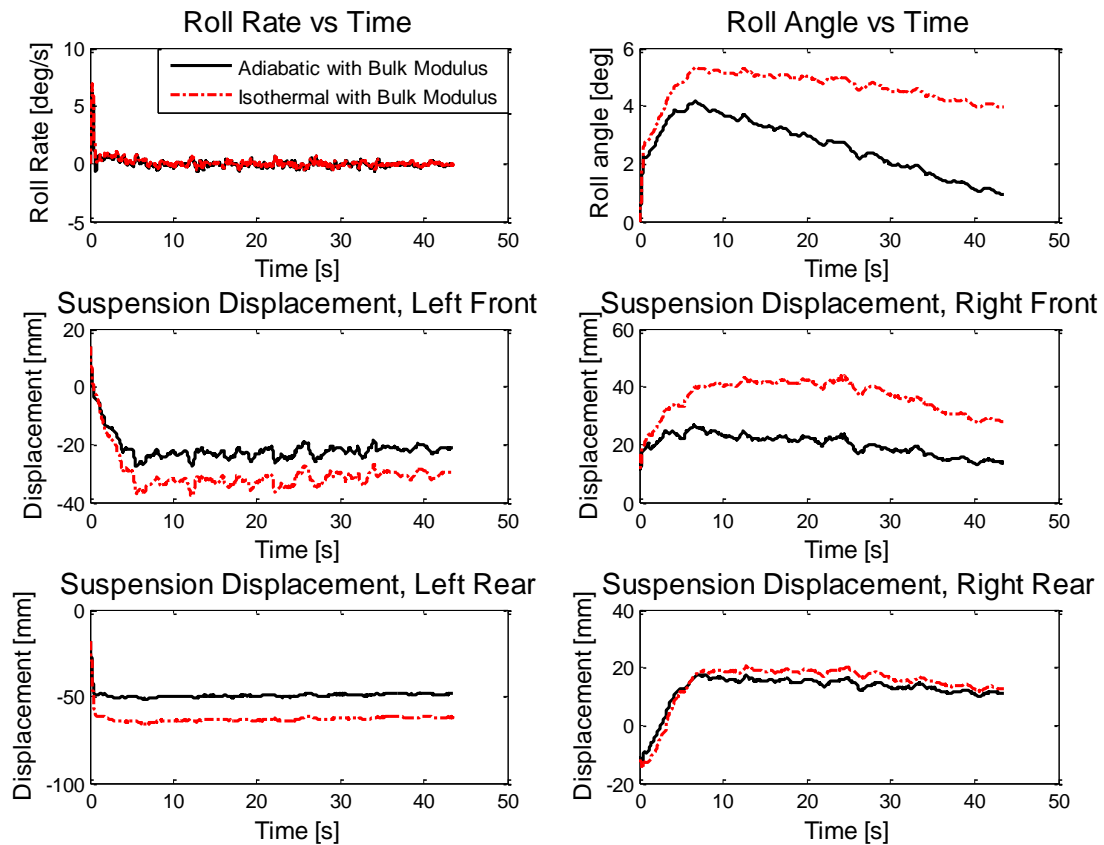


Figure 63: Adiabatic and Isothermal gas model effects on Constant Radius Test

The results shown indicate that the gas model is more notably affected by the bulk modulus effect in the suspension, especially the roll angle and suspension displacements, compared to the effect witnessed for a Double-Lane change. The more pronounced effect of the bulk modulus on the Constant Radius Test simulations, are simply due to the larger relative suspension displacements compared to those experienced during the Double Lane Change. It is also clear that the adiabatic suspension model yields much lower suspension displacements than the isothermal which is as expected as the adiabatic model effectively models a stiffer spring. The roll-rate shows very little dependence on the gas models and bulk modulus effect.

#### 4.1.2. Discussion: Gas-Spring Modelling Effects on Simulation

It is clear that the gas modelling approach affects the dynamic responses of the simulation model. The two sub-sections for discussion will be the effect of the bulk modulus and the effect of the gas modelling methodology.

##### 4.1.2.1. Bulk Modulus Effect

Assuming the bulk modulus effect is negligible, results in the suspension spring characteristics being merely defined by the gas model used. However, the bulk modulus characteristic of the oil yields some compressibility to the oil, effectively resulting in two

springs in series. The springs in series must physically have a lower spring rate than the lowest spring rate in the series of springs.

Assuming the bulk modulus effect is negligible and the working fluid is perfectly incompressible, results in lower suspension displacement compared to the case when taking bulk modulus effects into account. The change in spring rate also becomes non-negligible especially at higher velocity manoeuvres. Oil compressibility on the soft suspension setting is almost negligibly small when considering dynamic manoeuvres. This is due to the large difference in the spring stiffness characteristic between the oil and the gas and the relatively low suspension displacements. The effect of bulk modulus is clearly shown on the soft suspension simulation of the constant radius test, where the suspension displacements are considerably larger than those seen in the double-lane change.

The bulk modulus effect is not negligible for the stiff suspension setting. The effect of oil compressibility on the hard suspension setting is more pronounced due to the fact that the spring stiffness is much higher compared to the case of the soft suspension spring setting. The bulk modulus effect is again not clearly noticeable for manoeuvres with relatively low strut velocities, refer to Figure 60, but with manoeuvres with higher strut velocities the effect becomes much more pronounced and not including this can lead to major simulation errors.

#### ***4.1.2.2. Thermal time constant, Adiabatic, and Isothermal Ideal Gas modelling effects***

The adiabatic, isothermal and thermal time-constant ideal gas model approaches have an appreciable effect on both the ride and handling suspension setting simulation results of the 4S<sub>4</sub> system. Most notably on the simulated suspension displacements and computational time required to complete each simulation. Due to the perfect-heat transfer characteristic of the isothermal approach, the spring stiffness is seen to be lower than the adiabatic case, resulting in larger dynamic suspension displacements compared to the adiabatic and thermal time-constant approach on both ride and handling settings. The adiabatic formulation, where no heat transfer takes place, results in a stiffer spring characteristic when compared to the isothermal and Thermal Time Constant formulations (as seen during model validation).

The frequency dependence of the thermal time-constant model was clearly shown during model validation, where the model tends toward isothermal characteristics at low frequencies while tending toward adiabatic behaviour at higher frequencies. Frequency dependence in the gas model, with the additional accuracy obtained with the frequency dependence, is highly desirable during simulation. The frequency dependence and increased accuracy does however come at an additional computational cost. The increase in computational time is due to the heat transfer differential equation, which must be numerically solved at each step during simulation. The increase in simulation time of the

thermal time constant model, compared to using a lookup table (set up using the adiabatic or isothermal ideal gas formulation) is around 25 %, when using the modified LuGre friction model. The increase in simulation time of the thermal time constant model is around 60 % when using a more rudimentary lookup friction model. The computational demands for the adiabatic and isothermal formulations are equal.

## **4.2. Friction modelling Effects on Simulation Model**

Friction inherent to the suspension system clearly affects the damping characteristics. The additional friction induced damping effects of each different friction compensation method is shown in this section. Simulations using the same vehicle model and variables with the different friction implementations are used to show their effects on the predicted vehicle dynamics, compared to the case of no friction. The expectation should not be to notice large effects on the final/steady reactions of the system, but rather to see the effects on overshoot, reaction rates and the dynamic behaviour of the system. The three different friction models used for simulation show significant differences in computational expense, due to the complexity of each of the models.

### **4.2.1. Simulation Results: Friction Modelling effects on Simulation**

Friction is a highly non-linear manifestation of damping, and undoubtedly affects the reaction of most physical systems. It is expected to affect the ride-comfort setting of the 4S<sub>4</sub> system more than the handling setting, due to the low design damping rate for that setting. The three friction modelling approaches, all three highly non-linear, will be shown to affect the suspension displacements, roll-rate and roll-angle, in varying degrees for both the Double Lane Change and the Constant Radius Test. The effects of the different friction models on the vehicle dynamics will be shown using the thermal time constant ideal gas model for the double lane change manoeuvres, while the isothermal ideal gas model is used for the constant radius tests. Due to the highly nonlinear nature of the friction models, the simulation time increments must be reduced, effectively increasing the simulation frequency, to enable effective capturing of frictional effects. This also affects the computational demand of the model.

#### **4.2.1.1. Friction Effects on Double Lane Change**

The effects of the three friction models will be shown in this section along with the case of no friction, with regard to the Double Lane Change manoeuvre on the hard and the soft suspension settings. Figure 64 shows the results from simulation using the different friction compensation approaches for a 60 km/h double lane change manoeuvre on the soft suspension setting. A more detailed view of the effects of the different friction models is shown in Figure 65 for the left front suspension unit.

The difference between the friction compensation models and the model without friction is clear. The model with no friction effects shows higher peaks in roll rate and suspension



displacements. It also shows an under damped characteristic clearly visible on the roll rate where the model overshoots the steady state value at the end of the manoeuvre before settling. Friction effects are also clear when considering displacement rates. The differences in vehicle dynamics caused by the three friction models are small when compared with one another. The visible differences in suspension displacement between the three friction implementations, is caused by the velocity reversal dynamics of each model. The highly non-linear force characteristic near the zero velocity in the models is also seen to affect the static suspension displacement. The effect on static displacement is however small when compared to the differences seen in dynamic displacement responses.

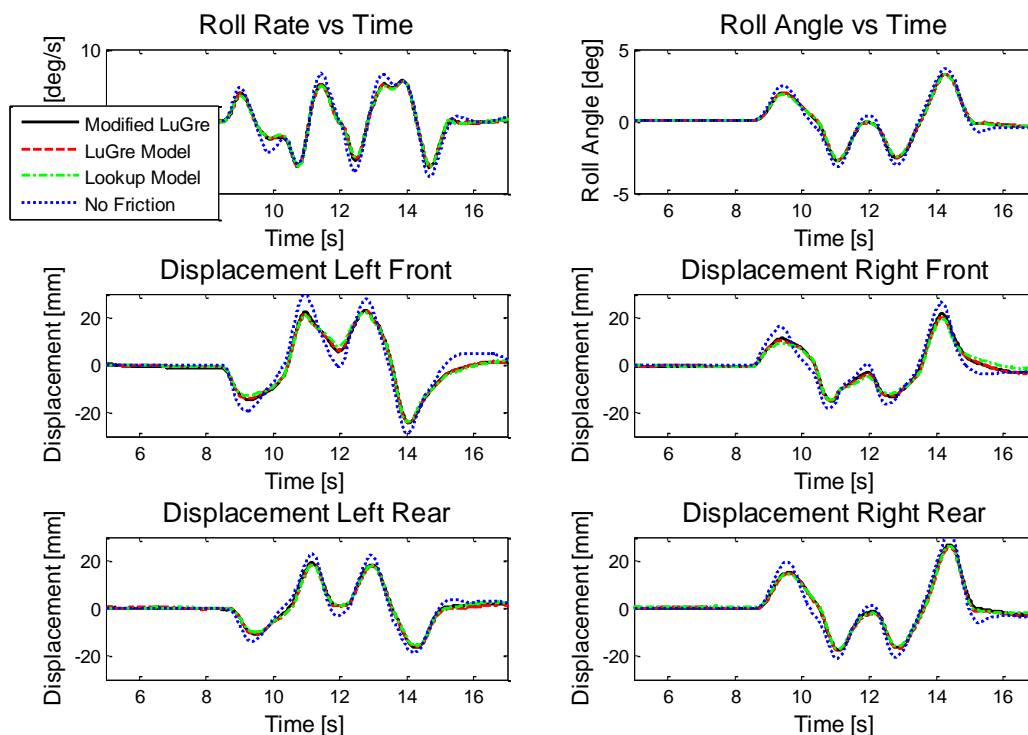


Figure 64: Friction Effects on Soft suspension dynamics for a Double Lane Change

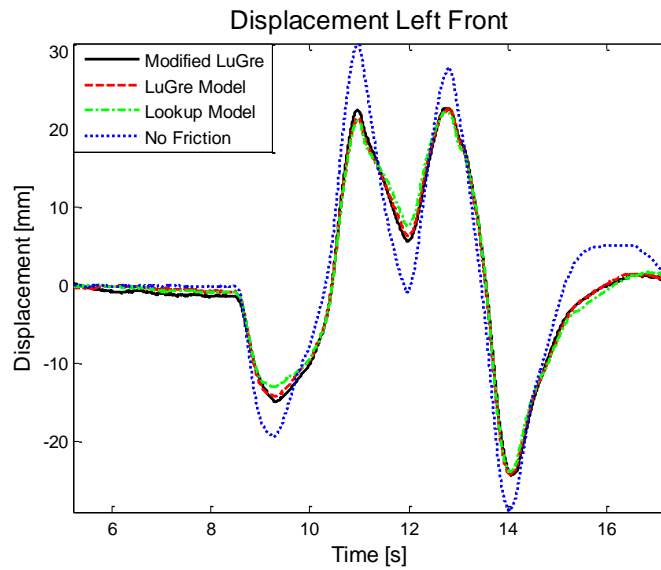


Figure 65: Detailed view of frictional effects on Left Front Soft suspension displacement for a Double Lane Change

Figure 66, shows simulation results of a  $60\text{km/h}$  double lane change manoeuvre using the different friction models for the hard suspension setting. Figure 67, shows a more detailed view of frictional effects on suspension displacement dynamics for the hard suspension setting.

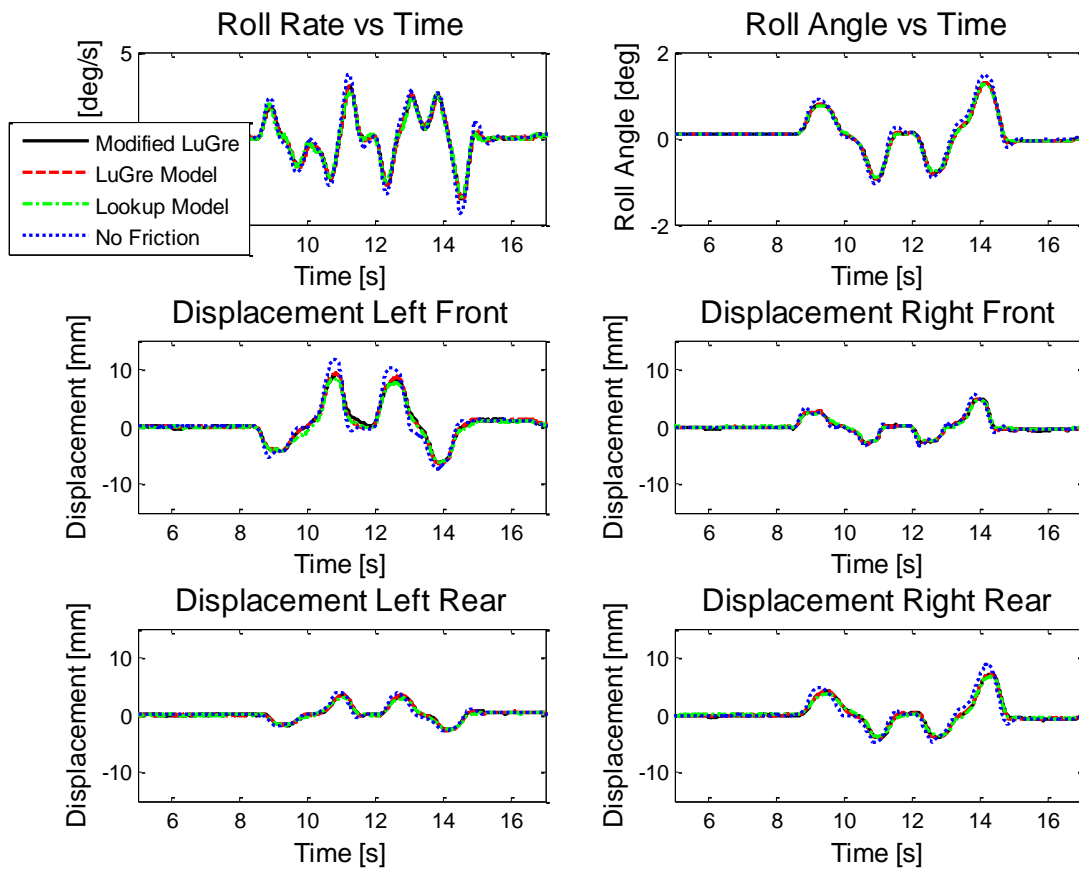


Figure 66: Friction Effects on Hard suspension dynamics for a Double Lane Change

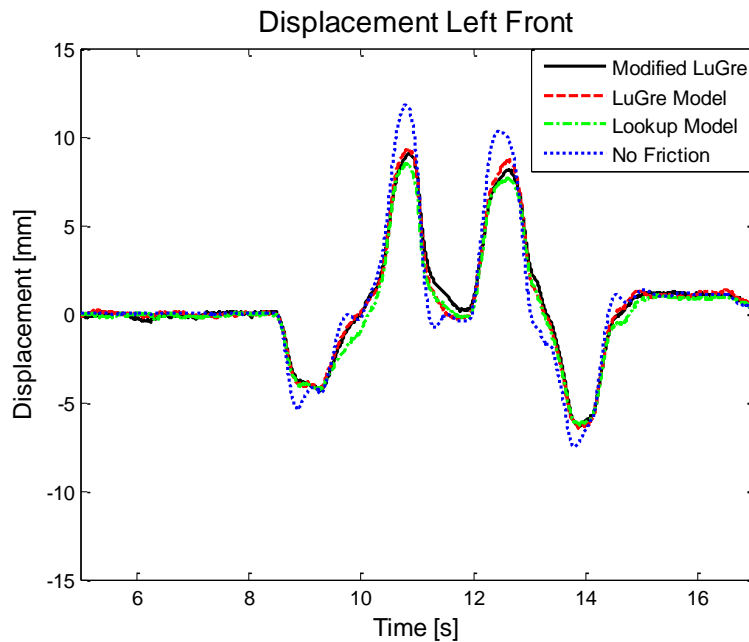


Figure 67: Detailed view of frictional effects on Left Front Hard suspension displacement for a Double Lane Change

The difference between the models with friction compensation and the model neglecting friction is clear. The model without friction shows higher peak suspension displacements, especially in rebound, roll-rate and roll angle. Due to the higher damping ratio on the handling setting of the  $4S_4$ , additional friction induced damping is not as clear in the hard suspension setting as compared to the soft setting. This is clearly visible in the steady state settling at the end of the Double Lane Change Manoeuvre. The friction effect on the handling setting is also not negligible just as it was not negligible for the ride-comfort setting on the suspension system. The effects of friction on the vehicle dynamics for higher velocity manoeuvres are shown in Annexure D: Friction Effects Additional figures.

#### 4.2.1.2. Friction Effects on Constant Radius Test

The effects of friction on the constant radius test are shown in Figure 68, where the model uses the isothermal ideal gas model formulation. Figure 69 shows a detailed view of the frictional effects on the right rear suspension unit displacement.

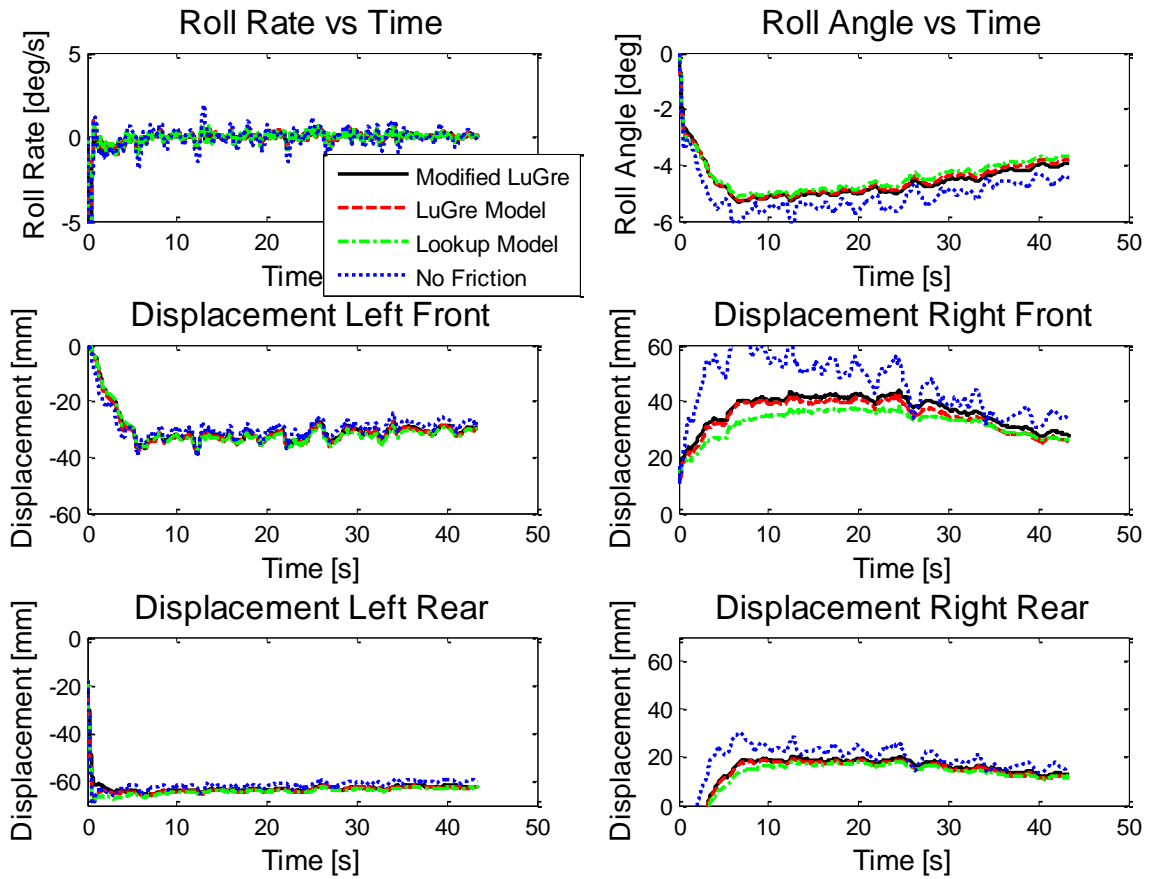


Figure 68: Friction Effects on suspension dynamics for a Constant Radius test

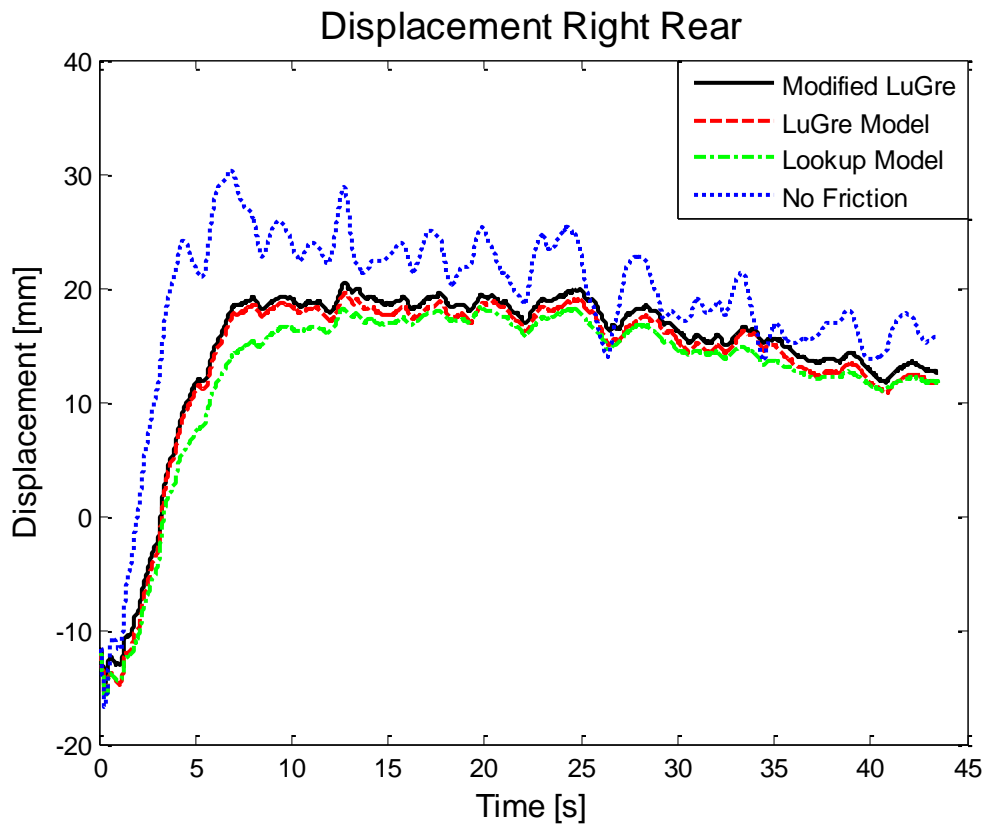


Figure 69: Detailed view of Friction effects on Right Rear Suspension displacement for a Constant Radius Test

Clear differences are visible between the three friction models for the constant radius test simulation. The model with no friction is clearly more sensitive to small steering corrections as were necessary during physical testing. The displacement rates and overshoot for the model without friction is clear throughout the simulation. The lack of friction causes the suspension displacements to be overly sensitive to any small steering corrections.

#### 4.2.2. Discussion: Friction Modelling effects on Simulation

The effect of friction, aside from seemingly inducing numerical noise in the steady state, is not clearly visible on suspension forces. The three implemented friction models yielded force correlations that upon first glance shows the same characteristics. The small differences in these forces, although not clearly visible when looking directly at forces, do affect the roll-rate, roll-angle, and suspension displacements much more noticeably, compared to the case where friction is neglected.

The computational expense of each friction model is summarised in terms of the time taken to complete the simulation in Table 13. The simulation used for comparative purposes was that of the 60 km/h double lane change on the soft suspension setting using the adiabatic ideal gas model formulation, translating to a 20.35 s simulation. It is clear that using the Modified LuGre friction model is much more computationally demanding than either of the other two friction modelling approaches. The table shows the modelling approach, the time required to complete the simulation as well as the percentage difference in time required relative to the case of no friction compensation.

Table 13: Comparison of simulation times with different friction modelling approaches

Friction Modelling Approach	Time to complete Simulation	Percentage Difference
No Friction Compensation	285.912 s	Reference Value
Lookup Rudimentary Model	478.476 s	67.35 %
LuGre Friction Model	1050.42 s	267.39 %
Modified LuGre Friction Model	1230.12 s	330.27 %

In terms of computational efficiency the Lookup model is clearly the most efficient of the three models accounting for friction. The increased accuracy of the simulation model therefore justifies the increase in computational expense. The LuGre and Modified LuGre friction models are much more computationally expensive due to the stiff differential equations requiring numerical solution at each simulation step. Due to the stiff nature of the differential equations, numerical solution is more time consuming than would be the case for non-stiff differential equations (stiff differential equations are required to model the highly non-linear frictional behaviour).

Table 14, summarises the percentage difference in suspension displacement peak values comparing different friction models with the case where friction is neglected on the hard and soft suspension settings. The reason for using the case where friction is neglected as

reference value is the fact that most sources found using full vehicle simulation models neglect frictional effects. For the sake of simplicity and comparison the left front suspension unit is used taking the first positive displacement peak of the 60 km/h Double Lane Change to compare reactions. The largest difference between the three friction models is less than 5 mm on the peak displacement. The largest difference between simulation accounting for and ignoring friction was seen to be larger than 15 mm.

**Table 14: Friction Effect Peak Percentage Differences, Suspension Displacements**

Friction Modelling Approach	Percentage Difference Soft	Percentage Difference Stiff
No Friction Compensation	Reference Value	Reference Value
Lookup Rudimentary Model	-32.61 %	-28.20 %
LuGre Friction Model	-31.26 %	-22.08 %
Modified LuGre Friction Model	-27.71 %	-24.77 %

Table 15, summarises the percentage difference in vehicle roll-rate and roll-angle peaks. The different friction models are compared to the case where friction is neglected. Again for the sake of simplicity and comparison the first peak of the roll-angle and roll-rate results from the 60 km/h Double Lane Change are used. The largest difference in roll rate and roll angle are less than 1 degree/s and 0.1 degree respectively when considering the three friction models. The differences between ignoring and accounting for friction is seen to be more than 2 degrees/s and more than 0.5 degrees respectively for roll-rate and roll-angle.

It is clear from the tables shown that friction has a more pronounced effect on the soft suspension settings' displacement compared to the hard setting. This is as expected due to the much higher damping rate of the hard setting. The apparent sensitivity in the suspension setting, the hard setting seeming more sensitive compared to the soft setting, is however easily explained when considering the magnitude of the reference values used to compare the different models. (The magnitude of roll-rate and roll-angle are much lower for the hard suspension setting, therefore the reference values for comparison are much lower, causing the apparent increased sensitivity.)

**Table 15: Friction effect Peak Percentage Differences, Roll Rate and Roll Angle**

Friction Modelling Approach	% Difference Roll Rate		% Difference Roll Angle	
	Hard	Soft	Hard	Soft
No Friction Compensation	Reference	Reference	Reference	Reference
Lookup Rudimentary Model	-14.65 %	-25.24 %	-18.40 %	-23.27 %
LuGre Friction Model	-23.33 %	-19.86 %	-13.35 %	-20.05 %
Modified LuGre Friction Model	-22.60 %	-18.60 %	-13.21 %	-19.72 %

The Modified LuGre model gives the closest comparison to the case of no friction. This is due to the inclusion of a lubricant film dynamics model which lowers the peak friction in continued dynamic motions. The lookup and LuGre models do not account for lubrication effects and therefore do not account for the lower break-away force for continued dynamic

motions. It is interesting to note that the stiff suspension settings' displacement is almost equally sensitive to the friction model used when compared to the soft suspension settings' displacement. The percentage variation between the friction models on the soft suspension is 4.90 %, while the stiff suspension shows, 6.11 % variability.

It is clear that the inclusion of friction in the simulation model has a pronounced effect on the peak suspension displacements, roll-rate as well as roll-angle. Friction effectively lowers the peak responses in all the cases mentioned by a non-negligible margin each time. The differences in vehicle dynamics when comparing each different friction model implementation to the others, is seen to be almost negligibly small. The difference of less than 5 *mm* in displacement variability, the less than 0.2 *degree* difference in roll-angle and less than 2 *degrees/s* difference in roll rate, reflects the minute influence of the specific friction model implementation. It is also reasonable to expect the differences between the simulation models with and without friction to grow at higher velocities of the simulated manoeuvres.

### 4.3. Discussion: Friction Effects on Ride and Rollover Dynamics

Frictional effects as seen in the results from simulation clearly affect vehicle dynamics. The effects on suspension displacement, roll-rate and roll-angle as discussed in the previous section have implications on various parts of vehicle dynamics responses, including ride- and roll over dynamics. The effects of friction on the simulation results for ride and roll-dynamics are discussed in this section.

Suspension displacement specifically ties in with ride dynamics and vehicle mobility. Contact with bump- or rebound-stops is dependent on suspension displacement. The forces and accelerations caused by bump and rebound stop contact, negatively impact the ride-dynamics and perception. This is due to the highly non-linear nature of the bump and rebound-stops. Neglecting friction in ride comfort optimisation studies not only induces the possibility of convergence to the wrong optimal point, but could also cause convergence issues due to the highly non-linear bump-stop contact effects. Bump-stop contact affects structural fatigue life due to the highly nonlinear induced loads when bump-stop contact occurs. Therefore if friction is neglected and bump-stop contact is over-predicted, the structural fatigue simulation will predict a lower fatigue life compared to the actual system. Vehicle mobility is also affected when neglecting suspension friction. The higher displacement dynamics seen when neglecting friction also causes the possibility of optimisation and simulation issues when considering vehicle mobility.

Aside from bump-stop contact issues, additional friction induced damping in the system may influence the damped sprung- and un-sprung-mass natural frequencies. It is reasonable to expect the damped natural frequency to be affected by the additional frictional damping, especially on suspension systems tuned toward ride comfort, where frictional damping is in the same order of magnitude as the hydraulic damping in the system. The effects on the natural frequencies could have a noticeable effect on ride dynamics.

Roll-rates, roll-angles, and suspension displacements all form part of vehicle roll over dynamics. Friction in the system was seen to have substantial effects on the suspension displacements, roll-rate and roll-angle. Neglecting friction in the system leads to an over-prediction of roll-angle, roll-rate and suspension displacements. Over-predictions in parameters affecting roll over dynamics once again induce errors in optimisation studies. It could allow vehicle simulation models to over-predict roll over incidences, depending on the parameters used to quantify roll over.

The Dynamic Stability Index (DSI), discussed in section 2.2.3, relies on roll-acceleration to quantify roll energy. From the definition of the DSI, vehicle roll over will occur if the DSI exceeds the value of the SSF. The frictional effects seen in the roll-velocity and roll-angle, also affects roll-acceleration. The effect of ignoring friction on the DSI when using the 4S<sub>4</sub> ride-comfort setting is shown in Figure 70 and Figure 71 for a 60 and 80 *km/h* Double Lane Change respectively.



### Friction Effects on Vehicle Roll-over Prediction

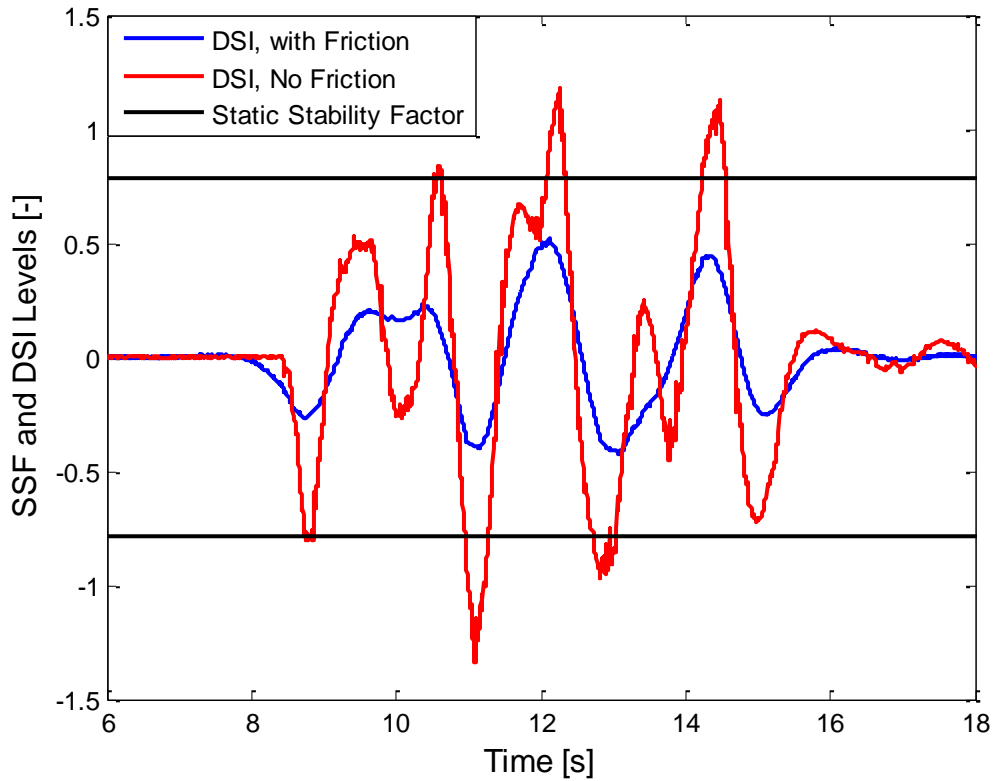


Figure 70: Friction Effects on the DSI for a 60km/h Double Lane Change, Ride-Setting

### Friction Effects on Vehicle Roll-over Prediction

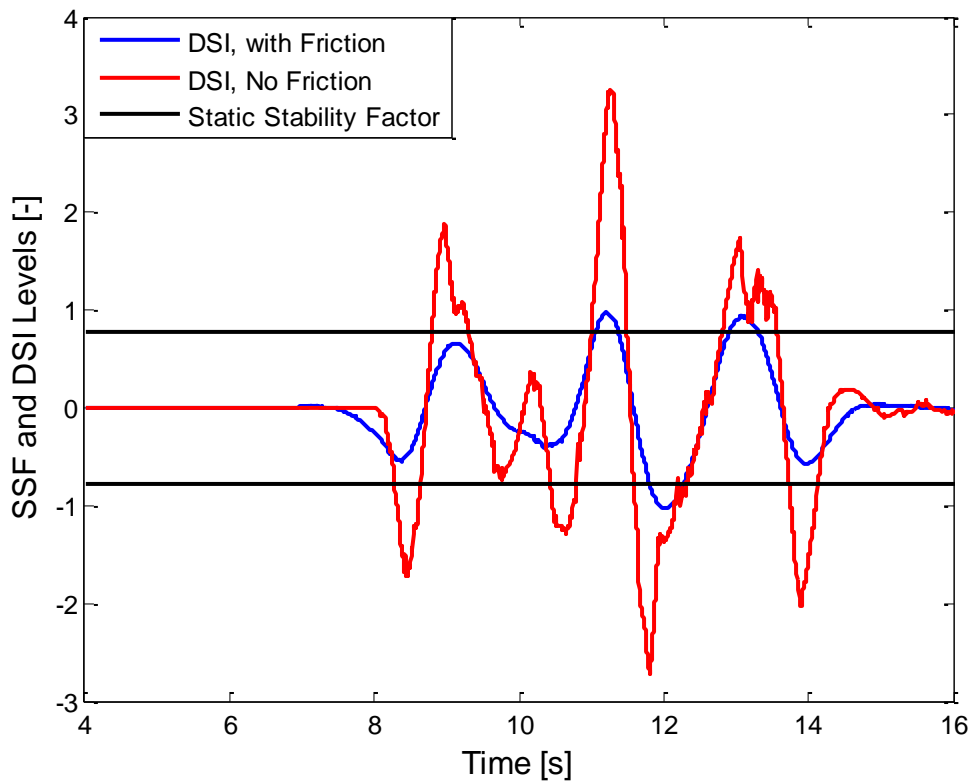


Figure 71: Friction Effects on the DSI for an 80km/h Double Lane Change, Ride Setting

Figure 72 and Figure 73 show the effects of friction on the 4S<sub>4</sub> handling setting for a 60 and 80 km/h Double Lane Change respectively.

### Friction Effects on Vehicle Roll-over Prediction

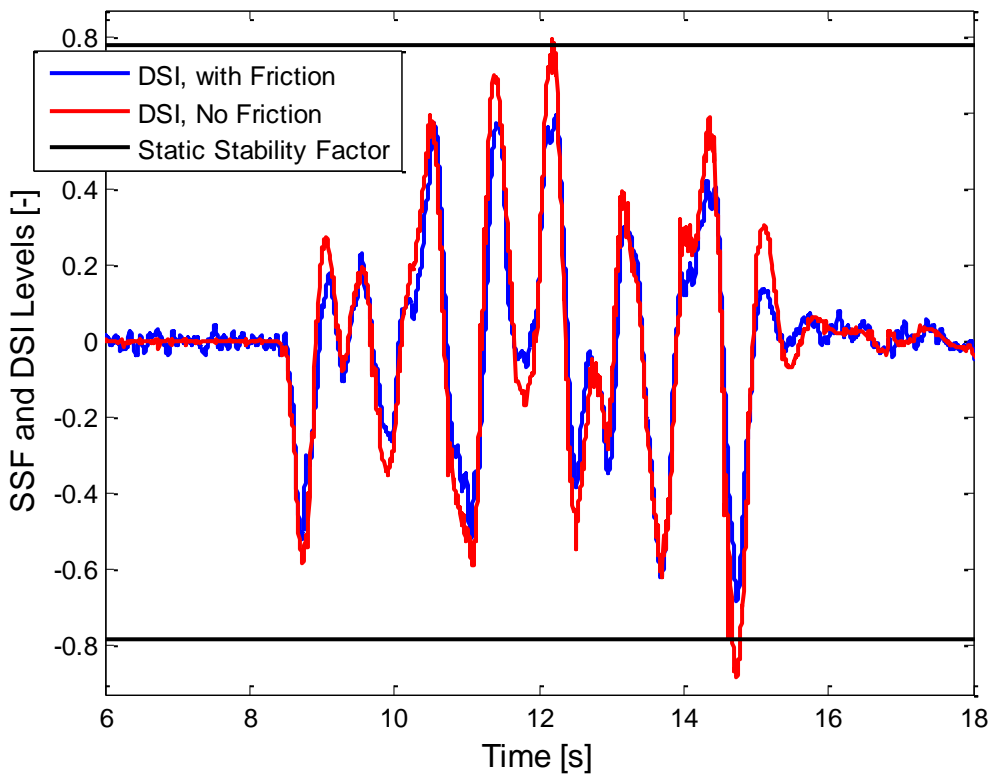


Figure 72: Friction Effects on the DSI for a 60km/h Double Lane Change, Handling Setting

### Friction Effects on Vehicle Roll-over Prediction

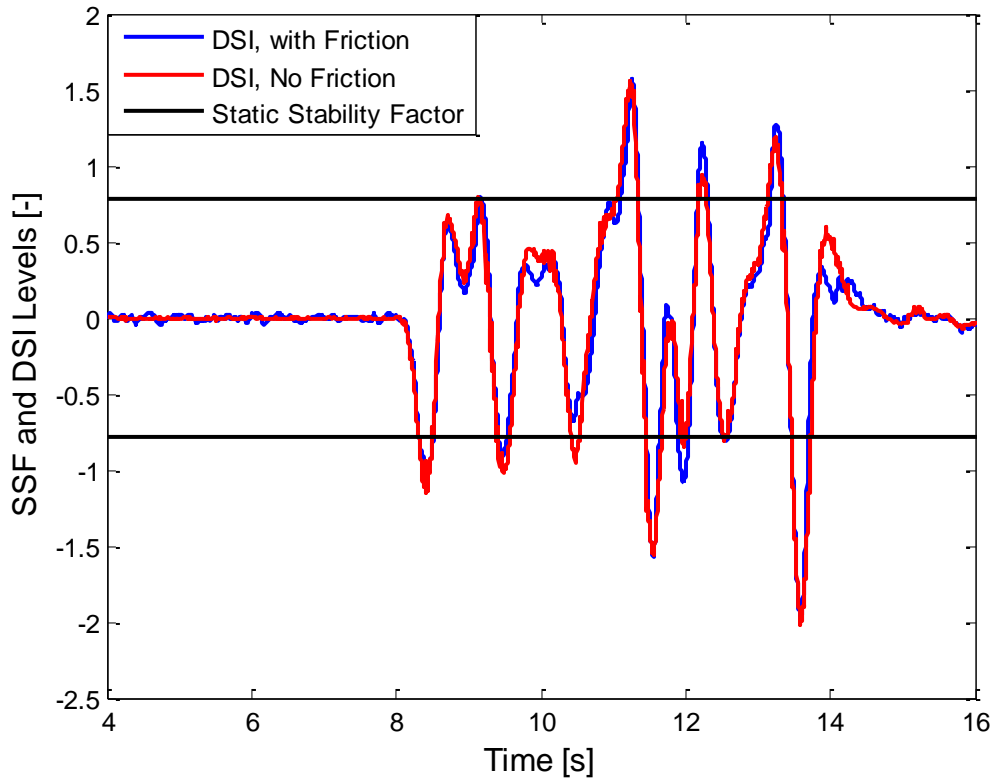


Figure 73: Friction Effects on the DSI for an 80km/h Double Lane Change, Handling Setting

From Figure 70 to Figure 73 it is clear that friction has a more pronounced effect on vehicle roll over when using the ride-setting of the 4S<sub>4</sub> system compared to the much stiffer

handling setting. Ignoring frictional damping results in a higher prediction of the DSI, due to the higher predicted roll-acceleration; therefore the DSI would be more prone to predicting roll over instances.

Friction induced damping is seen to be advantageous due to the effective increase in roll-damping. Frictional-damping, especially in low damping instances, improves roll over stability of the vehicle model, reducing the peak predicted roll-accelerations, roll-rates and roll-angles.

Ignoring friction in simulation would most certainly impact negatively on the validity and accuracy of a vehicle model. The effects of neglecting friction as shown previously and discussed here may induce errors in optimality when using such models for parameter optimisation studies. Especially if one considers vehicle roll dynamics. As shown it influences the DSI roll over metric quite substantially, which could effectively cloud the understanding of the already complex roll over phenomena seen in vehicle dynamics.

## 5. Conclusions, Recommendations and Future Work

Conclusions and recommendations will be made in this section regarding the investigation of the gas modelling effects as well as frictional effects on simulation modelling. This section is broken into two sub-sections the first being the conclusions section, and the second being the recommendations and future work section.

### 5.1. Conclusions

The conclusions drawn in this section are based upon the evidence provided. The effect of the gas modelling strategy, as well as frictional effects on the vehicle simulation model, is handled in the sub sections that follow.

#### 5.1.1. Gas-modelling effects

The gas modelling strategy used affects the spring stiffness characteristic of the vehicle system. It therefore affects the roll, pitch, vertical acceleration response, and suspension displacements calculated during simulation. This study investigated the effect of modelling the gas as an Isothermal, Adiabatic and Thermal Time-Constant dependent Ideal gas, the latter, taking heat transfer into account resulting in something between the isothermal and adiabatic formulations.

From the model validation it may be concluded that the Isothermal approach yields acceptable correlation to measured data at low frequencies (0.001 Hz). It was seen that at frequencies above 0.01 Hz the accuracy of the adiabatic ideal gas formulation yielded lower accuracies compared to the Thermal time-constant approach, but at a much lower computational cost. Suspension displacements in the Double-Lane Change manoeuvre are generally in the higher frequency range where the adiabatic approach yielded more acceptable accuracies while the displacements during a constant Radius test conversely are in the low frequency spectrum, where the isothermal approach yielded acceptable accuracies. The effects of friction on the gas model-predicted force, was also seen to be non-negligible. Taking account of friction improved the accuracy and general correlation of all three gas model implementations when compared to measured data.

Oil compressibility influences suspension force-displacement characteristics and therefore general vehicle dynamics also. Oil compressibility was shown to effectively decrease spring stiffness characteristics of the suspension system. The decrease in spring stiffness was more notable on the stiff suspension setting where the high spring rate of the small gas volume is much closer to the spring rate of the oil. The effects of oil compressibility were also seen on the soft suspension setting of the 4S<sub>4</sub>, although this was only at large suspension displacements (where high gas pressures are induced).

The modelling strategy employed clearly affects simulation model reactions. Steady manoeuvres such as the Constant Radius Test or manoeuvres that do not induce suspension

displacements over a short time period, are suited to be modelled with the isothermal ideal gas model formulation showing acceptable correlation. Manoeuvres such as the Double-lane change or driving over rough terrain, where large suspension displacements are induced over a short time period, the adiabatic ideal gas model formulation shows acceptable correlation.

It may be concluded that adequate accuracy may be achieved when using the Isothermal or Adiabatic Ideal gas model formulations for specific frequency ranges, however the effect of oil compressibility must be accounted for as this may lead large errors in suspension characteristics. The Ideal Gas model implementing the Thermal Time constant approach, generally yields better correlation compared to the isothermal and adiabatic formulation results. The thermal Time constant formulation is also a frequency dependent model, thus making the simulation model independent of the suspension excitation frequency.

### **5.1.2. Friction modelling and Frictional effects**

Friction inherent in the system adds additional damping to the system. Simulation in the ride setting on the 4S<sub>4</sub> system is especially sensitive to the frictional effects due to the low hydraulic damping rate of this setting. The handling setting is less sensitive to frictional effects due to its high hydraulic damping rate. Frictional effects were seen to greatly affect the suspension displacement dynamics for both the Ride and Handling settings on the 4S<sub>4</sub> system, whereas the suspension force dynamics were much less affected.

It may be concluded that friction cannot be ignored in vehicle dynamics studies. The additional damping induced by friction causes large discrepancies in the roll-rate, roll-angle, and suspension displacements when ignored. The predicted suspension displacements for a model with friction, shows displacements of up to 50 % lower than the model ignoring friction. The differences between the friction models implemented showed exceptional correlation between the three compensation methods showing a difference of less than 10 % between the three models. The simulation time, and computational demand, between the three compensation methods was seen to differ substantially, as expected.

It is concluded that complex high computational demand friction models is not suited to optimisation studies in vehicle dynamics simulation. The friction modelling strategies yielded results within 10 % of one another, and showed a difference of up to 50 % when compared to the case where friction is neglected. It can therefore be concluded that the improvement in accuracy from including friction in the system is justifiable for a rudimentary friction modelling approach as the increase in computational demand is comparable to the difference in suspension displacement dynamics. The additional computational expense for the more advanced friction models, is however much more difficult to justify, as they show a gross increase in simulation time while not yielding the significant increases in accuracy over the rudimentary approaches.

It is concluded that friction could have major implications in studies pertaining to ride comfort, mobility and roll over. The reduction in suspension displacement associated with realistic friction modelling will reduce predicted incidences of bump- or rebound-stop contact in ride comfort optimisations for rough terrain, which could change the optimal design damping and spring rates. The reduction in suspension displacement will also most certainly affect the predicted roll over dynamics of the vehicle. The predicted roll-rate and roll-angle were also seen to be greatly affected by friction.

## 5.2.Recommendations

Considering that vehicle dynamics simulations are widely used for optimisation, the recommendations from this study will be summarised for the Gas modelling strategy as well as the effects of friction, after which the Future work will be discussed in a similar format.

The gas modelling strategy has an appreciable effect on the predicted suspension, and thus predicted vehicle dynamics, especially suspension displacements. The following recommendations are made:

- Isothermal gas-spring models are useful for steady manoeuvres, yielding acceptable accuracy for low frequency inputs.
- Adiabatic gas-spring models are useful for dynamic manoeuvres, yielding acceptable accuracy for higher frequency inputs.
- Thermal Time-Constant ideal gas models are recommended for high fidelity suspension models, where the exact displacement frequency range is unknown, although this comes at the cost of additional computational expense.
- Bulk-Modulus Effects (Oil Compressibility) cannot be ignored especially in systems with high spring-rates and/or high operating pressures.
- Bulk-Modulus Effects can be implemented by making use of the force balance method as described in this text as a computationally efficient manner of accounting for oil compressibility.
- For optimisation purposes, it is recommended that initial optimisation be done using either the adiabatic, or isothermal ideal gas formulation.
- The Thermal Time-Constant Approach to the Ideal Gas model, is recommended for final stages of optimisation, where increased accuracy and computational demand can be justified.

The friction modelling strategy is seen to have major implications on both hard and soft settings of the 4S<sub>4</sub> hydropneumatic suspension system. The difference between the different compensation strategies is low compared to the un-compensated case. The following recommendations are made with regard to friction modelling:

- Friction modelling cannot be neglected.
- Suspension friction should be characterised for each specific sub-system.

- High fidelity Friction data should be used to create friction models.
- Rudimentary Friction Compensation effects should be included in vehicle optimisation models.
- Advanced High Fidelity Friction models could be included in the final stages of optimisation if higher accuracy is required.
- Using Advanced High Fidelity Friction models throughout the optimisation process is not recommended due to increased computational demand.

### 5.3.Future Work

During the study certain areas of concern and areas requiring additional attention were identified. While some areas of concern like the effect of Oil Compressibility were addressed, others that could not be addressed that require further attention will be noted here.

A major area of concern is the effect of the lateral tyre force model used. The tyre model specifically is not the concern, but the tyre data upon which the tyre model is based is of questionable quality in the operational vertical load range. This may lead to major errors in simulations compared to measured results. The errors would be especially noticeable in the lateral acceleration dynamics of the vehicle, but also in the roll-, pitch-, and yaw-responses and suspension displacements. More tyre data should be collected that would enable a more realistic and accurate tyre model to be created and used within simulation. More complex tyre models could also be introduced. However more complex models may only produce marginal improvements in simulation accuracy, necessitating a trade-off between accuracy and computational demand. The effect of different tyre models on simulation accuracy and fidelity requires further attention.

The uncertainty of the position of the vehicle Centre of Gravity (CG) is another area of concern. It is known that the roll-dynamics of a vehicle is highly sensitive to the CG height, while the CG lateral and longitudinal position affects the handling dynamics of a vehicle. The exact CG position is thus of paramount importance for accurate vehicle dynamics simulation models. A simple procedure of obtaining the CG position should be investigated or developed such that it could be performed as part of a general vehicle dynamics testing. The correct CG height should also be used in vehicle simulations, especially where vehicle roll over is concerned.

The suspension setting for reducing vehicle roll over propensity is also a field that requires further investigation. The suspension settings for good handling and good ride-comfort are well documented, although the settings on reducing roll over propensity have not been investigated to a large extent. Improving the understanding of the required suspension type required to reduce roll over propensity could prove invaluable, given vast improvements made in controllable suspension technology and design.

The effect of friction on optimal ride- and handling-damping settings also requires some quantification. Optimal damper settings for ride dynamics especially could be greatly affected by friction in suspension systems tuned to yield good ride comfort. The effects of friction in suspension joints may also be investigated to ascertain what effect these have on vehicle dynamics.

The effects of the Ideal gas model or the specific permutation of the ideal gas model used may also influence the fidelity of the model as shown in this text. Another option that may



be explored in future is the possibility of implementing the polytropic ideal gas model as done by Mikulowski, Wiszowaty, and Holnicki-Szulc, (2014). This method estimates the polytropic coefficient for every time-interval during simulation, thereby updating the polytropic coefficient to be closer to isothermal or adiabatic depending on the energy balance in the system.

## 6. References

- AL-BENDER, Farid, Vincent LAMPAERT, and Jan SWEVERS. 2005. The Generalized Maxwell-Slip Model: A Novel Model for Friction Simulation and Compensation. *IEEE TRANSACTIONS ON AUTOMATIC CONTROL*. **50**(11), pp.1883-1887.
- BAKKER, Egbert, Hans B PACEJKA, and Lars LIDNER. 1989. *A New Tire Model with an Application in Vehicle Dynamics Studies*. Warrendale, USA: Society of Automotive Engineers.
- BATTACHARJEE, Subrata. *Thermofluids.net*. [online]. [Accessed 4 September 2013]. Available from World Wide Web: <[thermo.sdsu.edu/testhome/Test/Solve/basics/tables/tablesRG/zNO.html](http://thermo.sdsu.edu/testhome/Test/Solve/basics/tables/tablesRG/zNO.html)>
- BAUER, Wolfgang. 2011. *Hydropneumatic Suspension Systems*. Berlin Heidelberg: Springer.
- BERGMAN, L A, T K CAUGHEY, A G CHASSIAKOS et al. 1997. Structural Control: Past, Present, and Future. *Journal of Engineering Mechanics*., pp.897-971.
- BIRCH, S. 2002. Global Vehicles: 2002 Paris Mondial De L'Automobile, Tech highlights. *Automotive Engineering International*, November, pp.22-24.
- BLUNDELL, Mike and Damian HARTY. 2004. *The Multibody Systems Approach to Vehicle Dynamics*. Burlington, MA: Elsevier Ltd.
- BONCHIS, Adrian, Peter I CORKE, and David C RYE. 1999. A Pressure-Based, Velocity Independent, Friction Model for Asymmetric Hydraulic Cylinders. In: *International Conference on Robotics & Automation*. Detroit, Michigan, pp.1746-1751.
- BREYTENBACH, Hendrik. 2009. *Optimal vehicle suspension characteristics for increased structural fatigue life - Masters Degree Thesis - University of Pretoria*.
- BRITISH STANDARDS INSTITUTION. 1987. *BS 6841-1987: British Standard Guide to Measurement and Evaluation of Human Exposure to Whole-Body Mechanical Vibration and Repeated Shock*.
- CRONJÉ, P.H. 2008. *Improving off-road vehicle handling using an active anti-roll bar - Masters Degree Thesis - University of Pretoria*.
- DAHLBERG, Erik. 2002. Parameter Sensitivity of the Dynamic Rollover Threshold. In: *7th International Symposium on Heavy Vehicle Weights & Dimensions*. Delft, Netherlands, pp.51-62.
- DE WIT, Carlos Canudas, Henrik OLSSON, Karl Johan ÅSTRÖM, and Pablo LISCHINSKY. 1995. A New Model for Control of Systems with Friction. *IEEE TRANSACTIONS ON AUTOMATIC CONTROL*. **40**(3), pp.419-425.
- DICKERSON, Charles P., Stephen M. ARNDT, Gregory A. MOWRY, and Mark W. ARNDT. 1994. Effects of Outrigger Design on Vehicle Dynamics. *Concepts in Vehicle Dynamics and Simulation SP-1016*, February, pp.81-98.
- DUKKIPATI, Rao, Jian PANG, Mohamad QATU et al. 2008. *Road Vehicle Dynamics*. Warrendale: Society of Automotive Engineers.

ELS, Pieter Schalk. 1993. *Die Hitteprobleem op Hidropneumatiese Veer-en-Demperstelsels - Masters Degree Thesis - University of Pretoria.*

ELS, Pieter Schalk. 2006. *The Ride Comfort vs. Handling Compromise for Off-Road Vehicles - PhD Dissertation - University of Pretoria.*

ELS, Pieter Schalk and B GROBBELAAR. 1999. Heat transfer effects on hydropneumatic suspension systems. *Journal of Terramechanics*. **36**, pp.197-205.

ELS, Pieter Schalk, Nicolaas Johannes THERON, Petro E UYS, and Michael John THORESSON. 2007. The ride comfort vs. handling compromise for off-road vehicles. *Journal of Terramechanics*. **44**, pp.303-317.

FACILITIES, Gerotek Test. [online]. [Accessed 3 September 2013]. Available from World Wide Web: <[www.armscordi.com/SubSites/Gerotek1/Gerotek01\\_landing.asp](http://www.armscordi.com/SubSites/Gerotek1/Gerotek01_landing.asp)>

FISCHER, Daniel and Rolf ISERMANN. 2004. Mechatronic semi-active and active vehicle suspensions. *Control Engineering Practice* **12.**, pp.1353-1367.

FRIMBERGER, Manfred, Florian WOLF, Gerd SCHOLPP, and Jürgen SCHMIDT. 2004. Influences of Parameters at Vehicle Rollover. *SAE International*. **101**, pp.333-340.

GARROT, W Riley, J Gavin HOWE, and Garrick FORKENBROCK. 1999. *An Experimental Examination of Selected Maneuvers That May Induce On-Road Untripped, Light Vehicle Rollover - Phase II of NHTSA's 1997-1998 Vehicle Rollover Research Program*. Washington, DC: Department of Transportation.

GILLESPIE, Thomas D. 1992. *Fundamentals of Vehicle Dynamics*. Warrendale: Society of Automotive Engineers, Inc.

GRAU, César A. 2002. *A Parametric Study of the Lateral Dynamics of a Nonlinear Four-Wheel Road-Vehicle Model*. Cincinnati.

HAC, Aleksander, Todd BROWN, and John MARTENS. 2004. *Detection of Vehicle Rollover*. Detroit, Michigan: Society of Automotive Engineers.

HOLDMANN, Peter and Michael HOLLE. 1999. Possibilities to improve the ride and handling performance of delivery trucks by modern mechatronic systems. *JSAE Review*. **20(4)**, pp.505-510.

HOWE, J Gavin, W Riley GARROT, Garrick FORKENBROCK et al. 2001. *An Experimental Examination of Selected Maneuvers That May Induce On-Road, Untripped Light Vehicle Rollover - Phase I-A of NHTSA's 1997-1998 Vehicle Rollover Research Program*. Washington, DC: Department of Transportation.

INTERNATIONAL ORGANISATION FOR STANDARDISATION. 1975. *International Organisation for Standardisation ISO 3888-1975*.

KARNOPP, D and D MARGOLIS. 1984. Adaptive suspension concepts for road vehicles. *Vehicle System Dynamics*. **13(3)**, pp.145-160.

- KAT, Cor-Jacques and Pieter Schalk ELS. 2012. Validation metric based on relative error. *Mathematical and Computer Modelling of Dynamical Systems: Methods, Tools and Applications in Engineering and Related Sciences*.
- LAMPAERT, Vincent, Jan SWEVERS, and Farid AL-BENDER. 2002. EXPERIMENTAL COMPARISON OF DIFFERENT FRICTION MODELS FOR ACCURATE LOW VELOCITY TRACKING. In: *Proceedings of the 10th Mediterranean conference on control and Automation*. Lisbon, Portugal.
- LAWNICZAK, Sebastian and Przemyslaw SIMINSKI. 2009. Hydropneumatic Suspension Modelling for Wheeled Armoured Fighting Vehicle. *Journal of KONES Powertrain and Transport*. **16**(2), pp.285-297.
- MÀRTON, Lőrinc and Béla LANTOS. 2007. Modelling, Identification, and Compensation of Stick-Slip Friction. *IEEE TRANSACTIONS ON INDUSTRIAL ELECTRONICS*. **54**(1), pp.511-521.
- MIKULOWSKI, Grzegorz, Rafal WISZOWATY, and Jan HOLNICKI-SZULC. 2014. Analysis and Thermodynamic modeling of a pneumatic adaptive absorber. In: *Six World Conference on Structural Control and Monitoring*. Barcelona, Spain, pp.3057-3066.
- MITCHELL, William C. 2012. *Neohio Sports Car Club of America*. [online]. Available from World Wide Web: <[http://www.neohio-scca.org/comp\\_clinic/hand\\_out\\_reprints/LoadTransfer%20reduced%202.pdf](http://www.neohio-scca.org/comp_clinic/hand_out_reprints/LoadTransfer%20reduced%202.pdf)>
- NATIONAL HIGHWAY TRAFFIC SAFETY ADMINISTRATION. 2011. *Traffic Safety Facts 2009 Data*. Washington.
- OTIS, D R and A POURMOVAHED. 1985. An Algorithm for Computing Nonflow Gas Processes in Gas Springs and Hydropneumatic Accumulators. *Journal of Dynamic Systems, Measurement, and Control*. **107**, pp.93-96.
- OZAKI, Akinori. 2002. Basic study of vehicle roll motion and possibility of inward roll: examination by a mechanical model of rigid axle suspension. *Journal of the Society of Automotive Engineers.*, pp.465-471.
- RAZENBERG, J. A. 2009. *Modelling of the hydro-pneumatic suspension system of a rally truck - PhD Dissertation - Eindhoven University of Technology*. Eindhoven.
- SAKAI, Hideki and Yukiharu SATOH. 1994. The impact of roll center height on vehicle dynamic behavior. *Journal of the Society of Automotive Engineers Review.*, pp.329-333.
- SARAMI, Shahriar. 2009. *Development and Evaluation of a Semi-active Suspension System for Full Suspension Tractors*. Berlin.
- SONTAG, Richard E, Claus BORGNÄKKE, and Gordon John VAN WYLEN. 2003. *Fundamentals of Thermodynamics*. John Wiley and Sons.
- SOUTH-AFRICAN DEPARTMENT OF TRANSPORT. 2004. *Road Traffic and Fatal Crash Statistics 1990-2003*.

TAKANO, Shuichi, Masao NAGAI, Tetsuo TANIGUCHI, and Tadashi HATANO. 2003. Study on a vehicle dynamics model for improving roll stability. *Journal of the Society of Automotive Engineers.*, pp.149-156.

THORESSON, Michael John. 2003. *Mathematical Optimisation of the Suspension System of an Off-Road Vehicle for Ride Comfort and Handling - Masters Degree Thesis - University of Pretoria.*

THORESSON, Michael John. 2007. *Efficient Gradient-Based Optimisation of Suspension Characteristics for an Off-Road Vehicle - PhD Dissertation - University of Pretoria.*

UNGOREN, Ali Y and Huei PENG. 2004. Evaluation of Vehicle Dynamic Control for Rollover Prevention. *International Journal of Automotive Technology.* 5(2), pp.115-122.

UYS, Barend Petrus. 2007. *Omrol van Veldvoertuie - Masters Degree Thesis - University of Pretoria.*

UYS, Petro E, Pieter Schalk ELS, and Michael John THORESSON. 2006. Criteria for handling measurement. *Journal of Terramechanics.*, pp.43-67.

UYS, Petro E, Pieter Schalk ELS, Michael John THORESSON et al. 2006. Experimental determination of moments of inertia for an off-road vehicle in a regular engineering laboratory. *International Journal of Mechanical Engineering Education*, October, pp.291-314.

VAN DER WESTHUIZEN, Sarel Francois and Pieter Schalk ELS. 2011. Slow Active Suspension Control for Rollover Prevention.

VAN GEFFEN, V. 2009. *A study of friction models and friction compensation - PhD Dissertation - Technische Universiteit Eindhoven.*

WHITEHEAD, Randal John, George T FLOWERS, W TRAVIS, and David M BEVLY. 2004. A Study of the Effect of Various Vehicle Properties on Rollover Propensity. *Journal of the Society of Automotive Engineers.*

YANADA, Hideki and Yuta SEKIKAWA. 2008. Modelling of dynamic behaviours of friction. *Mechatronics.*, pp.330-339.

## Annexure A: Previous attempts at bulk modulus compensation

The bulk modulus compensation in the model as previously implemented by Breytenbach (2009), approaches the problem in terms of two equations that must be solved simultaneously. The simultaneous solution of the equations is extremely time-consuming, and the result from this approach is ultimately incorrect as will be shown. The approach followed by Breytenbach (2009), is discussed below.

Breytenbach (2009), modelled the suspension gas-spring characteristic in the same way as was done for this study, the specific equation set up by him is given as the following.

$$F = p_{stat}A \left( \frac{x_{stat}}{x} \right)^{n_p}$$

with

- $F$  = Pneumatic spring force,
- $p_{stat}$  = Static Pressure,
- $A$  = Area,
- $x_{stat}$  = Static Displacement,
- $x$  = Hydro-pneumatic spring displacement,
- $n_p$  = Polytropic gas constant.

He modelled the stiffness of the oil as a linear spring in series with the non-linear air spring. The system is then solved for the displacement of the air spring and of the bulk oil given an initial estimate of the displacements. He then proceeds to use the displacement of either the air spring or the oil spring to predict the force characteristic. The system of equations is given by the following.

$$[F] = \begin{bmatrix} k_{\beta_f} x_{oil} - F_{air}(x_{air}) \\ x_{oil} - (x_{air} + x_{oil}) \end{bmatrix} = \bar{0}$$

where

- $k_{\beta_f}$  = Bulk oil stiffness,
- $x_{oil}$  = Displacement of the oil volume,
- $x_{susp}$  = Total suspension displacement,
- $F_{air}(x_{air})$  = Air spring force as a function of air volume.

The system of equations was then solved using the non-linear Matlab fsolve.m function using the initial estimates of zero oil displacement and the total suspension displacement for the air spring displacement. Breytenbach (2009), noted the solution of the system of equations to introduce a large computational expense into the model, therefore the bulk modulus effects were neglected in his study.

A comparison between the results obtained in the fashion described above is shown in Figure 74 where it is compared to the bulk modulus implementation followed in this study which has previously been shown to be correct.

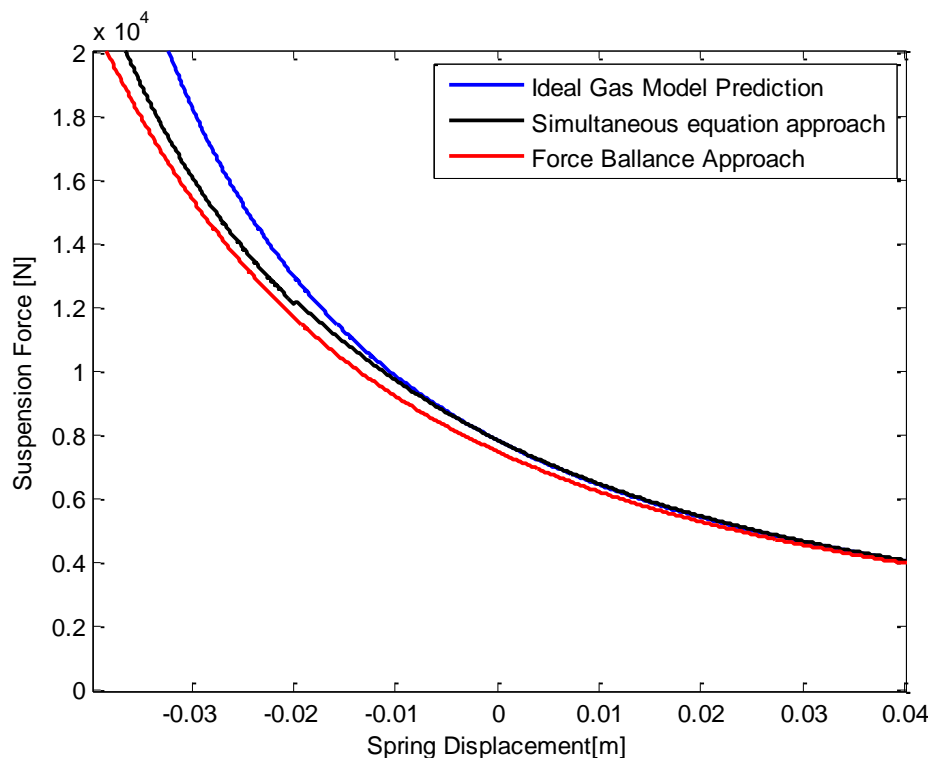


Figure 74: Spring Force Displacement Bulk Modulus Compensation Comparison

It is clear that the simultaneous equation approach does not yield the same characteristic as the force-balance approach. The simultaneous equation approach in fact crosses the ideal gas model prediction at the zero-displacement position, predicting higher suspension forces in the rebound stroke of the characteristic. The force balance approach is not only less computationally expensive than the simultaneous equation approach, it is also more accurate.

The fact that the simultaneous equation approach crosses over the ideal gas model prediction on the rebound stroke, indicates that the model only takes the static force into account on the gas spring. Neglecting the static force on the oil effectively results in oil expansion when the suspension unit is in rebound, which is not physically the case. In reality the oil has a measure of compression from any pressure above zero, and during normal operation, the 4S<sub>4</sub> system is pressurized for the entire operational range. This is not encapsulated in the simultaneous equation approach presented here.

The conclusion made by Breytenbach (2009), that the bulk modulus effect is negligible, is valid in the context of his study where only the suspension forces were of interest. It has been shown in this text that the bulk modulus, although not having noticeable effects on suspension forces, does affect the vehicle displacement dynamics in a manner which is not negligible.

## Annexure B: Friction model comparisons for various test inputs

Friction characteristics for Sinusoidal and Triangular displacement inputs at various frequencies are shown here for the three friction models implemented. This section is divided into two sub sections, the first showing the sinusoidal input reactions, while the second shows the triangular input reactions.

### Annexure B-1: Friction Characteristics for sinusoidal displacement inputs

Figure 75, shows the Force characteristic for a,  $0.05\text{ Hz}$ ,  $0.025\text{m}$  amplitude Sinusoidal displacement input, as a function of time.

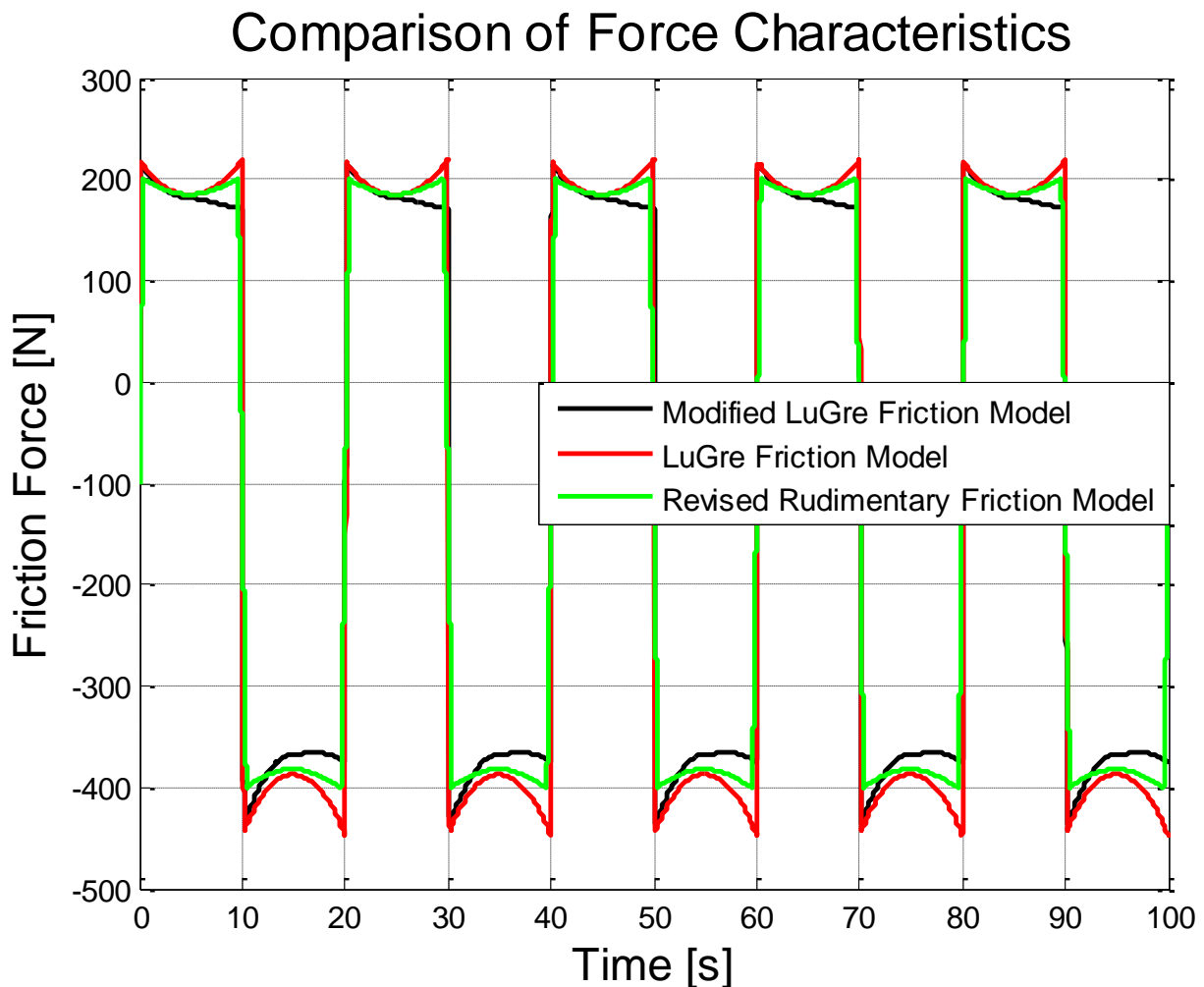


Figure 75:  $0.05\text{Hz}$ ,  $0.025\text{m}$  Amplitude Sinusoidal Displacement input Force Characteristic

Figure 76, shows the Force-Velocity Characteristic for a,  $0.1\text{Hz}$ ,  $0.025\text{m}$  Amplitude Sinusoidal Displacement input.



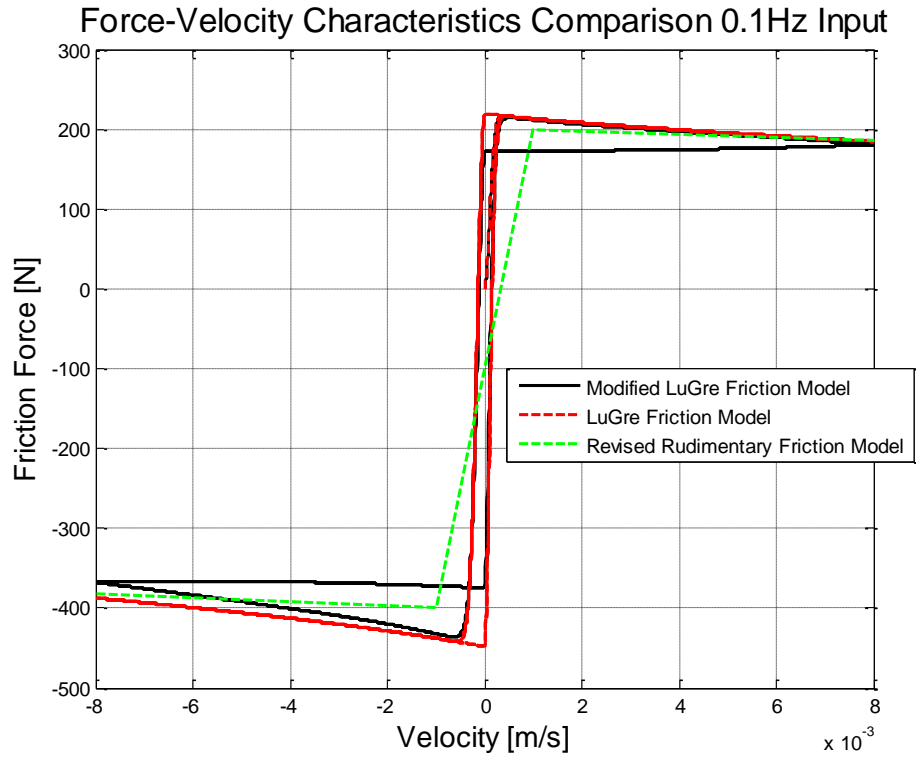


Figure 76: 0.1Hz, 0.025m Amplitude Sinusoidal Displacement input Force-Velocity Characteristics

Figure 77, shows the force characteristic for a, 0.25Hz, 0.025m Amplitude Sinusoidal displacement input, as a function of time.

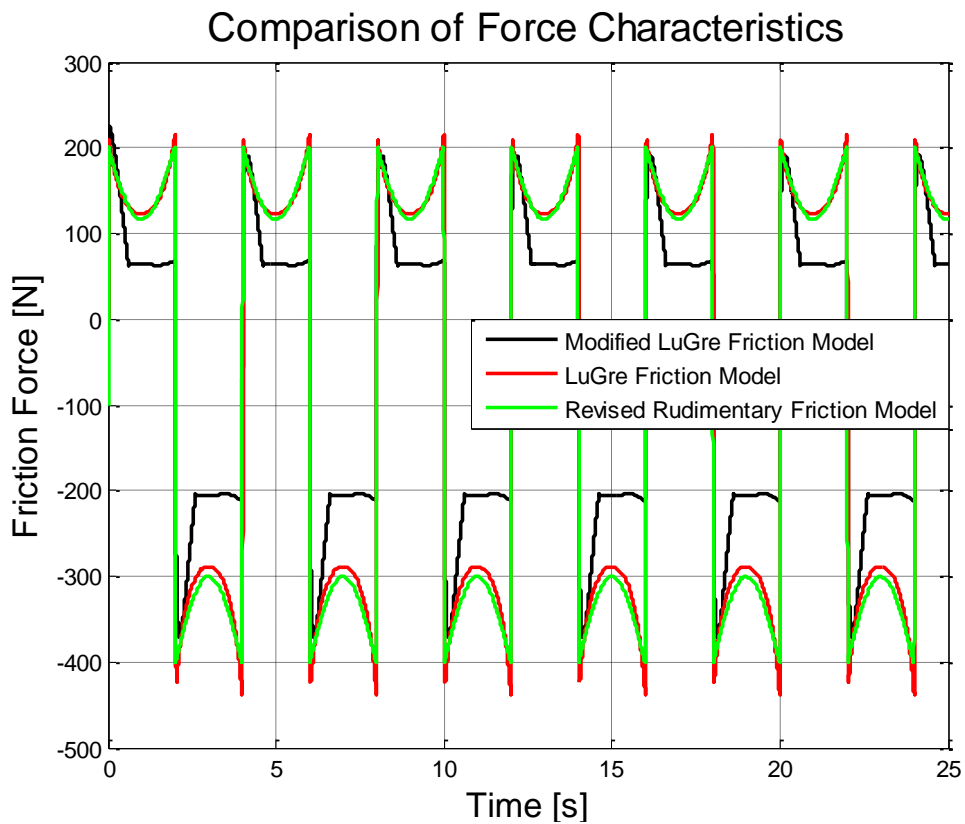


Figure 77: 0.25Hz, 0.025m Amplitude Sinusoidal Displacement input Force Characteristic

Figure 78, shows the Force-Velocity Characteristic for a,  $0.5\text{Hz}$ ,  $0.025\text{m}$  Amplitude Sinusoidal Displacement input.

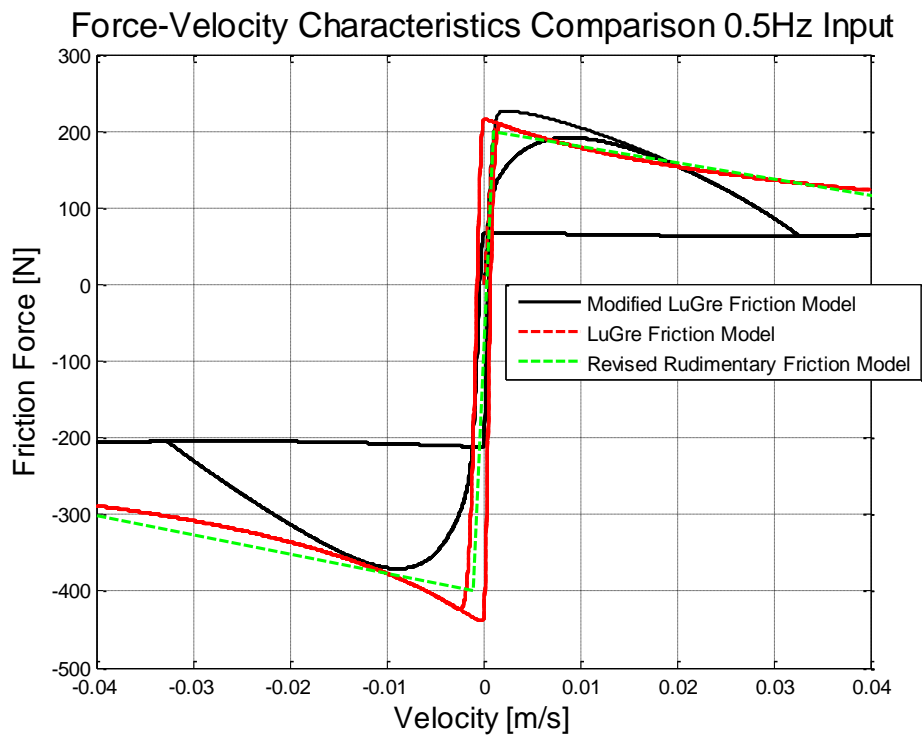


Figure 78:  $0.5\text{Hz}$ ,  $0.025\text{m}$  Amplitude Sinusoidal Displacement input Force-Velocity Characteristics

Figure 79, shows the force characteristic for a,  $0.5\text{Hz}$ ,  $0.025\text{m}$  Amplitude Sinusoidal displacement input, as a function of time.

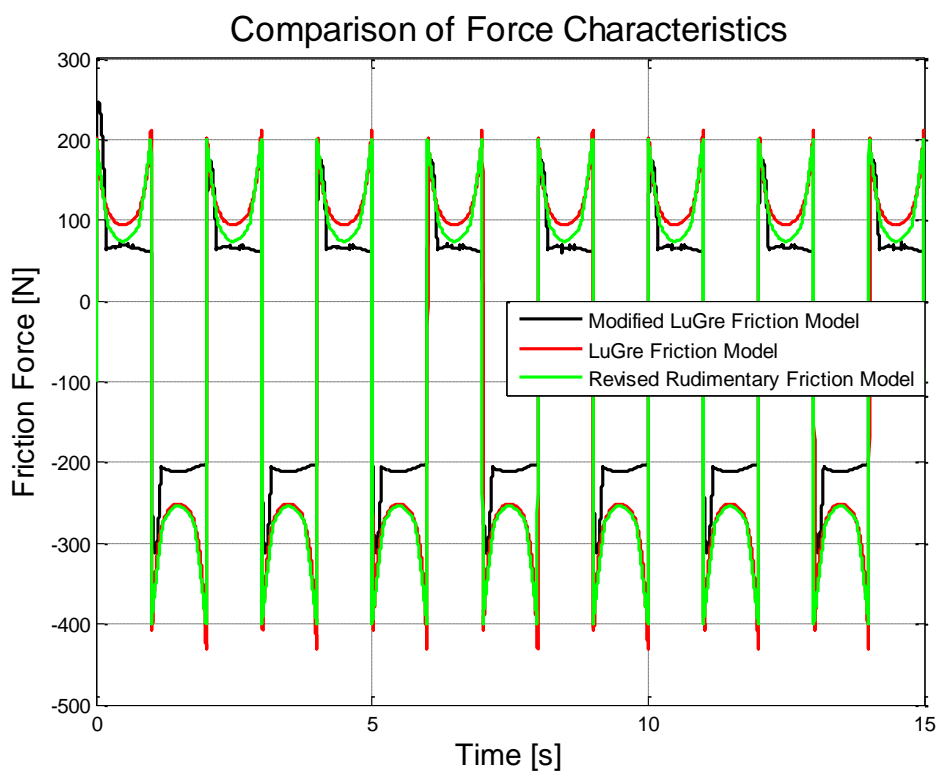


Figure 79:  $0.5\text{Hz}$ ,  $0.025\text{m}$  Amplitude Sinusoidal Displacement input Force Characteristic

Figure 80, shows the Force-Velocity Characteristic for a, 1Hz, 0.025m Amplitude Sinusoidal Displacement input.

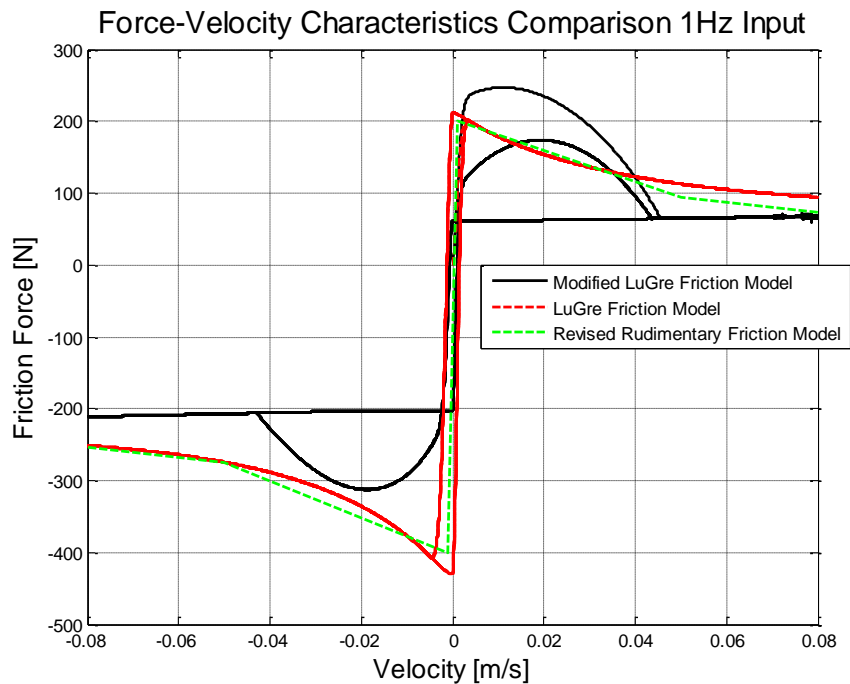


Figure 80: 1Hz, 0.025m Amplitude Sinusoidal Displacement input Force-Velocity Characteristics

Figure 81, shows the Force characteristic for a, 0.75 Hz, 0.025m Amplitude Sinusoidal displacement input, as a function of time.

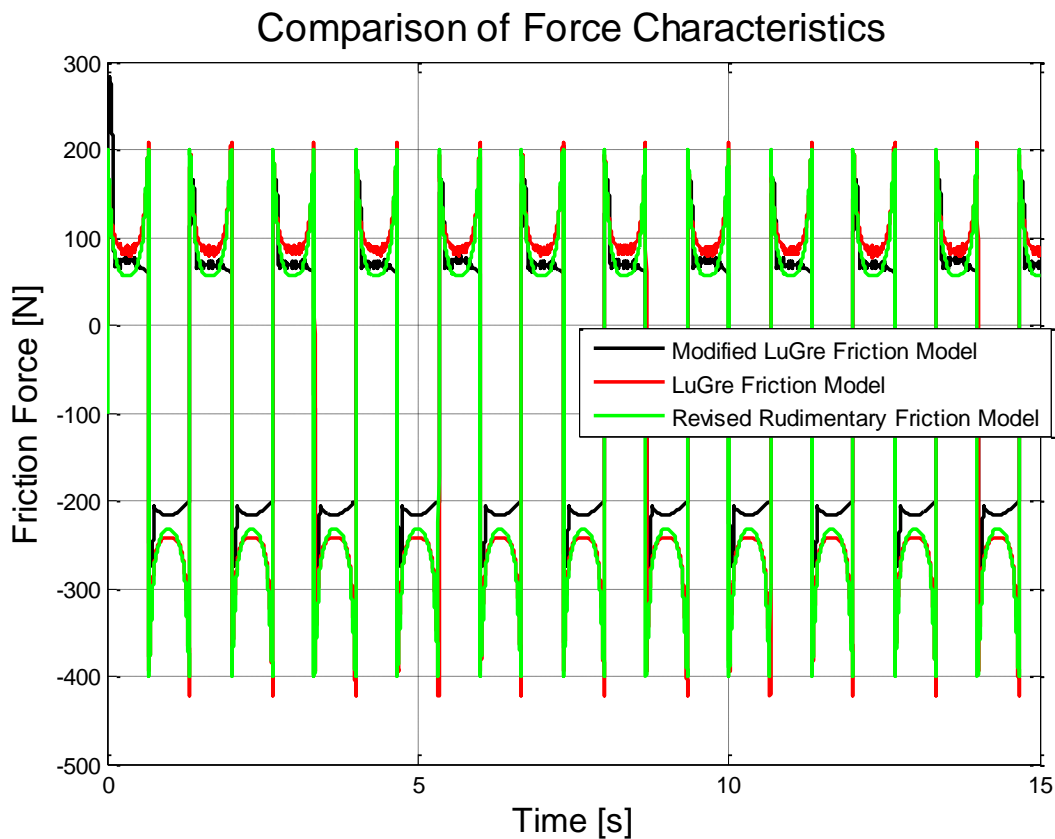
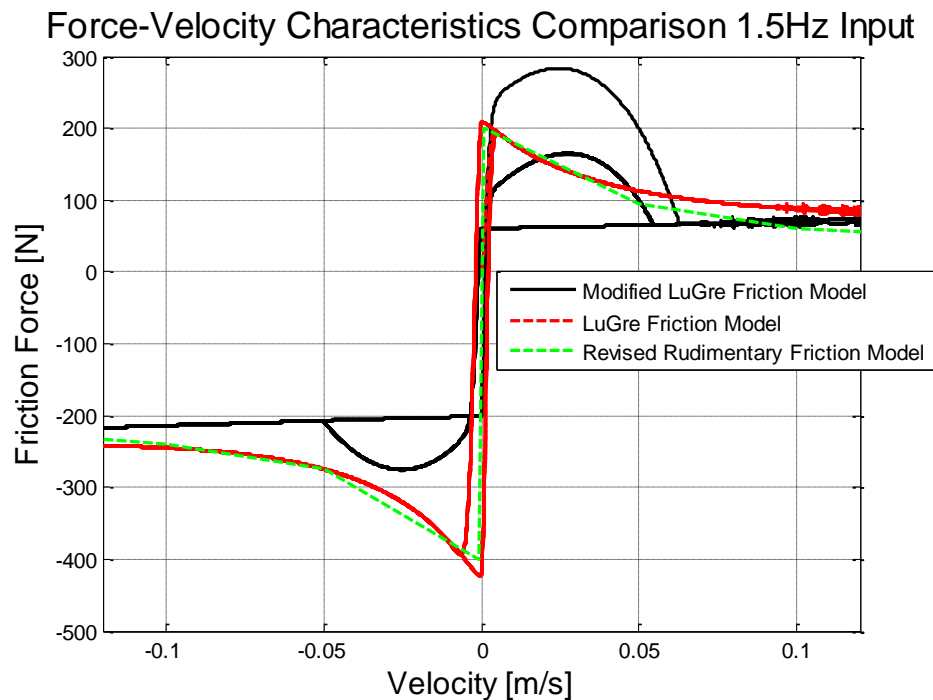


Figure 81: 0.75Hz, 0.025m Amplitude Sinusoidal Displacement input Force Characteristic

Figure 82, shows the Force-Velocity Characteristic for a, 1.5 Hz, 0.025m Amplitude Sinusoidal Displacement input.



**Figure 82: 1.5Hz, 0.025m Amplitude Sinusoidal Displacement input Force-Velocity Characteristics**

It is notable that the LuGre and Modified LuGre Friction models both exhibit hysteretic behaviour. It is also notable that the Modified LuGre model reacts in a substantially different way compared to the LuGre or Rudimentary friction models during velocity reversals. The differences in the friction models are clearly visible at the higher end of the frequency spectrum, where the LuGre and Rudimentary models correlate well, as well as at the low frequency region, where the LuGre and Modified LuGre models show good correlation on the extension stroke.

## Annexure B-2: Friction Characteristics for Triangular displacement inputs

Figure 83, shows the Force response for a Triangular displacement input with a  $0.001m/s$  steady state velocity.

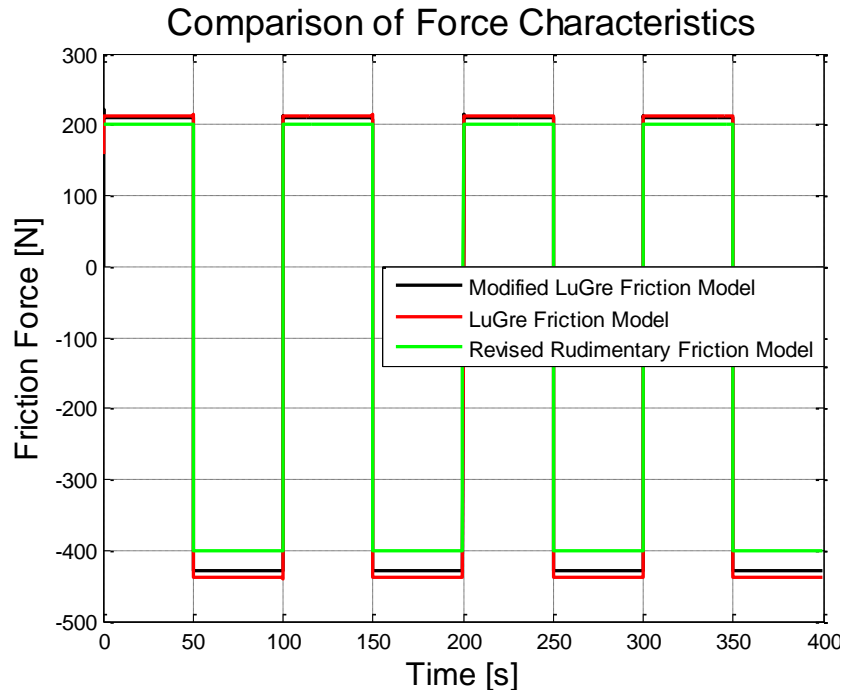


Figure 83: 0.25m Amplitude, 0.01Hz Triangular displacement input Force response

Figure 84, shows the Force response for a Triangular displacement input with a  $0.005m/s$  steady state velocity.

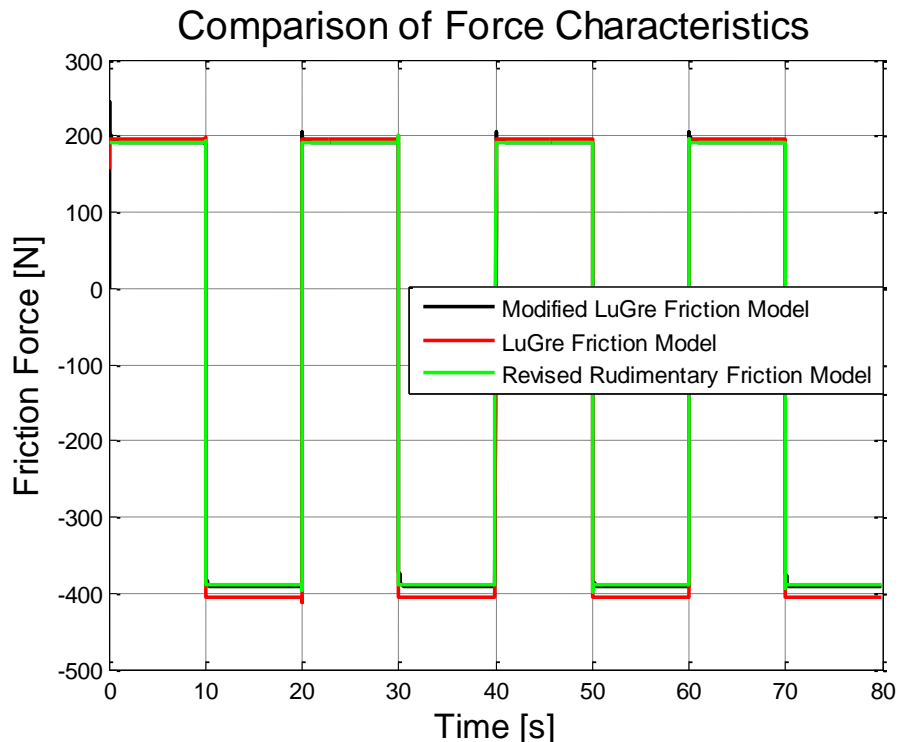


Figure 84: 0.25m Amplitude, 0.05Hz Triangular displacement input Force response

Figure 85, shows the Force response for a Triangular displacement input with a  $0.01m/s$  steady state velocity.

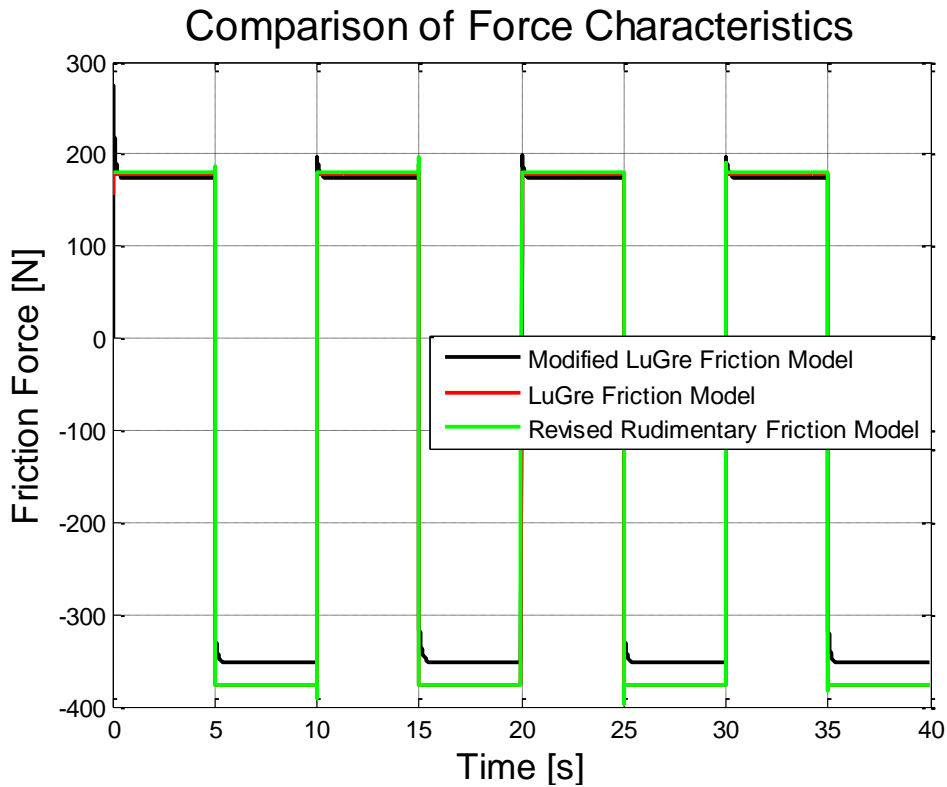


Figure 85: 0.25m Amplitude, 0.1Hz Triangular displacement input Force response

Figure 86, shows the Force response for a Triangular displacement input with a  $0.05m/s$  steady state velocity.

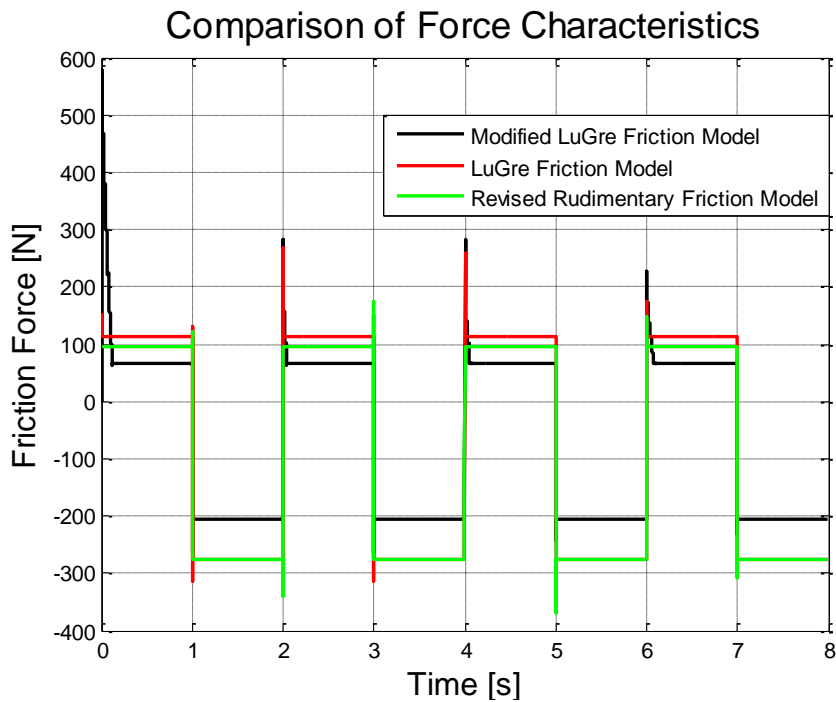


Figure 86: 0.25m Amplitude, 0.5Hz Triangular displacement input Force response

Figure 87, shows the Force response for a Triangular displacement input with a  $0.1m/s$  steady state velocity.

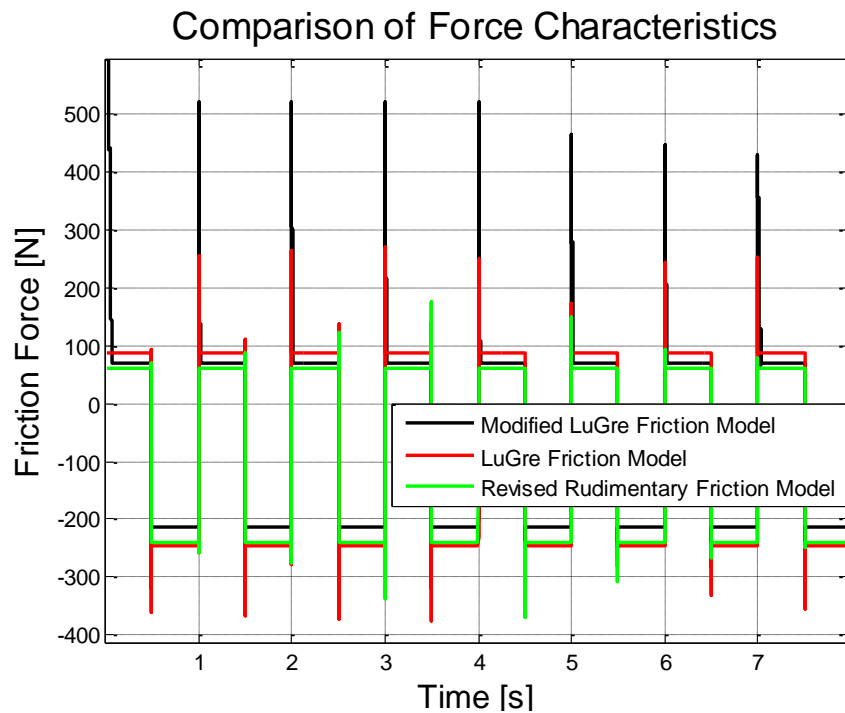


Figure 87: 0.25m Amplitude, 1Hz Triangular displacement input Force response

Figure 88, shows the Force response for a Triangular displacement input with a  $0.2m/s$  steady state velocity.

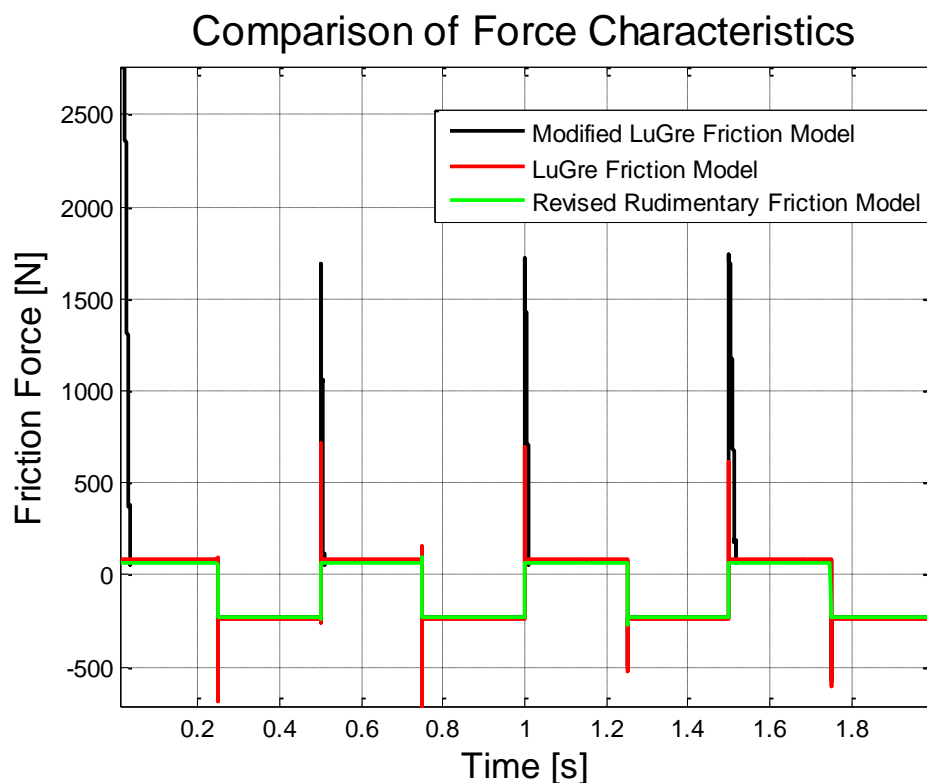


Figure 88: 0.25m Amplitude, 2Hz Triangular displacement input Force response

The differences in the friction models can clearly be seen in the higher frequency/velocity range. The film dynamics models' effect is clearly visible on the Modified LuGre model on velocity reversals, where the initial peak friction level is much higher than the subsequent peaks at velocity reversals. The reason for the reversal friction peaks in the negative velocity range is due to the sampling frequency being too low, where the test input missed the low velocity points during the velocity reversal. The steady frictional force for the different models shows good correlation especially at higher frequencies.

It may also be noticed that the Modified LuGre Friction model predicts in most of the velocity range predicts a lower steady-velocity friction force compared to the LuGre and Rudimentary models. The LuGre and Modified LuGre friction models show much higher frictional peaks on velocity reversals compared to the Rudimentary model.

The lower predicted steady state friction force for the Modified LuGre model is clearly visible in the suspension displacement reactions albeit small considering the overall displacements. The higher frictional peaks from the LuGre and Modified LuGre models also affect the overall suspension displacement, although the effects are again small in the overall displacement reaction.



## Annexure C: Model Validation Additional figures

Additional figures for purposes of model validation are given in this section. Higher velocity double lane change validation figures for the soft suspension are given in the first section. The second section shows the validation figures for the stiff suspension setting.

### Annexure C-1: Higher Velocity Double Lane Change Soft Suspension

Additional figures for the soft suspension model validation are given in this section for Double Lane Change manoeuvres at higher velocities are given in this section. The correlation figures shown here use the same layout as used in the main report.

Suspension displacements are shown in Figure 89 while suspension forces are shown in Figure 90 for a 70 km/h Double Lane Change manoeuvre on the ride suspension setting.

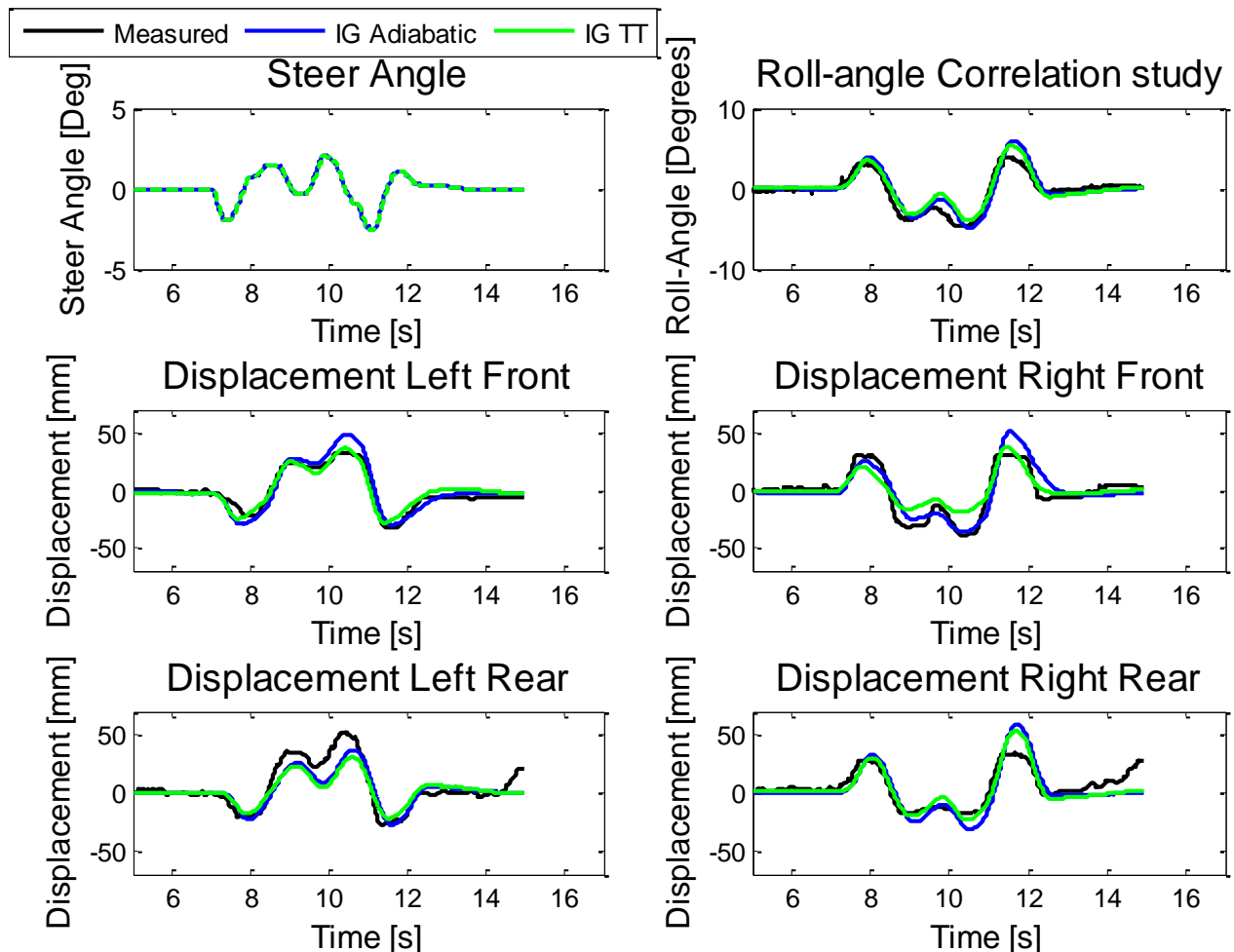


Figure 89: Double Lane Change Displacement validation 70km/h Soft

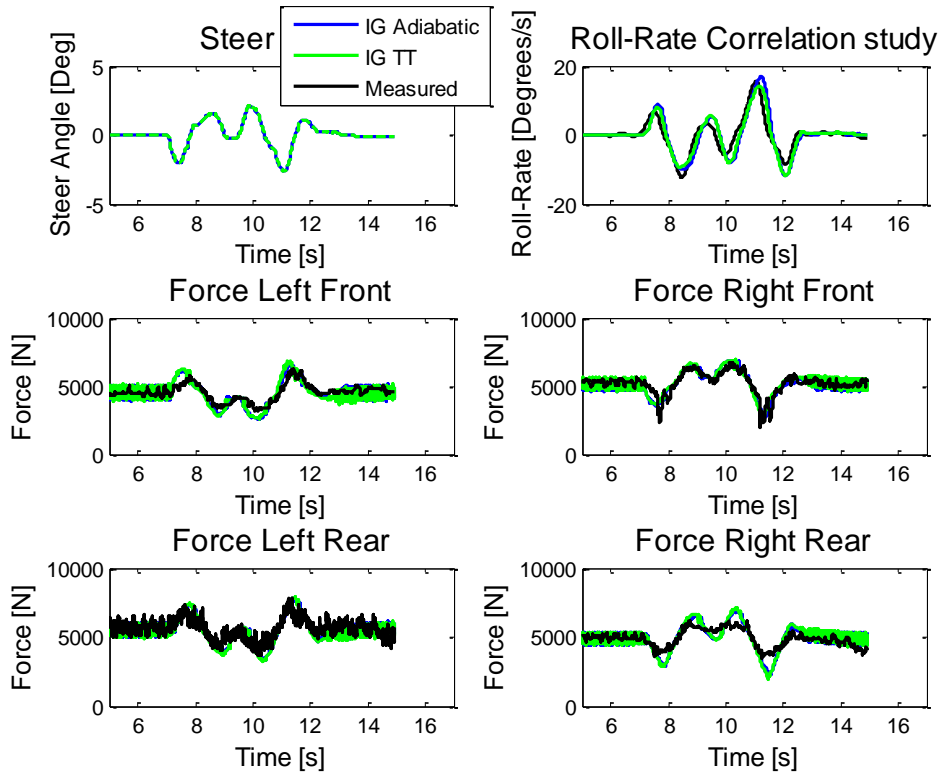


Figure 90: Double Lane Change Force validation 70km/h Soft

Figure 91 and Figure 92 shows the validation for displacements and forces respectively for an 80 km/h Double Lane Change manoeuvre.

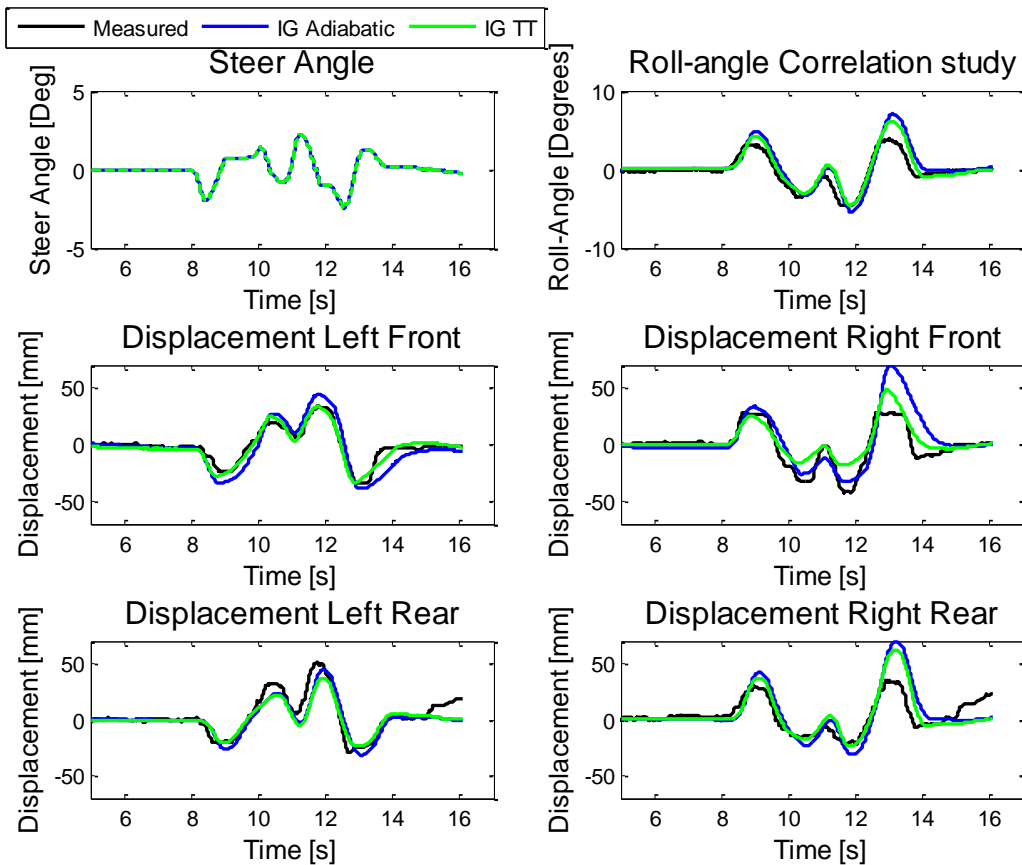


Figure 91: Double Lane Change Displacement validation 80km/h Soft

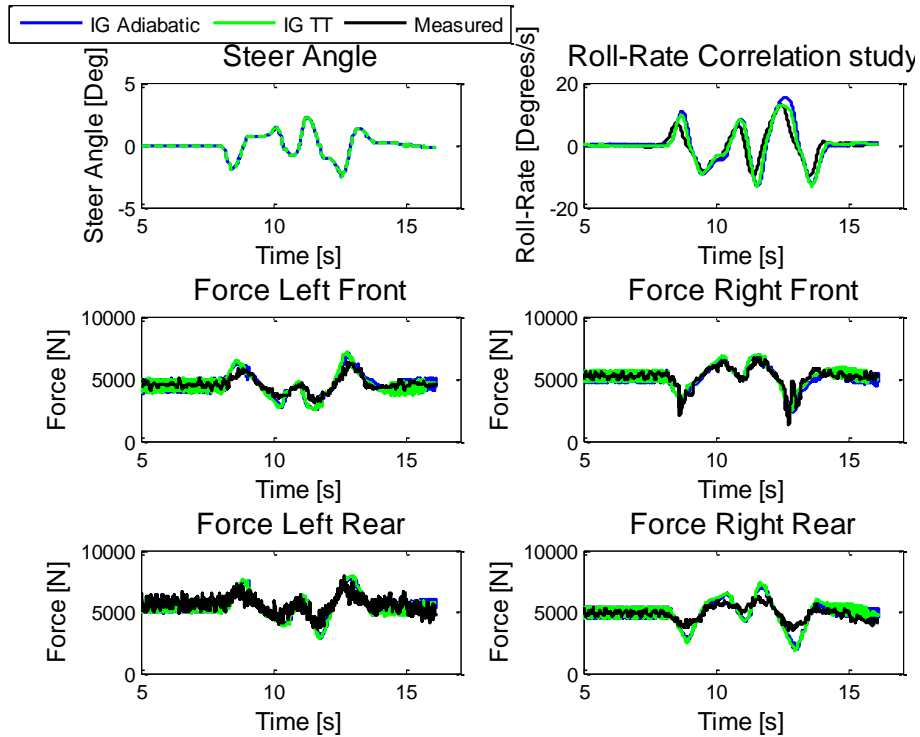


Figure 92: Double Lane Change Force validation 80km/h Soft

### Annexure C-2: Higher Velocity Double Lane Change Stiff Suspension

Additional figures for the Stiff suspension model validation are given in this section for Double Lane Change manoeuvres at higher velocities are given in this section. The correlation figures shown here use the same layout as used in the main report. Suspension displacements are shown in Figure 93. Suspension forces are shown in Figure 94, for a 70 km/h Double Lane Change manoeuvre on the Handling suspension setting.

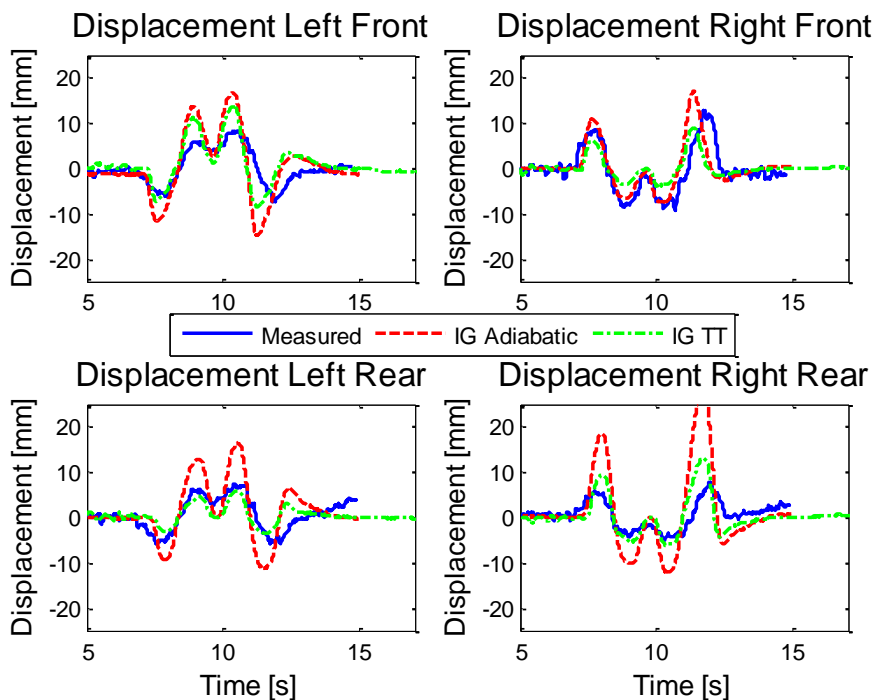


Figure 93: Double Lane Change Displacement validation 70km/h Stiff

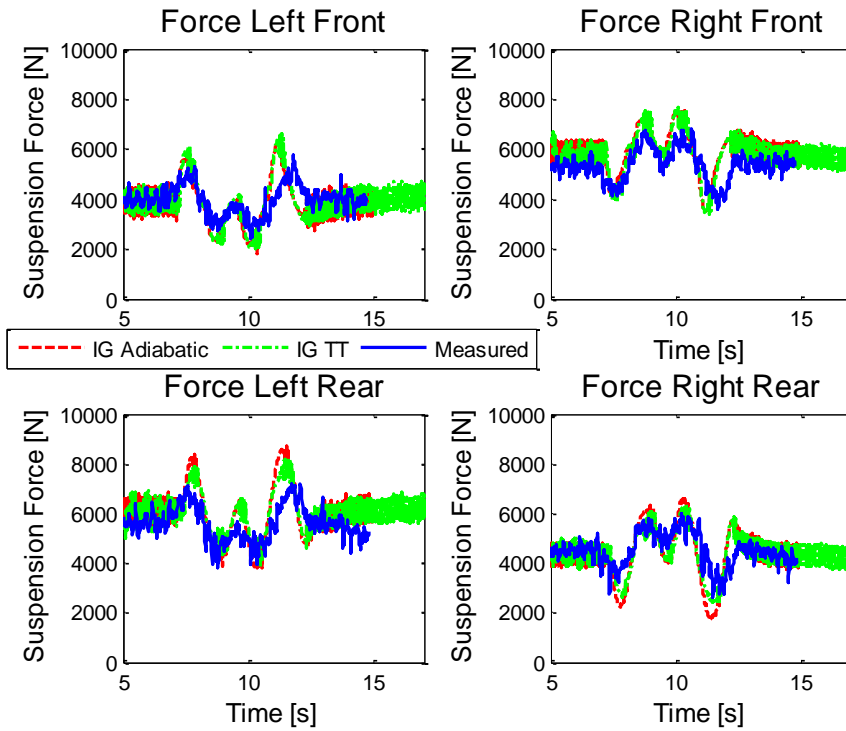


Figure 94: Double Lane Change Force validation 70km/h Stiff

Suspension displacements are shown in Figure 95, suspension forces are shown in Figure 96, for an 80 km/h Double Lane Change manoeuvre on the Handling suspension setting.

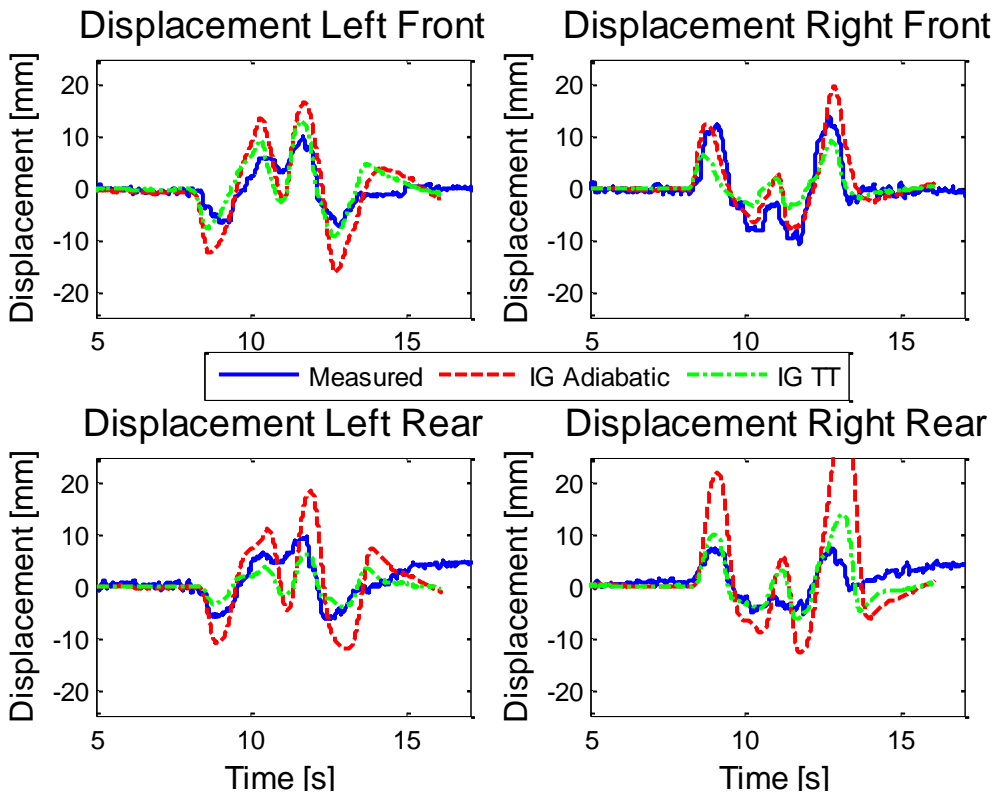


Figure 95: Double Lane Change Displacement validation 80km/h Stiff

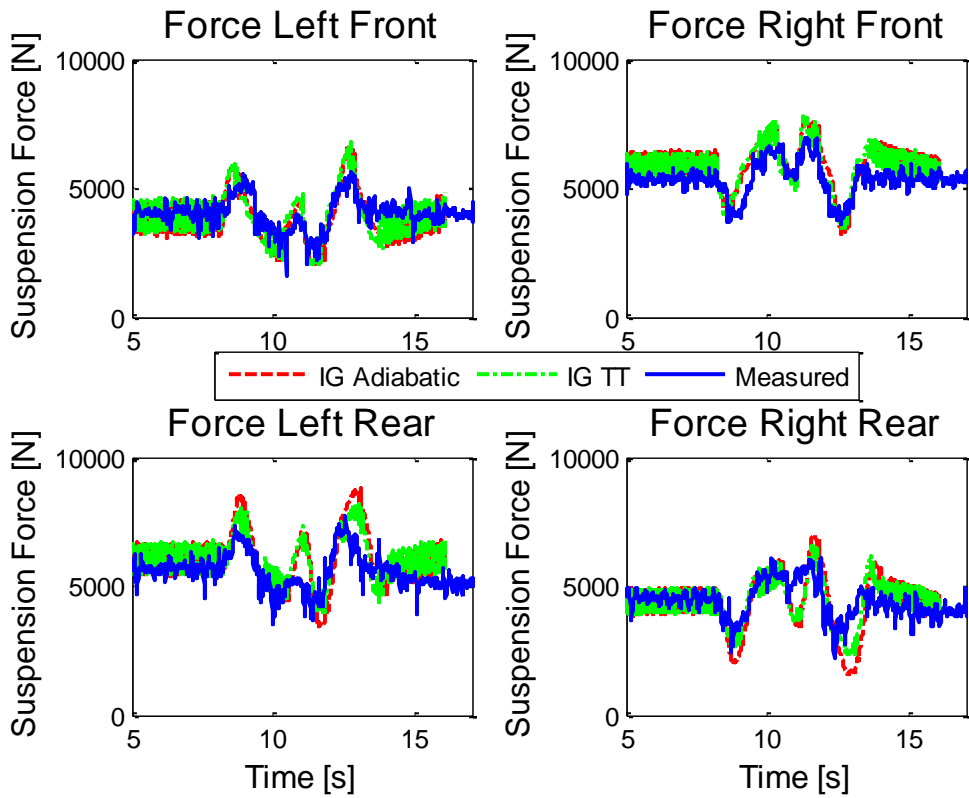


Figure 96: Double Lane Change Force validation 80km/h Stiff

## Annexure D: Friction Effects Additional figures

The effects of suspension friction on the displacement characteristics for higher velocity simulations on the hard and soft suspension settings are shown in this section. Figure 97 shows the reactions of the suspension displacements and roll dynamics of the vehicle for a 70 km/h Double Lane Change on the soft suspension setting.

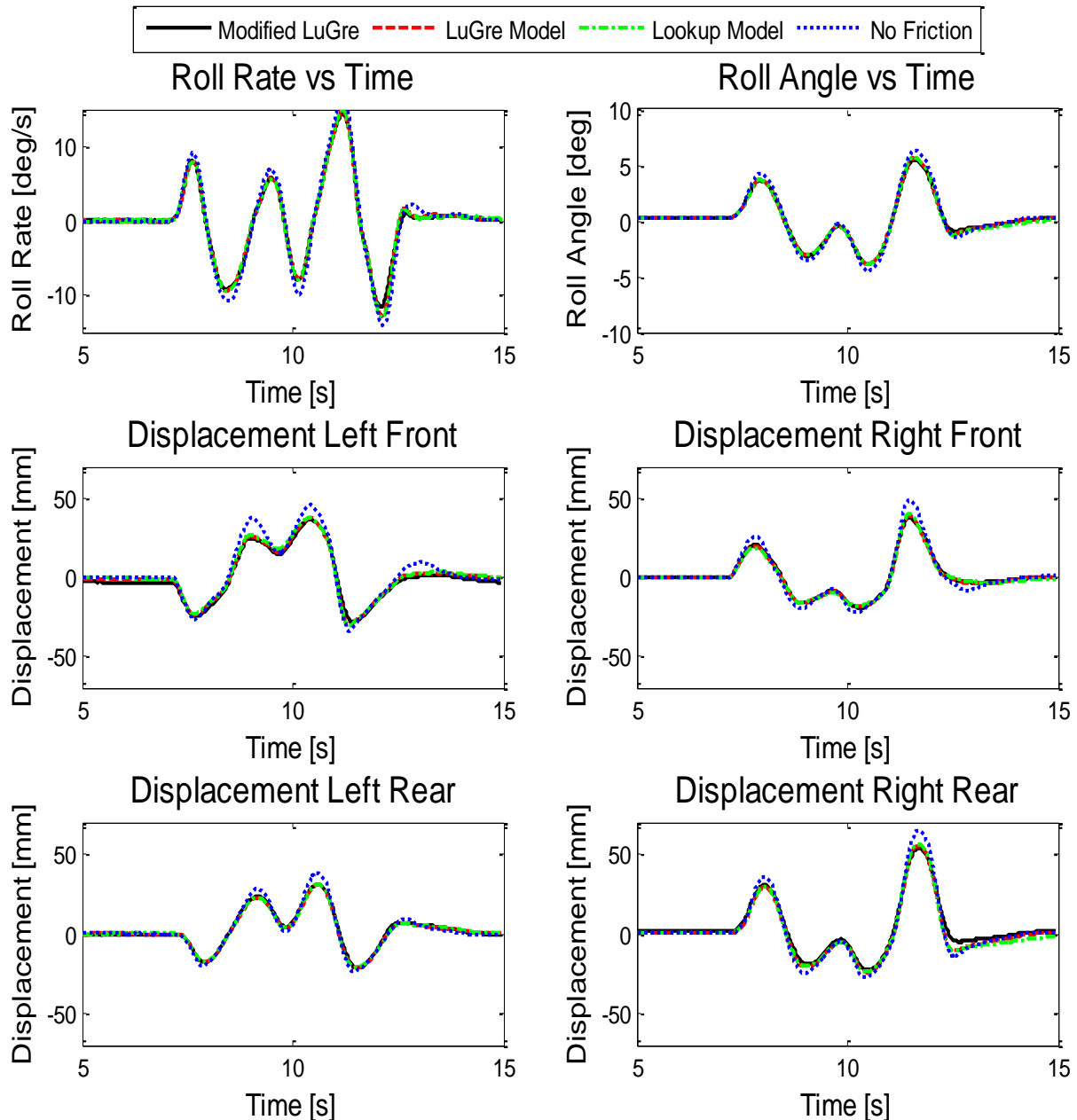


Figure 97: Friction Effects for 70km/h Double Lane Change Soft Suspension

Figure 98 shows the detailed view of friction effects on the left front suspension unit for a Double Lane Change using the soft suspension setting.

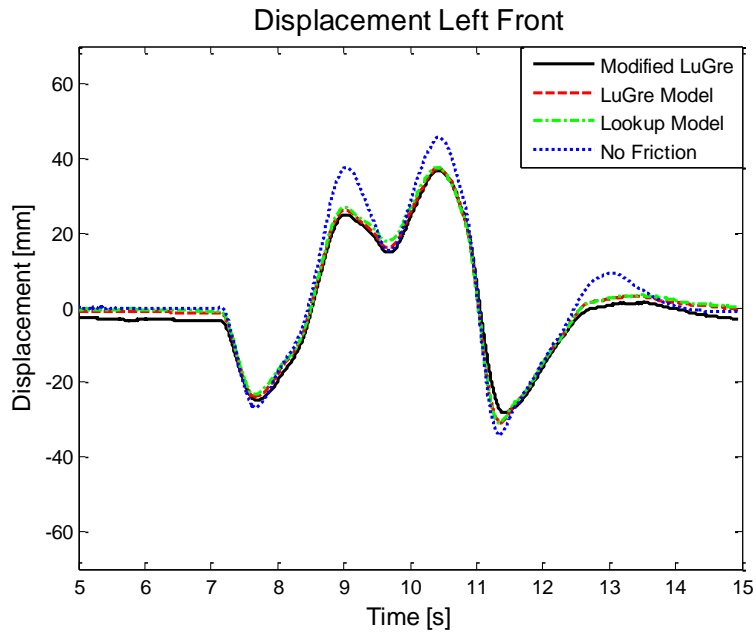


Figure 98: Friction effects on 70km/h Double Lane Change Soft Suspension, Left Front Detailed view

Figure 99 shows the effects of friction on suspension displacements and roll dynamics for a 80 km/h Double Lane Change manoeuvre. Figure 100 shows a detailed view of the friction effects on the left front suspension displacement using the soft suspension setting.

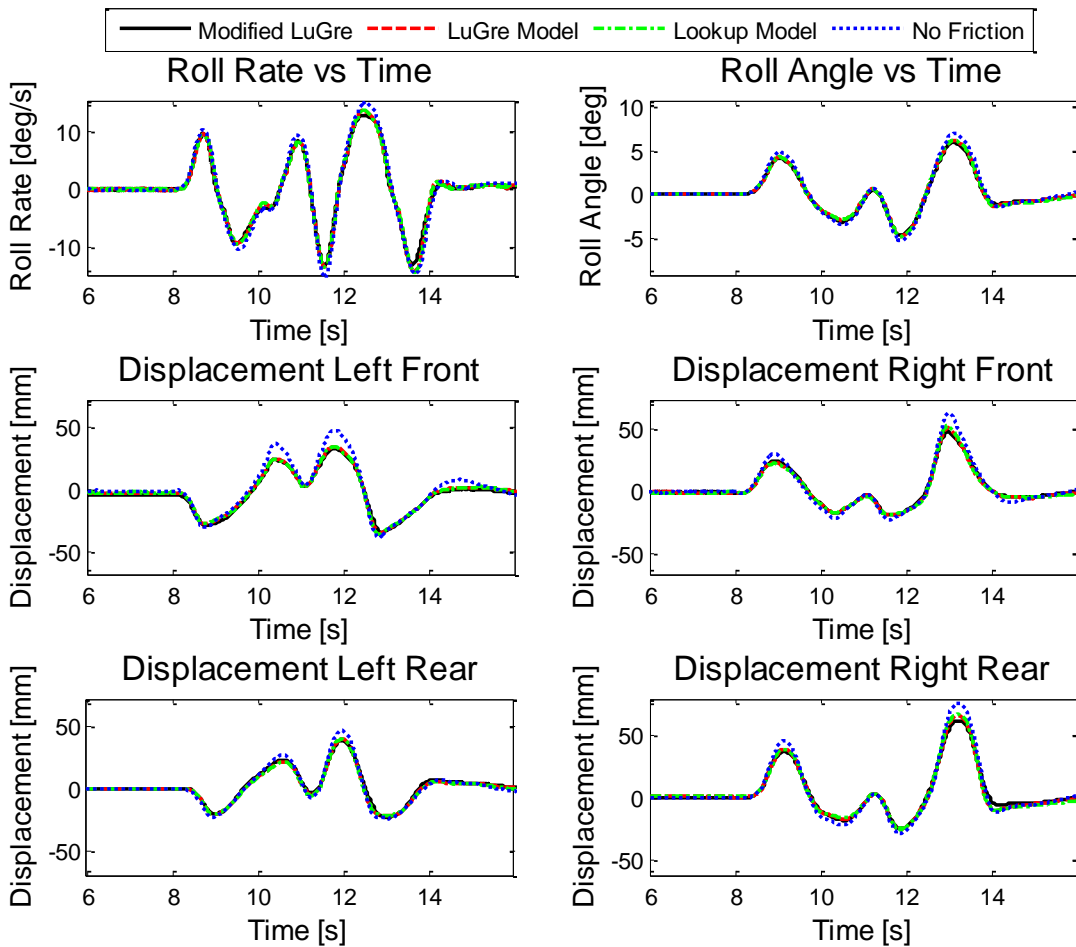


Figure 99: Friction Effects suspension displacements for an 80 km/h Soft Suspension Double Lane Change

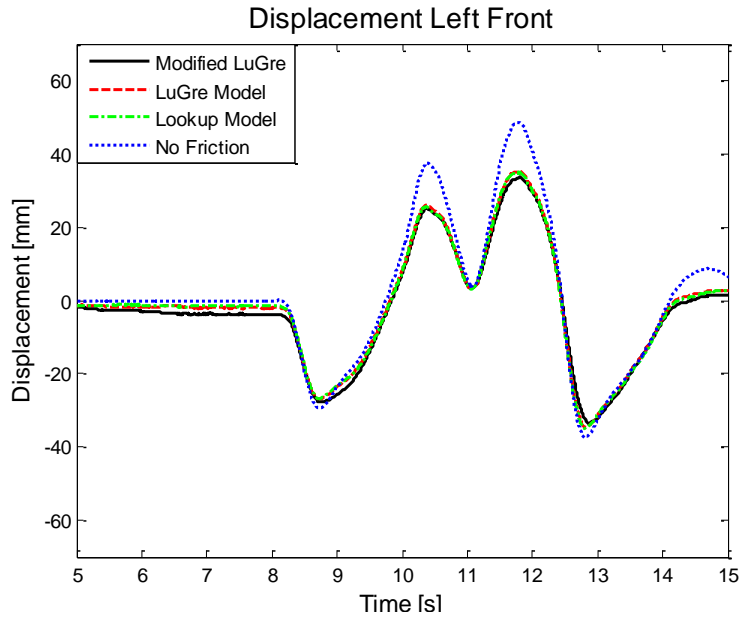


Figure 100: Friction Effects on 80km/h Soft Suspension Double Lane Change, Left Front detailed view

Friction not only affects the soft suspension setting but also the stiff suspension setting. The Frictional effects on suspension displacements and roll dynamics during a 70km/h Double Lane Change Manoeuvre using the Stiff suspension setting is shown in Figure 101.

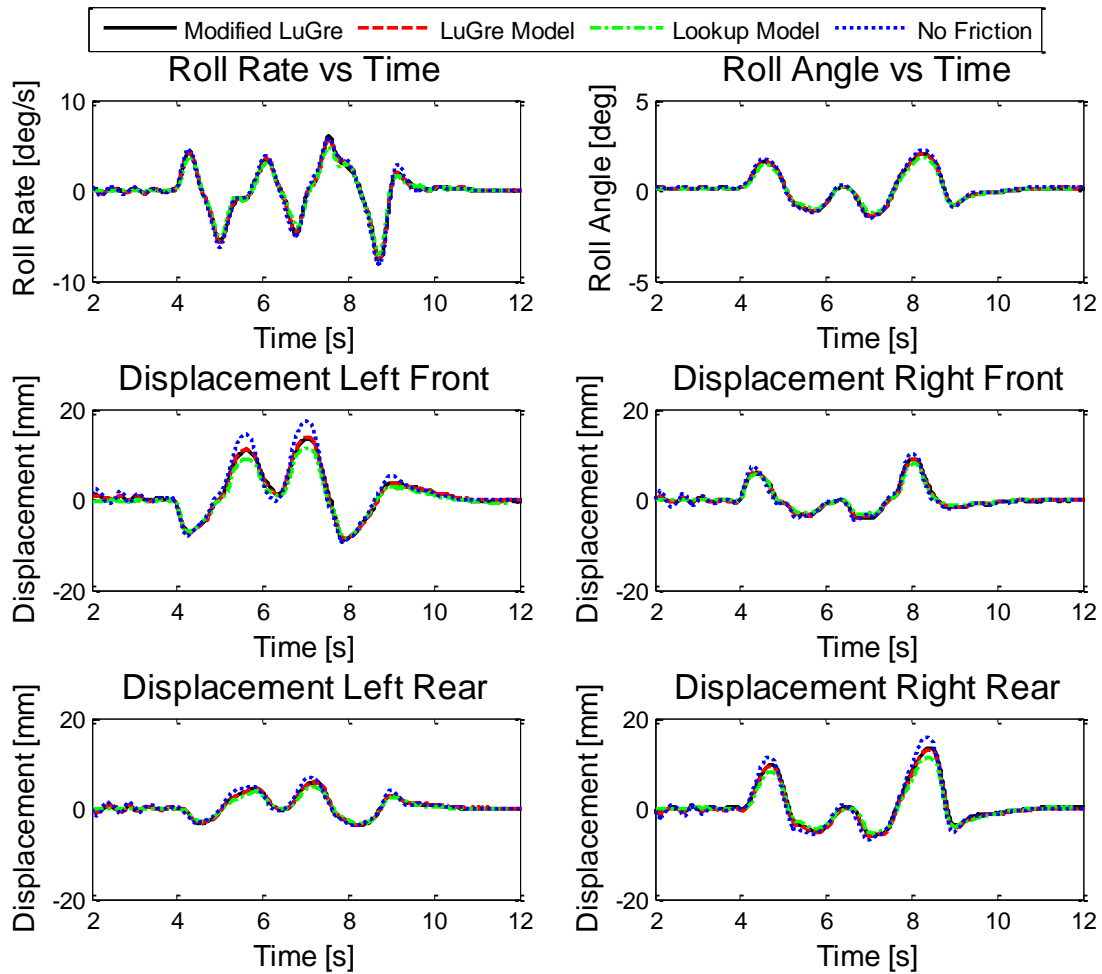


Figure 101: Friction Effects suspension displacements for a 70 km/h Stiff Suspension Double Lane Change



Figure 102, shows a detailed view of the friction effects on the left front suspension displacement using the stiff suspension setting.

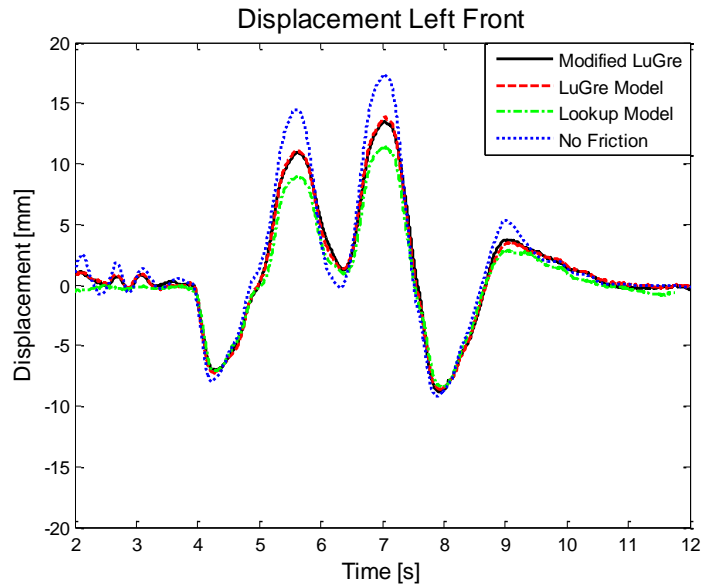


Figure 102: Friction Effects on 70km/h Stiff Suspension Double Lane Change, Left Front detailed view

Figure 103 shows the effects of friction on suspension displacements and roll dynamics for a 80 km/h Double Lane Change manoeuvre. Figure 104 shows a detailed view of the friction effects on the left front suspension displacement using the stiff suspension setting.

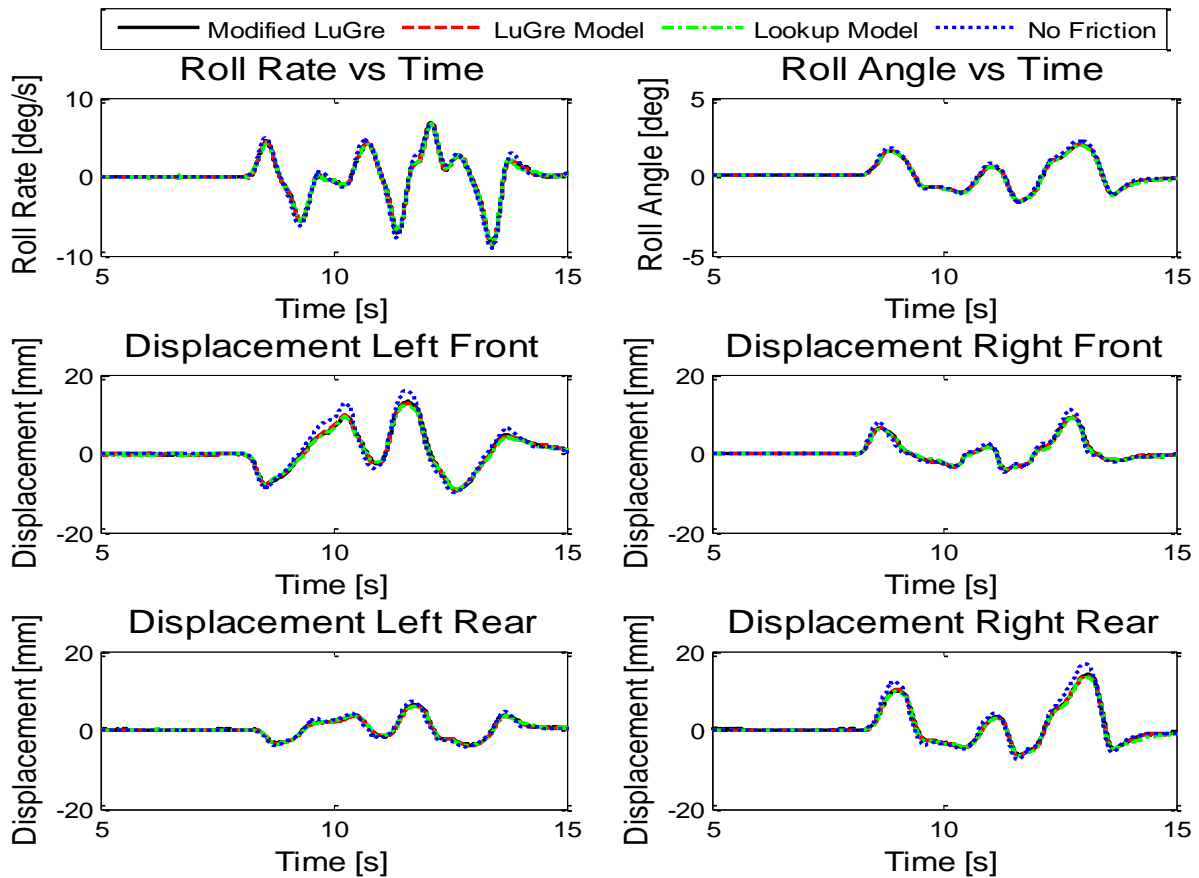


Figure 103: Friction Effects suspension displacements for an 80 km/h Stiff Suspension Double Lane Change

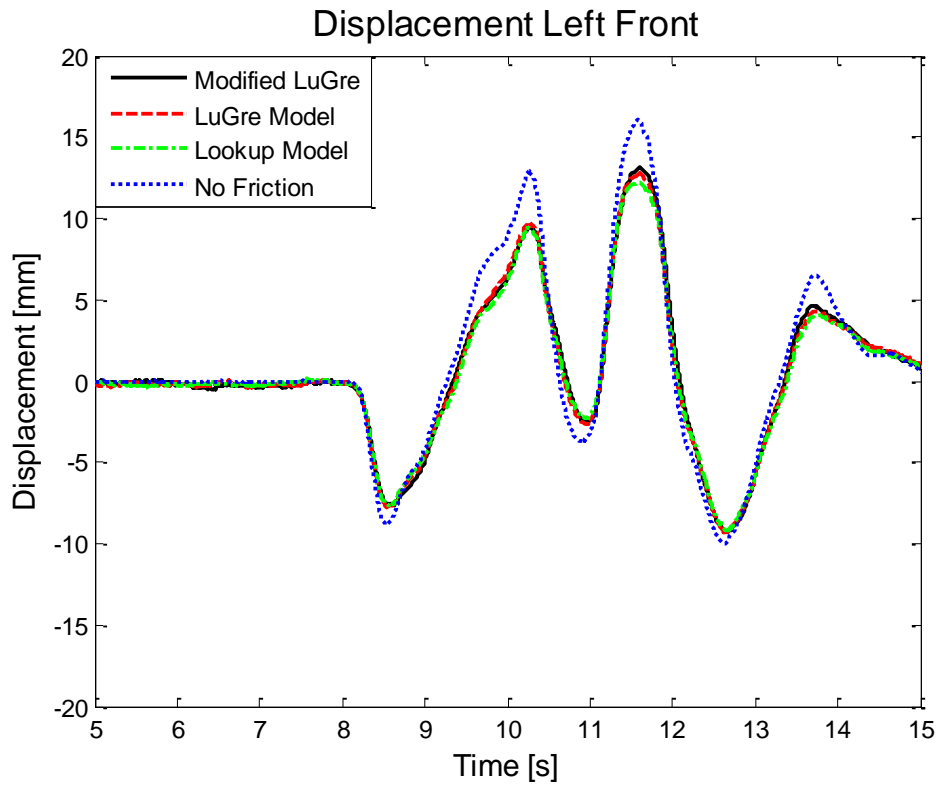


Figure 104: Friction Effects on 80km/h Stiff Suspension Double Lane Change, Left Front detailed view